

**CHARACTERIZATION OF OIL WATER FLOW IN  
HORIZANATAL PIPES**

BY

**AYMAN WAJEEH MUKHAIMER**

A Thesis Presented to the  
DEANSHIP OF GRADUATE STUDIES

**KING FAHD UNIVERSITY OF PETROLEUM & MINERALS**

DHAHRAN, SAUDI ARABIA

In Partial Fulfillment of the  
Requirements for the Degree of

**MASTER OF SCIENCE**

In

**MECHANICAL ENGINEERING**

December 2012

KING FAHD UNIVERSITY OF PETROLEUM & MINERALS

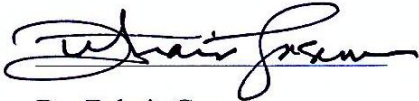
DHAHRAN- 31261, SAUDI ARABIA

**DEANSHIP OF GRADUATE STUDIES**

This thesis, written by AYMAN WAJEEH MUKHAIMER under the direction his thesis advisor and approved by his thesis committee, has been presented and accepted by the Dean of Graduate Studies, in partial fulfillment of the requirements for the degree **MASTER OF SCIENCE IN MECHANICAL ENGINEERING.**



Dr. Abdelsalam Al-Sarkhi  
(Advisor)



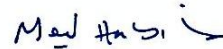
Dr. Zuhair Gasem  
Department Chairman



Dr. Luai Al-Hadhrami  
(Co-Advisor)



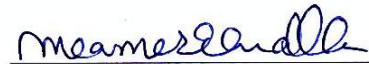
Dr. Salam A. Zummo  
Dean of Graduate Studies



Dr. Mohamed A. Habib  
(Member)

24/2/13

Date



Dr. Meamer El Nakla  
(Member)



Dr. Wael Ahmed  
(Member)

© AYMAN WAJEEH MUKHAIMER

2012

*Dedication*

*This thesis is dedicated to my family who have encouraged me and supported me through  
my study*

## **ACKNOWLEDGMENTS**

Special thanks for my advisor Dr. Al-Sarkhi and co-advisor Dr. Al-Hadhrami for their advice and support during my MS study and their guidance during working in this study. I'm also grateful for their quick response and help whenever a problem in my work comes. Appreciations are also to committee Dr. Habib, Dr. El Nakla, and Dr. Wael Ahmed for their significant suggestions and support.

I am extremely grateful to my family for their encouragement and prayers that I needed to finish this study, also for their support during the years of study.

Finally, thank you KFUPM for giving me this opportunity and providing me with everything I needed. Also my appreciation and thanks to all my colleagues, for your friendship, help and support and making the MS years pleasant.

# TABLE OF CONTENTS

ACKNOWLEDGMENTS .....	V
TABLE OF CONTENTS .....	VI
LIST OF TABLES.....	VIII
LIST OF FIGURES.....	IX
NOMENCLATURE .....	XIII
ABSTRACT .....	XV
<b>1 CHAPTER 1 INTRODUCTION .....</b>	<b>1</b>
<b>2 CHAPTER 2 LITERATURE REVIEW.....</b>	<b>3</b>
2.1 Flow Pattern and Flow Pattern Map .....	3
2.1.1 Flow Pattern Classification .....	5
2.1.2 Flow Pattern Transition .....	6
2.1.2.1 Prediction of Stratified flow .....	6
2.1.2.2 The Transition Criteria .....	9
2.1.2.3 Prediction of Dispersed Flow .....	13
2.2 Pressure Drop .....	24
2.2.1 Pressure Drop in Dispersion Flow .....	24
2.2.1.1 Mixture Viscosity .....	26
2.2.1.2 Inversion Point.....	30
2.2.2 Pressure Drop in Stratified Flow .....	33

<b>3</b>	<b>CHAPTER 3 EXPERIMENTAL SETUP &amp; PROCEDURE .....</b>	<b>35</b>
3.1	Multiphase Flow Facility .....	35
3.2	Test section .....	38
3.3	Instrumentation .....	41
3.4	Procedure .....	45
3.5	Fluids Properties .....	45
<b>4</b>	<b>CHAPTER 4 EXPERIMENTAL RESULTS.....</b>	<b>49</b>
4.1	Flow Pattern Map .....	49
4.2	Pressure Drop .....	65
<b>5</b>	<b>CHAPTER 5 VALIDATION.....</b>	<b>80</b>
5.1	Flow Pattern .....	80
5.2	Pressure Drop .....	89
5.2.1	Single phase Pressure Drop .....	89
5.2.2	Two Phase Pressure Drop.....	90
5.2.2.1	Comparison with models.....	94
5.2.2.1.1	Modified Correlation of Mixture Viscosity.....	99
5.2.2.2	Inversion Point .....	103
	<b>CHAPTER 6 CONCLUSIONS AND RECOMMENDATION .....</b>	<b>106</b>
6.1	Conclusions .....	106
6.2	Recommendation .....	108
	<b>REFERENCES .....</b>	<b>109</b>
	<b>APPENDIX1: UNCERTAINTY ANALYSIS.....</b>	<b>114</b>
	<b>APPENDIX2: PRESSURE DROP DATA.....</b>	<b>116</b>
	<b>APPENDIX3: FLOW PATTERN DATA.....</b>	<b>125</b>
	<b>VITAE .....</b>	<b>129</b>

## LIST OF TABLES

Table1: “Safrasol 80” oil properties. ....	46
Table 2: Previous experimental studies on oil-water in horizontal pipes with low viscosity range.....	92
Table 3: Percent error in the new correlation.....	102
Table 4: Comparison between inversion point models and experimental data .....	104
Table 5: Evaluation of the uncertainty analysis .....	115



## LIST OF FIGURES

Figure 2-1: The effect of the density differential and the viscosity ratio on the locations of the ZNS and ZRC boundaries [Brauner [13]].....	12
Figure 2-2: stratified-dispersed region [Brauner [13]].....	14
Figure 2-3: Comparison of the theoretical flow pattern map (points) with the experimental flow pattern map (lines) [Trallero[10]] .....	17
Figure 2-4: The H-model predictions for transition to <i>DO/W</i> (boundary 4, $C_H=0.5$ ) and transition to <i>DW/O</i> (boundary 5) in horizontal oil–water system of $E_{oD}=5$ , with experimental data of Guzhov [40] [Brauner [36]]. .....	20
Figure 2-5: The calculated pressure drop using Pal [57], Phan & Pham [55], Brinkman [48], and Schowalter [53] models of mixture viscosity, where inversion point was found by Arirachakaran et al. [9] $\nu_o = 1.85$ cP, $\rho_o = 780$ kg/m <sup>3</sup> , $U_m=2$ m/s, and $d= 22.5$ cm. ....	32
Figure 2-6: Schematic diagram of the stratified flow .....	33
Figure 3-1: Schematic Representation of the Experimental Setup .....	37
Figure 3-2: Oil-water mixing section.....	38
Figure3-3: The Test Part of the Setup.....	40
Figure 3-4: The transparent part of the test section. ....	41
Figure 3-5: The water manometer.....	42
Figure 3-6: The variable area flow meter .....	42
Figure 3-7: A picture of the “king instrument” flow meters.....	44
Figure 3-8: “Safrasol 80” oil viscosity at different temperatures .....	47
Figure 4-1: Stratified flow pattern (ST), $U_o = 0.1$ m/s, $U_w = 0.2$ m/s.....	50
Figure 4-2: Stratified flow with mixing at interface (ST-MI), $U_o = 0.63$ m/s, $U_w = 0.2$ m/s .....	50
Figure 4-3: Oil-in-water emulsion (O/W), $U_o = 0.5$ m/s, $U_w = 1.6$ m/s .....	50
Figure 4-4: Water-in-oil emulsion (W/O), $U_o = 1.6$ m/s, $U_w = 0.08$ m/s .....	51
Figure 4-5: Dispersion of oil in water over a water layer ( <i>DO/W</i> & <i>W</i> ), $U_o = 0.08$ m/s, $U_w = 0.8$ m/s .....	51
Figure 4-6: Dispersion of oil in water and dispersion of water in oil ( <i>DO/W</i> & <i>DW/O</i> ), $U_o = 0.8$ m/s, $U_w = 1.6$ m/s .....	51

Figure 4-7: Dispersion of water in oil under an oil layer (DW/O &O), $U_o=0.6$ m/s, $U_w=1.26$ m/s .....	52
Figure 4-8: Dispersion of oil in water over a water layer (DW/O &W), $U_o=0.08$ m/s, $U_w=0.8$ m/s, Saline water.....	54
Figure 4-9: Dispersion of oil in water over a water layer (DW/O & W), $U_o=0.08$ m/s, $U_w=0.8$ m/s, Tap water .....	54
Figure 4-10: Dispersion of oil in water over a water layer (DW/O & W), $U_o=0.5$ m/s, $U_w=1.26$ m/s, Saline water.....	55
Figure 4-11: Dispersion of water in oil and oil in water (DW/O & DO/W), $U_o=0.5$ m/s, $U_w=1.26$ m/s, Tap water.....	55
Figure 4-12: Oil-in-water emulsion (DO/W), $U_o=0.1$ m/s, $U_w=1.6$ m/s, Saline water ...	56
Figure 4-13: Oil-in-water emulsion (DO/W), $U_o=0.1$ m/s, $U_w=1.6$ m/s, Tap water.....	56
Figure 4-14: Oil-in-water emulsion (DO/W), $U_o=0.1$ m/s, $U_w=1.6$ m/s, Saline water ...	57
Figure 4-15: Oil-in-water emulsion (DO/W), $U_o=0.1$ m/s, $U_w=1.6$ m/s, Tap water.....	57
Figure 4-16: Stratified flow with mixing at the interface (ST-MI), $U_o=1$ m/s, $U_w=0.5$ m/s, Saline water.....	58
Figure 4-17: Stratified flow with mixing at the interface (ST-MI), $U_o=1$ m/s, $U_w=0.5$ m/s, Tap water .....	58
Figure 4-18: Experimental flow pattern map for Tap water, $\mu_o/\mu_w=1.94$ , $\rho_o/\rho_w=0.78$ . .	61
Figure 4-19: Experimental flow pattern map for 75 ‰ saline water, $\mu_o/\mu_w=1.536$ , $\rho_o/\rho_w=0.732$ .....	62
Figure 4-20: Comparison of the flow pattern boundaries between Tap water and saline water.....	63
Figure 4-21: Single phase pressure drop for oil, 25 °C.....	66
Figure 4-22: Single phase pressure drop for Tap water, 25 °C.....	66
Figure 4-23: Single phase pressure drop for 75 ‰ saline water, 25 °C.....	67
Figure 4-24: The pressure drop of oil-tap water at 1.42 m/s mixture velocity and of oil-saline water at 1.61 m/s mixture velocity, 25 °C. ....	68
Figure 4-25: The pressure drop of oil with tap and saline water at 2.98 m/s mixture velocity, where the single phases pressure drops are found by calculation, 25 °C.....	69

Figure 4-26: The pressure drop of oil-Tap water, where SP is the calculated single phase pressure drop for oil and water, 17 °C.....	71
Figure 4-27: The pressure drop of oil -Tap water for 17 °C and 25 °C, where SP is the calculated single phase pressure drops for oil and water. ....	73
Figure 4-28: Pressure drop of oil -Tap water with mixture velocities (m/s) shown in chart; the flow pattern of first data line was ST&MI, 25 °C. ....	75
Figure 4-29: Pressure drop of oil -saline water with mixture velocities (m/s) shown in chart, 25 °C.....	76
Figure 4-30: Normalized pressure drop against oil fraction. The mixture velocities (m/s) are shown in chart, 25 °C. ....	78
Figure 4-31: Experimental Pressure drop profile along with a straight line profile of $V_m=2.98\text{m/s}$ , 25 °C.....	79
Figure 5-1: Comparison between Trallero [15] flow pattern map (lines) and this study experimental flow pattern map (points), Tap water, $\mu_o/\mu_w = 1.94$ , $\rho_o/\rho_w = 0.78$ .....	81
Figure 5-2: Comparison between Trallero [15] flow pattern map (lines) and this study experimental flow pattern map (points), saline water, $\mu_o/\mu_w = 1.536$ , $\rho_o/\rho_w = 0.732$ . ....	82
Figure 5-3: Comparison between Brauner flow pattern map (lines) and this study experimental flow pattern map (points), Tap water, $\mu_o/\mu_w = 1.94$ , $\rho_o/\rho_w = 0.78$ . ....	83
Figure 5-4: Comparison between Brauner flow pattern map (lines) and this study experimental flow pattern map (points), saline water, $\mu_o/\mu_w = 1.536$ , $\rho_o/\rho_w = 0.732$ . ....	84
Figure 5-5: Comparison between Torres [43] flow pattern map (lines) and this study experimental flow pattern map (points), Tap water, $\mu_o/\mu_w = 1.94$ , $\rho_o/\rho_w = 0.78$ . ....	85
Figure 5-6: Comparison between Torres [43] flow pattern map (lines) and this study experimental flow pattern map (points), saline water, $\mu_o/\mu_w = 1.536$ , $\rho_o/\rho_w = 0.732$ . ....	86
Figure 5-7: Experimental pressure drop of different mixture velocities taken from the present study along with the experimental work of Elseth [66] and Karolina et al. [64]	90
Figure 5-8: Experimental pressure drop for several previous works taken from Table 2 along with the present study .....	93
Figure 5-9: Comparison between the Homogenous Model along with the Two-Fluid-Model and the present experimental work.....	94

Figure 5-10: Comparison between the Homogenous Model and the present experimental work .....	95
Figure 5-11: Comparison between the Homogenous Model and the present experimental work, 17 °C.....	96
Figure 5-12: Comparison between theoretical and experimental values of pressure drop from this study using the Homogenous, pal [56], and phan and pham [55] models .....	97
Figure 5-13: Comparison between theoretical and experimental values of pressure drop of Elseth [66] and Karolina et al. [64] experimental data taken from Figure 5-7.....	98
Figure 5-14: Comparison between suggested model and the Homogenous model with the experimental work of this study for $U_m = 2.98$ m/s. ....	99
Figure 5-15: Comparison between the suggested model, pal [56] model, and phan and pham [55] model with the experimental work of this study. ....	100
Figure 5-16: Comparison between the suggested model and the experimental work of several works mentioned in Table 2 .....	101

## NOMENCLATURE

$A$	:	The area	$m^2$
$\beta$	:	Pipe inclination	degree
$C_s$	:	The sheltering effect	
$d_{cr}$	:	Critical diameter	m
$d_{max}$	:	The maximum droplet diameter	m
$\epsilon_o$	:	Critical oil holdup	
$f$	:	Friction factor	
$g$	:	Acceleration of gravity	$m/s^2$
$h,$	:	Holdup	
$H$	:	Water height	m
$\mu$	:	Viscosity	cP
$Re$	:	Reynolds number	
$S$	:	The perimeter	m
$\rho$	:	The density	$kg/m^3$
$S_g$	:	Specific gravity	
$\tau$	:	Shear stress	$N/m^2$

$U$	:	Superficial velocity	m/s
$V$	:	Velocity (actual)	m/s
$\sigma$	:	Interfacial tension	mN/m
$\text{‰}$	:	Parts per thousands	

## Subscripts

$c$	:	The continuous phase
$cr$	:	Critical
$d$	:	The dispersed phase
$i$	:	Interface
$m$	:	The mixture
$o$	:	Oil
$w$	:	Water
$os$	:	Superficial oil
$ws$	:	Superficial water

## **ABSTRACT**

Full Name : AYMAN WAJEEH MUKHAIMER  
Thesis Title : CHARACTERIZATION OF OIL WATER FLOW IN HORIZANATAL  
PIPES  
Major Field : MASTER OF SCIENCE IN MECHANICAL ENGINEERING  
Date of Degree : December 2012

The flow pattern and the pressure drop of oil-water flow in a 2.25 cm inner diameter acrylic horizontal pipe were studied experimentally. The used oil has a  $781 \text{ kg/m}^3$  density and a 1.85 cP viscosity at  $25^\circ\text{C}$ . The experimental data were compared with Trallero, Brauner, and Torres flow pattern models and with several models of mixture viscosity. The effect of water salinity on flow pattern map and pressure drop was investigated by making the water salinity 75 ‰ and comparing the data of oil-Tap water with that for oil-saline water. The added amount of salt caused the density ratio to change from 0.78 to 0.732, and the viscosity ratio to change from 1.94 to 1.536. It was noticed that due to the salt addition, the transition from dispersion of oil in water over a water layer flow pattern to the dispersion of water in oil and oil in water flow pattern was delayed. Also, it was noticed that in the stratified with mixture at the interface flow pattern, the waves in saline water has less amplitudes than that in tap water. For the pressure drop, it was noticed that the inversion in saline water case happened earlier, and the pressure drop decrease rate for saline water was found to be less than that for tap water.

## ملخص الرسالة

الاسم الكامل: أيمن وجيه مخيمر

عنوان الرسالة: خصائص تدفق الزيوت والمياه في الأنابيب الأفقية

التخصص: ماجستير في العلوم في الهندسة الميكانيكية

تاريخ الدرجة العلمية: ديسمبر 2012

تم إجراء تجارب لدراسة خسائر الضغط وشكل التدفق لماء وزيت يتدفقان معا في أنبوب مصنوع من الاكريليك ومثبت افقيا. وكانت كثافة الزيت المستخدم 780 كغ/م<sup>3</sup> ولزوجته 1.85 سم.بويز. وكان قطر الأنبوب المستخدم في الدراسة 2.25 سم. وقد تم مقارنة نتائج التجارب مع العديد من نظريات أشكال التدفق ونظريات حساب خسارة الضغط. وتم أيضا دراسة تأثير ملوحة الماء على انخفاض الضغط وشكل التدفق من خلال جعل ملوحة الماء 75 جزء بالألف و إجراء مقارنة بين نتائج تجارب الماء النقي مع الماء المالح. وقد تسببت كمية الملح المضافة في خفض نسبة كثافة الزيت للماء من 0.78 إلى 0.732 وفي انخفاض نسبة كثافة الزيت للماء من 1.94 إلى 1.536. وقد تم ملاحظة أن الملح قام بتأخير عملية الانتقال من شكل تدفق إلى آخر في بعض أشكال التدفق، وفي أشكال أخرى كانت الأمواج بين طبقة الزيت والماء أقل حدة في الماء المالح من تلك في الماء النقي. ولوحظ أيضا أن سلوك الضغط قد تأثر أيضا بالملح المضاف، حيث أن منطقة إنعكاس الضغط بدأت أولا في الماء المالح، وكما لوحظ أن مقدار الانخفاض في فرق الضغط للماء المالح أقل من ذلك للماء النقي.



# **CHAPTER 1**

## **INTRODUCTION**

Liquid-liquid flow appears in chemical, petrochemical, and food industries. More often, it is seen in petroleum industry, as some of the reservoirs consist of water and oil layers. So production lines will carry both components with different ratios. In this study, the oil-water flow in a horizontal pipe case is investigated.

While extracting oil from wells, the ratios of water and oil varies with time. The change in these ratios has a major influence on the pressure drop along the pipe and the flow pattern. This influence will cause the mass flow inside the pipe to vary as well. Therefore, it's essential to realize the relation between the components ratio and the pressure drop.

Predicting the flow pattern inside the pipe is the major concern in any petroleum process, since the knowledge of the flow patterns gives various advantages. For instance, knowing the flow pattern determines the behavior if the pressure drop inside the pipe, the right method of evaluating the pressure drop, the contact area of each fluid with the pipe wall for corrosion problems, and at the end, better reservoir management and flow assurance.

The aspects that affect the pressure drop and the flow pattern should be determined in order to predict the pressure losses inside the pipes, maintain the pressure at the required rate, and enhance the flow inside the pipe. The aspects which are considered in this study are the oil-water flow rate, oil fraction, oil-water viscosity and density ratio.

Extensive amount of experimental work were performed on different types of oil to study the effect of oil-water density ratio and viscosity ratio on both the flow pattern map and the pressure drop. The previous experimental works show the effect of oil-water density ratio and viscosity ratio by changing oil physical properties. The present work is conducted to show the effect of changing the oil-water density ratio and viscosity ratio on the flow pattern and the pressure drop by changing the water physical properties. This is achieved by dissolving food salt into the water. Since the added salt is organic, it dissolves only in water, and the oil properties will not change.

The objectives of this study are summarized as follows:

1. Produce experimental data for the flow pattern and the pressure drop using oil with low viscosity value due to the scarcity of the available data for this range.
2. Study the pressure drop behavior for low viscosity oils.
3. Study the effect of changing the water physical properties on both the flow pattern map and the pressure drop by dissolving salt into the water.
4. Validate previous models of the flow pattern map and pressure drop against the experimental results of this study.
5. Modify existing correlation or develop new one if needed.

A computer program is developed to generate the flow pattern map and the pressure drop inside a pipe using models from the literature. The program uses visual basic programming language as a micro impeded in MS excel to estimate and display the produced flow pattern map and the pressure drop profile.

## **CHAPTER 2**

### **LITERATURE REVIEW**

A state-of-the-art literature survey of previous studies on oil-water flow is presented in this chapter. Also, models of predicting flow patterns and pressure drop including inversion point is summarized as well.

Most of the available oil-water models in the open literature are considered as an extension of gas-water models since more attention was brought to gas-water flows than oil-water. Moreover, focus on oil-water flow started a while after gas-water. The main variances between gas-water and oil-water flow are the large differences in the density (of air compared to oil) and other thermo physical properties such as viscosity, surface tension, specific heat ...etc.

#### **2.1 Flow Pattern and Flow Pattern Map**

The flow pattern is a term which describes the oil-water flow shape inside a pipe, or it describes the structure of the interface between the two fluids. As oil and water flow in a pipe, they take different special configuration depending on their flow rates. For example, when the flow rates of oil and water are very low, they move as two continuous layers with one above the other without any mixing at the interface. The flow pattern for this

shape of interface is called the stratified flow pattern. Other flow patterns are seen in section 2.1.1.

The flow pattern map is a graph that is divided into regions; each region indicates a certain flow pattern. It can be found with different coordinates. These coordinates are usually represented by pipe geometry, or fluid property, or flow rate, or a combination between these parameters. There are two types of coordinates used in the flow pattern map. The first type uses dimensionless parameters that are found empirically or derived from the flow rate, pipe geometry, and fluid properties. An example of this type is Fair [1] flow pattern map, where the total mass flux is plotted against the Lockhart-Martinelli parameter [2]. Another example is Taitel and Dukler [3] flow pattern map which uses the Lockhart-Martinelli parameter [2] in the x-axis and gas Froude number with two other parameters they derived.

The other type of flow pattern map uses a simple coordinate system where one variable or more (such as the flow rate) is used in the diagram axes without complex derivations. This type is used to show the effect of changing the diagram axis parameter on the transition boundaries between the flow patterns while fixing the other parameters. So, this is not a generalized diagram that can be used for other fluids or pipes. This type of flow pattern map can be seen in many research work such as Bergelin and Gazley [4] and Johnson and Abou-Sabe [5] flow pattern maps that use the liquid and gas mass flow rates, and Baker [6] flow pattern map that uses the mass flow rate of gas and liquid as the y-axis and the x-axis respectively.

### 2.1.1 Flow Pattern Classification

Different techniques were used to identify each flow pattern. Visual observation is the most common way in recognizing a flow pattern. Other methods combine visual observation with pressure behavior and holdup, whereas other ways include tomography using x-ray or gamma ray.

The oil-water flow patterns in a horizontal pipeline are almost similar to those for gas-water. Back in 1959, Russell et al. [7] identified three flow patterns which are mixed flow, stratified flow, and bubble flow for oil having a 18 cP at 40 °C viscosity and 834 kg/m<sup>3</sup> density. Charles et al. [8] used three kinds of oils having a 6.29, 16.8, and 65 cP viscosity at 25 °C, and equal density with water. They categorized the observed flow patterns into water-droplets-in-oil, concentric oil-in-water, oil-slugs-in-water, oil-bubbles-in-water, and oil-drops-in-water. Arirachakaran et al. [9] performed experiments for oil viscosities of 4.7, 58, 84, 115, 237, and 2116 cP. They classified the flow patterns into stratified, mixed, annular, intermittent, and dispersed. Trallero [10] generated a flow pattern map for oil-water density ratio 0.85 and viscosity ratio 29.6. He classified the flow patterns into stratified, stratified with mixing at the interface, dispersion of oil in water over a water layer, emulsion of oil in water, emulsion of water in oil, and dual type of dispersions. Nadler and Mews [11] did the same classification and added the flow pattern “layers of water-in-oil dispersion and water”. Another classification seen in Abduvayt [12] who arranged the flow patterns in Horizontal and Hilly Terrain flow into twelve flow patterns grouped into three basic categories: segregated, semi-segregated, and semi-dispersed flow.

## **2.1.2 Flow Pattern Transition**

Charles et al. [8] indicated that the oil-water flow patterns are nearly independent of oil viscosity, as had been noticed also by Arirachakaran et al. [9]. They mentioned that the viscosity effect was very minor, and the flow pattern maps for the different oil viscosities were similar.

The density is noticed to have a stronger effect on the flow pattern map than viscosity, but still the change is slight. This effect is noticeable in the stratified region, as its area increases when the oil-water density ratio decreases. An example of density and viscosity effect is Brauner [13] model shown in Figure 2-1 in section 2.1.2.2.

The same gas-water flow pattern transition concepts are used for oil-water, where most of the oil-water models came after adapting gas-water models to be suitable for oil-water. The first transition models for liquid-liquid flow are seen in Brauner [14], Brauner [13], and later Trallero [15] who developed a general flow pattern map for oil-water flow.

### **2.1.2.1 Prediction of Stratified flow**

Stratified flow is a major flow pattern in the oil-water flow pattern map, it is located in the low velocities region, and the boundaries of this flow pattern are surrounded by several flow patterns. Prediction of the stratified flow boundary for oil-water flow is achieved with the instability analysis. Studying the instability of the stratified flow provides two benefits, the transition from stratified to other flow patterns criteria, and the

waves generation at the interface between the two phases which will lead to the wavy-stratified transition conditions. The Kelvin-Helmholtz (KH) instability analyses are used to determine the stability of stratified flow. The KH instability arises when a velocity difference at the interface between two fluids appears. The result of the instability reveals waves at the interface of the two fluids. Two types of KH analyses are used, one which neglects the effect of shear stresses, which is called the Inviscid Kelvin-Helmholtz (IKH) analysis, and the other takes into account the shear stresses in the derivation, which is called the Viscous Kelvin-Helmholtz (VKH) analysis. Many researchers used the IKH analysis in their work (mainly for gas-liquid), such as Kordyban [16], Taitel [3], Kordyban [17], Mishima [18], and Wallis [19]. While work on the VKH analysis can be seen in Wallis [20], Lin [21], Wu [22], Andritsos [23], Barnea [24], and Crowley [25].

The KH instability analysis is the main element in determining the transition condition from stratified flow, and several studies have been implemented on this analysis to study its validity and credibility for different liquid viscosities and densities.

The influence of liquid viscosities on IKH and VKH analyses can be seen in the gas-liquid study of Barnea [26], where the shear stresses are neglected in the first one and considered in the other. The study aimed to show the influence of neglecting the shear stresses in the analysis for low viscosity liquids. The results showed that considering or neglecting the shear stresses will give the same results for high viscosity liquids. However, different results are noticed for low viscosity liquids. Also the influence of viscosity is seen in Lin [21] who specified that the IKH theory correctly predicts the stability of a stratified flow only for very large liquid viscosities, and the inviscid theory is not accurate in predicting the stability of stratified flow. They involved the shear

stresses in their analysis and mentioned that the VKH theory predicts well the transition to slugs for thick enough liquid layers.

The instability at the interface either leads to the growth of short waves, which will give a stratified-wavy flow, or leads to long waves which will produce roll waves that may lead to the transition to other flow patterns. Hanratty [27] and Andreussi [28] mentioned that roll waves arise due to the instability of long waves that occur once the liquid inertia and pressure variation over long waves overcomes gravity. Barnea [24] used a combined model of viscous and inviscid KH analyses for the determination of roll waves or annular flow.

An example of the IKH analysis is Wallis [19] model, where he used simple IKH analysis to produce a simple model for the transition from stratified flow to slug or plug flow. The model uses an empirical factor to suite the experimental results. The model is widely used due to its simplicity and reasonable agreement with experimental data. Taitel [3] proposed a simple model using IKH analysis that is widely used. The model uses an empirical factor to fit the experimental results, the model shows good agreement with the experimental data especially for low viscosity liquids.

In addition of the KH analysis, Barnea and Taitel [29] and Barnea and Taitel [30] introduced the structural stability analysis that specifies the stability of the structures of the steady-state solutions.

later Barnea [31] and Barnea [32] used the structural stability analysis and the interfacial stability analysis (KH analysis), where the simplified method of Taitel [3] and Barnea's



[24] method of combining VKH and IKH analysis are considered to study the stability of the solutions for stratified flow, using linear and non-linear analyses. They listed that the KH analysis are not enough to determine the steady-state solutions validity in separated flow, the structural stability should also be considered in addition to the KH analysis.

Another method of analysis used besides the KH analysis is Jurman [33] work, who used the boundary-layer approximation to derive a nonlinear wave equation that is valid for Reynolds numbers up to the order 100 for a gas flow over a thin liquid film. The derivations revealed the presence of kinematic and dynamic processes. Also the linear stability analyses were used to distinguish the regions where waves will be dominated by kinematic or dynamic processes. Also, the one-dimensional wave model analysis method which was used by Crowley [25], where he used the one-dimensional wave model for incompressible flow to predict the transition from stratified to slug.

### 2.1.2.2 The Transition Criteria

The first step is to find the actual holdup, it can be found from the combined momentum equation:

$$F = -\frac{\tau_w S_w}{A_w} + \frac{\tau_o S_o}{A_o} + \tau_i S_i \left( \frac{1}{A_w} + \frac{1}{A_o} \right) - (\rho_w - \rho_o)g \sin(\beta) \quad (1)$$

Where  $\tau_o$ ,  $S_o$ ,  $\rho_o$ , and  $A_o$  are the shear stress, the perimeter, the density, and the area of oil.

The terms  $w$  and  $i$  stands for water and interface respectively,  $\beta$  is the inclination of the

pipe. The shear stresses, phase's areas and perimeters can be found in Trallero [15] or Brauner [14].

The second step is to make F (the left hand side of equation (1)) equals to zero to get the steady-state solutions, as  $T$ ,  $S$ , and  $A$  are functions of the holdup. Equation (1) needs only to change the holdup to find its root. When the above equation is equaled to zero, the actual holdup for the given oil and water flow rates is found.

The transition criteria is shown below as presented in Barnea & Taitel [32]:

$$(c_v - c_{IV})^2 + \frac{\rho_w \rho_o}{\rho^2 R_o R_w} (V_o - V_w)^2 - \frac{(\rho_w - \rho_o)}{\rho} \frac{A}{\dot{A}_w} g \cos \beta - \frac{\sigma A}{\rho \dot{A}_w} k^2 < 0 \quad (2)$$

Where:

$$c_v = \frac{\left( \frac{\partial F}{\partial R_L} \right)_{U_o, U_w}}{\left( \frac{\partial F}{\partial U_{os}} \right)_{h, U_w} - \left( \frac{\partial F}{\partial U_{Ls}} \right)_{h, U_o}}$$

$$c_{IV} = \frac{\rho_w V_w R_o + \rho_o V_o R_w}{\rho_w R_o + \rho_o R_w}$$

$K$  is the wave number ( $K \geq 0$ ) used to symbolize the waves length ( $k = 0$  for long waves),  $V_o$  is the actual velocity of oil in the pipe,  $U_o$  is the superficial velocity of the oil,  $Ro = \frac{A_o}{A}$ ,  $\sigma$  is the interfacial tension,  $\dot{A}_w = [1 - (2h - 1)^2]^{0.5}$ ,  $h$  is the water holdup,  $A$  is the cross sectional pipe area,  $\rho = \frac{\rho_o}{R_o} + \frac{\rho_w}{R_w}$ , and  $\left( \frac{\partial F}{\partial R_w} \right)_{U_{os}, U_{ws}}$  is the derivative of  $F$  with respect to  $R_w$  at constant  $U_o$ , and  $U_w$ .

Another term was added to equation (2) by Trallero [15] used in the IKH analysis:

$$\frac{\rho_f(V_w - V_o)^2 C_s A}{\rho} \left[ \frac{1}{A_w} - \frac{1}{A_o} \right] \quad (3)$$

Where  $C_s$  is the sheltering effect,  $\rho_f$  represents  $\rho_o$  if oil is faster and  $\rho_w$  if water is faster.

The last three terms of equation (2) represents the inviscid stability criteria, where no effects of viscous forces appear. While the viscous stability criteria uses the four terms. The IKH bring in two transition lines, one with oil faster than water, and the other with water faster than oil. The VKH analyses show the transition boundary between stable and unstable wavy interface, which represents the transition from smooth stratified (ST) into stratified with mixing at the interface (ST&MI). The boundaries of the IKH and the VKH analysis can be seen in Figure 2-1.

Equation (2) can be solved numerically. Numerical solution allows using complex friction factor correlations in finding the transition criteria for rough pipes. Additional details about the solution steps and derivations can be found in Trallero [15].

Brauner [13] and [14] followed the same approach and introduced a model for predicting the stratified flow using the VKH and the IKH analysis. The IKH analysis produces two lines called the “zero real characteristics” (ZRC) lines, one with oil is faster than water and the other when water is faster. These lines represent the transition from stratified to non-stratified flow pattern. The VKH analysis produces the “zero neutral stability” (ZNS) line, which represents the smooth stratified flow region. The boundaries of the IKH and the VKH analyses are shown in Figure 2-1.

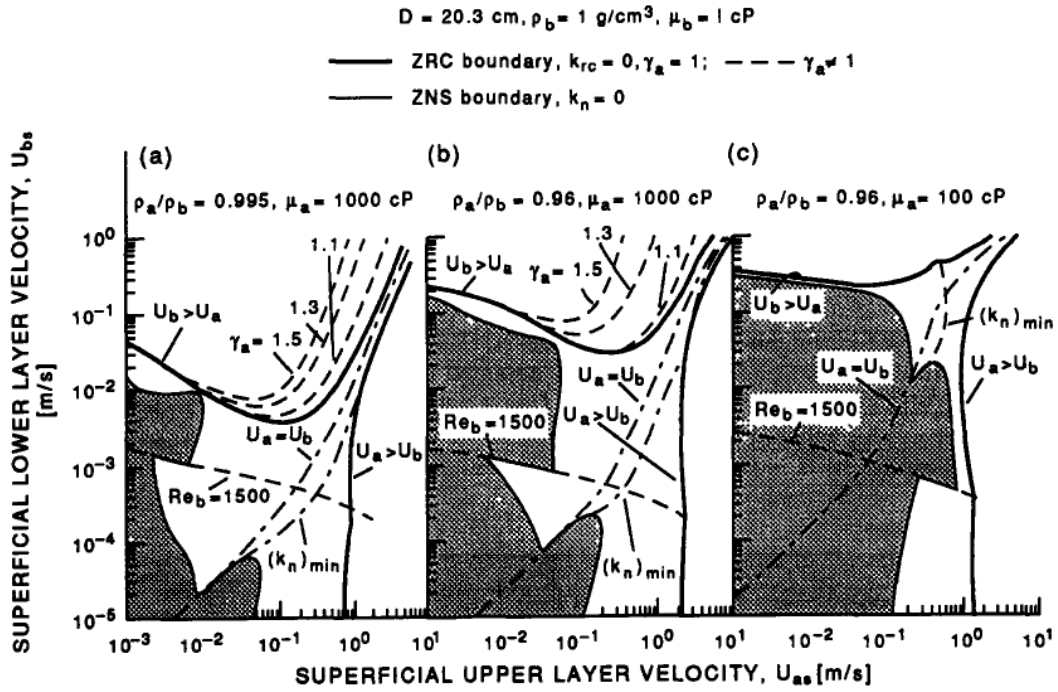


Figure 2-1: The effect of the density differential and the viscosity ratio on the locations of the ZNS and ZRC boundaries [Brauner [13]].

Looking at Figure 2-1, when the density difference between the two phases is reduced, the velocity needed to leave the stratified region is increased. Therefore, the stratified region is enlarged. As for viscosity, increasing the viscosity difference between the two liquids reduces the velocity needed to leave the stratified region. Therefore, the stratified region is reduced.

### **2.1.2.3 Prediction of Dispersed Flow**

Dispersed flow is located at higher oil or water velocities than the stratified flow for oil faster than water and for water faster than oil, where the dispersed phase flows not in a continuous layer but as drops or slugs in the continuous phase. Brauner [13] demonstrated the criteria of transition from an upper layer of oil drops into two continuous layers of liquids. The dispersed region comes between the stratified smooth and the “zero real characteristics” line as in Figure 2-2. In addition, a model was proposed for predicting the fully depressed flow pattern and oil slugs using Hinze [34] model of liquid-liquid dispersion for finding the maximum diameter of oil drops. The transition to fully depressed flow occurs if the velocity of the dispersed phase is much smaller than the velocity of the continuous phase with maximum oil drops diameter less than oil critical diameter. However, when the velocity difference is not large enough, oil slugs might be seen.

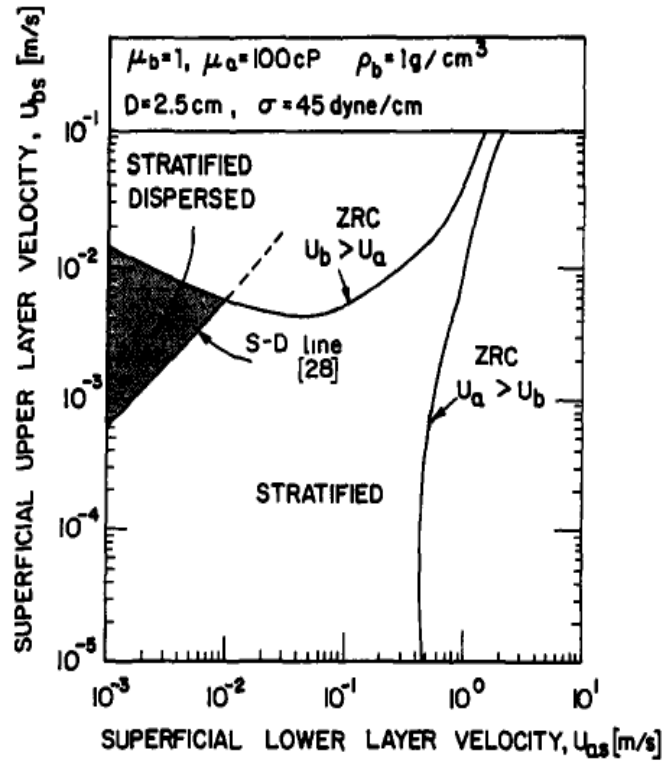


Figure 2-2: stratified-dispersed region [Brauner [13]].

In the model, assuming oil will be dispersed; oil drops will stay dispersed and will not convert to a continuous layer when the viscous and inertia forces are insufficient to cause coalescence, which can be seen at very low oil velocity. When oil drops maintain their shape the surface tension forces of the drops overcome the buoyancy forces due to weight difference, where buoyancy keeps these drops at the top of the pipe. From using the above balance, the critical diameter was introduced.

$$d_{cr} = \left[ \frac{6\sigma}{(p_w - p_o)} g \right]^{0.5} \quad (4)$$

The transition occurs when the upper layer height is smaller than the critical diameter, which occurs at very low oil velocity compared with the high velocity of water, meaning

that drops with diameter larger than the critical diameter will form a continuous layer of oil. Dispersion happens when the upper layer height is small ( $d - H \ll d_{cr}$ ) as proposed by Brauner [13], where  $d$  is pipe diameter and  $H$  is water high inside the pipe. When ( $d - H \ll d_{cr}$ ), no enough space to form drops with diameter larger than the critical diameter, and so the flow is stratified-dispersed. But when the height is large enough ( $d - H \gg d_{cr}$ ), the available upper space will allow the formation of drops with diameter lager than the critical diameter, and thus a continuous layer from the drops might form. From the critical diameter, the transition based on the critical area is:

$$A_o \ll A_{cr} \tag{5}$$

$$A_{cr} = \frac{\pi d_{cr}^2}{4}$$

Where  $A_o$  is the area of oil. If the density difference between oil and water is reduced or surface tension is increased, the dispersed flow region is extended to cover more area on the flow pattern map curve.

The fully-dispersed flow pattern is achieved at high water velocities with low oil velocities. Using Hinze [34] model for liquid-liquid dispersion, the maximum dispersed phase diameter is given to be:

$$d_m = C_1 h_d l_d^{-\frac{5}{2}} \left( \frac{\sigma}{\rho_b} \right)^{\frac{3}{5}} \tag{6}$$

$$l_d = \frac{2fU_m^3}{d}$$

$$f = 0.046 \left( \frac{dU_m \rho_b}{\mu_b} \right)$$

Where  $h_d$  is the dispersed phase no-slip holdup,  $U_m$  is the mixture velocity which equals the sum of the superficial velocities of the two liquids, and  $C_1$  is a constant which depends on the in situ hold-up and is to be determined experimentally. Hinze [34] had  $C_1 = 0.725$  in a Couette flow field.

When  $\frac{d_m}{d_{cr}}$  is smaller than one, or if  $d_m$  is smaller than  $d_{cr}$ , transition to fully depressed might occur if the velocity of the dispersed phase is much smaller than the continuous phase. However, if  $\frac{d_m}{d_{cr}} < 1$  and  $\frac{U_a}{U_b}$  is almost one, then oil slugs might be seen (Brauner [13]).

Trallero [15] proposed a model of predicting the dispersion flow pattern which includes gravity and turbulent fluctuation forces, along with the Hinze [34] and Levich [35] models of drop sizes prediction in dispersed flow, taking into account the dispersed phase concentration and water holdup. The proposed model included numerical parameters which were found experimentally. The proposed model and the experimental work are shown in Figure 2-3 below:



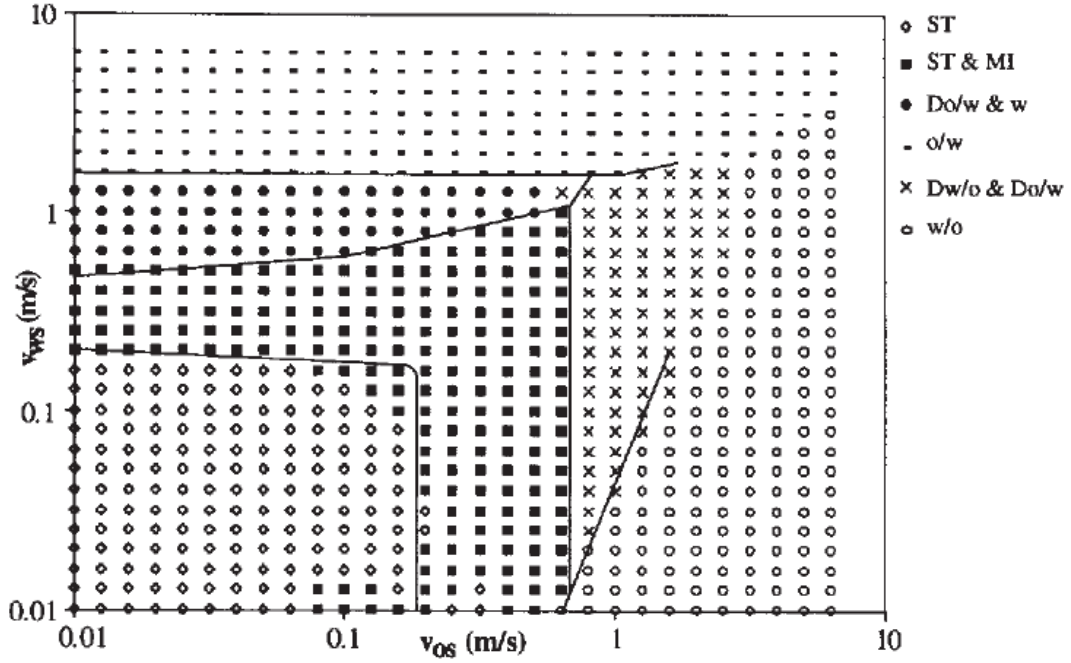


Figure 2-3: Comparison of the theoretical flow pattern map (points) with the experimental flow pattern map (lines) [Trallero[10]]

Brauner [36] proposed a unified model for predicting phase dispersion using different mechanisms and models of dispersion to cover all ranges and all kinds of dispersion. The model predicts the transitions to dispersed flow patterns in a variety of gas–liquid and liquid–liquid systems. Eötvös number was used to determine the applicability of these models. The models includes Hinze [34] and Kolmogorov [37] model which considers dilute dispersion with extension to cover dense dispersion, Barnea [38] method of finding drops critical diameter, and Brodkey [39] maximum droplet diameter above which drops are deformed.

The suggested model predicts the phase dispersion when turbulence forces of the continuous phase are strong enough to break the dispersed phase into droplets smaller

than the critical diameter ( $d_{\text{crit}}$ ). Dispersion happens when drops of the dispersed phase have smaller diameter than the critical diameter.

$$d_{\text{max}} \leq d_{\text{crit}} \quad (7)$$

Where  $d_{\text{max}}$  is the maximum droplet diameter of the dispersed phase inside the pipe.  $d_{\text{max}}$  is found by taking the greater value of Hinze [34] and Kolmogorov [37] models for dilute dispersion, with an extended Hinze's [34] and Kolmogorov [37] model for dense dispersion.

$$d_{\text{max}} = \max\{(d_{\text{max}})_o, (d_{\text{max}})_e\} \quad (8)$$

Where  $(d_{\text{max}})_o$  is the maximal drop size diameter in a dilute dispersion, and  $(d_{\text{max}})_e$  is the maximal drop size in a dense dispersion.  $\left(\frac{d_{\text{max}}}{D}\right)_o$  (the nondimensionalized form of the  $(d_{\text{max}})_o$ ) is found using Hinze's [34] and Kolmogorov [37] model. As mentioned earlier, their models are established based on the continuous phase buoyancy force which tends to break the dispersed phase into drops, and the surface tension force which tends to form a continuous layer of the phase.

$$\left(\frac{d_{\text{max}}}{D}\right)_o = 0.55 \left(\frac{\rho_c U_c^2 d}{\sigma}\right)^{-0.6} \left[\frac{\rho_c (1-h_d)}{f \rho_m}\right]^{0.4} \quad (9)$$

Where the subscript  $c$  stands for the continuous phase,  $m$  for the mixture.  $\sigma$  is the surface tension between the two liquids,  $h_d$  is the holdup of the dispersed phase, and  $f$  is the friction factor.

$\left(\frac{d_{\text{max}}}{D}\right)_e$  is found from the extended Hinze's [34] and Kolmogorov [37] model. The extended model takes into account the coalescence between drops which happens in

dense dispersion. This means that more turbulence in the continuous phase is needed to prevent the coalescence and to disperse other phase. The resulted model is shown below:

$$\left(\frac{d_{\max}}{D}\right)_e = 2.22 C_H^{3/5} \left(\frac{\rho_c U_c^2 d}{\sigma}\right)^{-0.6} \left[\frac{\rho_c (1-h_d)}{f \rho_m}\right]^{0.4} \left(\frac{h_d}{1-h_d}\right)^{0.6} \quad (10)$$

Where:  $C_H$  is a constant found experimentally. For friction factor  $f = 0.046/Re^{0.2}$ , we have:

$$\left(\frac{d_{\max}}{D}\right)_o = 1.88 \left[\frac{\rho_c (1-h_d)}{\rho_m}\right]^{0.4} We_c^{-0.6} Re_c^{0.08} \quad (11)$$

$$\left(\frac{d_{\max}}{D}\right)_e = 7.61 C_H^{3/5} We_c^{-0.6} Re_c^{0.08} \left(\frac{h_d}{1-h_d}\right)^{0.6} \left[1 + \frac{\rho_d}{\rho_c} \frac{h_d}{1-h_d}\right]^{-0.4} \quad (12)$$

$$We_c = \rho_c U_c^2 d / \sigma, \quad Re_c = \rho_c U_c d / \mu_c$$

The critical drop size  $d_{crit}$  is found using Barnea [38] technique:

$$\frac{d_{crit}}{D} = \min\left(\frac{d_{c\sigma}}{D}, \frac{d_{cb}}{D}\right) \quad (13)$$

Where  $d_{c\sigma}$  is the maximal size of drop diameter above which drops are deformed and thereby enhancing coalescence. It can be found using Brodkey [39] model as below:

$$d_{c\sigma} = \frac{0.224}{(\cos \beta)^{0.5} Eo_D^{0.5}} \quad (14)$$

$$Eo_D = \frac{\Delta \rho g d^2}{8\sigma} \quad \check{\beta} = \begin{cases} |\beta| & |\beta| < 45^\circ \\ 90 - |\beta| & |\beta| > 45^\circ \end{cases}$$

$Eo_D$  is the Eötvös number.  $d_{cb}$  is the maximal size of drop diameter above which the buoyant forces will cause the dispersed phase drops to move towards the tube walls:

$$\tilde{d}_{cb} = \frac{3}{8} f \frac{\rho_c}{\Delta \rho g} * \frac{U_c^2}{d g \cos \beta} \quad (15)$$

Where  $\beta$  is the inclination angle of the pipe (positive for downward inclination).

This model was called the H-model, the transition boundaries of this model is shown in Figure 2-4 below. The limitation of this models is that the flow should be turbulent, and in the range  $1.8 Re_c^{-7} < d_{max} = d_{crit} < 0.1$ . And with  $d_{crit} = d_{c\sigma}$ ,  $Eo_D < 1.5 \times 10^{-2} Re_c^{1.4}$ .

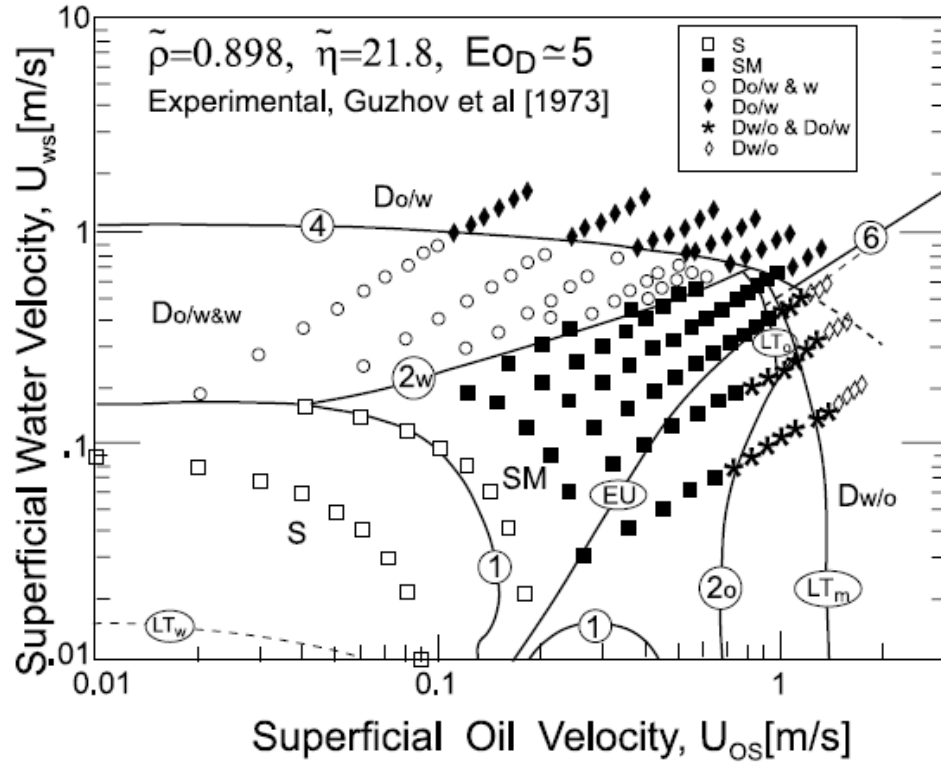


Figure 2-4: The H-model predictions for transition to DO/W (boundary 4,  $C_H=0.5$ ) and transition to DW/O (boundary 5) in horizontal oil–water system of  $Eo_D=5$ , with experimental data of Guzhov [40] [Brauner [36]].

In Figure 2-4, Boundary 4 and 5 were found from the H-model, they represent the transition to the dispersion flow pattern, the H-model uses equation (7) to determine the transition criteria. 1 is the neutral stability boundary for smooth stratified flow. 2w and 2o represents the upper boundary of stratified flow. Line 6 represents the inversion line which is found by Arirachakaran [9] as will be seen in section 2.2.1.2. EU is the equal velocity of fluids line in stratified layers. And LTo is the laminar/turbulent transition in the oil layer.

2w and 2o boundaries represent the transition criteria to dispersion of water in oil over an oil layer and to dispersion of oil in water over a water layer respectively. A transition criterion was found in Brauner [41] to describe this semi dispersed flow. The transition criteria is the same for the H-model, where equation (7) is used. However this model is only used when water is the continuous phase, the flow is turbulent, and for shallow inclinations, while for  $\frac{\Delta\rho}{\rho_c} \ll 1$ ,  $d_{cb} > d_{co}$ ,  $d_{crit} = d_{co}$  the following model is used Brauner [42]:

$$\Delta U_c = U_w - U_o \geq 4.36 \left[ \frac{\sigma \Delta \rho g \cos \beta}{\rho_c^2} \right]^{1/4} \{1 + 1.443(N_{vd} \cos \beta)^{0.4}\}^{1/2} \quad (16)$$

$$N_{vd} = \frac{\mu_d^4 \Delta \rho g}{\rho_d^2 \sigma^3}$$

The subscript d denotes to the dispersed phase, and c to the continuous phase. The 4.36 value could be modified to fit the experimental data. However, for  $Eo_D \approx 1$ , the transition criterion uses Brauner [13] models previously discussed:

$$A_d \cos \beta \ll \frac{\pi d_{cr}^2}{4} \quad (17)$$

Where  $d_{cr}$  is found from equation (4). When finding 2w boundary, the dispersed phase is oil and the continuous phase is water. While in finding 2o boundary, the opposite is applied.

Another model of predicting the transition to dispersed flow was presented by Torres [43], first the maximum droplet size needs to be found from:

$$d_{\max} = \max\{(d_{\max})_o, (d_{\max})_a\} \quad (18)$$

Where  $(d_{\max})_o$  is the maximal drop size diameter in a dilute dispersion, and  $(d_{\max})_a$  is the maximal drop size in a dense dispersion.  $(d_{\max})_o$  was found using Hinze's [34] and Kolmogorov [37] model to be:

$$\left(\frac{d_{\max}}{D}\right)_o = 0.549 \left(\frac{\rho_m U_m^2 d}{\sigma}\right)^{-0.6} f_m^{-0.4} \quad (19)$$

$$f_m = C \left(\frac{\rho_m U_m d}{\mu_c}\right)^{-n}$$

$$\rho_m = \rho_o h_o + \rho_w (1 - h_o)$$

Where  $\rho_m$  is the mixture density,  $c$  and  $n$  are equal to 0.046 and 0.2 respectively.

$\left(\frac{d_{\max}}{D}\right)_a$  was found using Hinze's [34] and Kolmogorov [37] model and Chen [44] model as below:

$$\left(\frac{d_{\max}}{D}\right)_a = 2.221 \left(\frac{\rho_m U_m^2 d}{\sigma}\right)^{-0.6} f_m^{-0.4} \left(\frac{h_d}{1-h_d}\right)^{0.6} \quad (20)$$

After finding the maximum droplet diameter, the transition to Semi-Dispersed flow is found by:

$$d_{\max} \leq d_{\text{CD}} \quad (21)$$

$d_{\text{CD}}$  can be found using Brodkey [39] model as below:

$$\tilde{d}_{\text{CD}} = \frac{1.265}{(\cos \beta)^{0.5} \text{Eo}_D^{0.5}} \quad (22)$$

$$\text{Eo}_D = \frac{\Delta \rho g d^2}{\sigma}$$

Where  $\text{Eo}_D$  is the Eötvös number. The transition to fully-dispersed flow is found by:

$$d_{\max} \leq d_{\text{CB}} \quad (23)$$

$d_{\text{cb}}$  is the maximal size of drop diameter above which the buoyant forces will cause the dispersed phase drops to move towards the tube walls:

$$\tilde{d}_{\text{cb}} = \frac{3}{8} f_c \frac{\rho_c}{\Delta \rho} * \frac{U_c^2}{g \cos \beta} \quad (24)$$

Where  $\beta$  is the inclination angle of the pipe (positive for downward inclination).  $f_c$  is the friction factor of the continuous phase.

## 2.2 Pressure Drop

Two models are presented for pressure drop calculations, one for stratified flow, and the other for dispersed flow.

### 2.2.1 Pressure Drop in Dispersion Flow

In dispersed flow, where the dispersed phase travels as drops in the continuous phase, two liquids are in contact with the pipe wall, one of them transfers as drops. For a given oil-water flow, the oil-water pressure drop for fully developed dispersed flow with neglecting the acceleration gradient is found by the following relation:

$$\left(\frac{dp}{dL}\right)_{TP} = \left(\frac{dp}{dl}\right)_g + \left(\frac{dp}{dl}\right)_f \quad (25)$$

Where the two phase pressure gradient  $\left(\frac{dp}{dL}\right)_{TP}$  equals to the sum of gravitational pressure losses  $\left(\frac{dp}{dl}\right)_g$  plus the frictional pressure losses  $\left(\frac{dp}{dl}\right)_f$ , the above equation can be written as:

$$\left(\frac{dp}{dL}\right)_{TP} = \rho_m * g * \sin(\beta) + 2 \frac{f * \rho_m * U_m^2}{d} \quad (26)$$

Where  $\rho_m$  is the mixture (oil-water) density,  $g$  is the gravitational acceleration,  $\beta$  is the angle of inclination,  $U_m$  is the mixture superficial velocity which is equal to the sum of the oil and water superficial velocities,  $U_m = U_{sw} + U_{so}$ ,  $f$  is the friction factor, and  $d$  is the pipe diameter.



The mixture density ( $\rho_m$ ) can be found from the actual oil holdup,  $h_o$ . The actual oil holdup should be found from the experiment by any method, or it is considered to equal the oil fraction (no-slip holdup) as considering no slip happens between the dispersed and the continuous phase. The mixture density in terms of the oil holdup is:

$$\rho_m = h_o \rho_o + (1 - h_o) \rho_w \quad (27)$$

Where  $\rho_o$ ,  $\rho_w$  are the oil and water densities respectively. The friction factor, for homogenous models can be obtained from the following correlation:

$$f = C \cdot Re^{-n} \quad (28)$$

Where  $C$ , and  $n$  are constants that depends on the flow type whether it is laminar or turbulent,  $C=16$ ,  $n=1$  for laminar, and  $C=.079$ ,  $n=0.25$  for turbulent. The Reynolds number  $Re = \frac{\rho_m \cdot d \cdot U_m}{\mu_m}$ , is a function of the mixture velocity, mixture density, and mixture viscosity.

The next step which is need in the pressure drop calculations is the value of the mixture viscosity. Many researchers introduced models for predicting the accurate mixture viscosity value for different oil-water flow rate ratios, some of them will be considered and compared in the next section.

### 2.2.1.1 Mixture Viscosity

The mixture viscosity for two phases flowing inside a pipe represents the viscosity as considering a single phase flowing inside that pipe. Different correlations were proposed to find the mixture viscosity due to its complex behavior while changing phase's ratio.

The simplest model in finding the mixture viscosity is the simple average used in the homogenous model as:

$$\mu_m = h_o\mu_o + (1 - h_o)\mu_w \quad (29)$$

This model gives high error in many cases compared with other models, but still it is commonly used due to its simplicity and validity for some cases.

Prediction goes back to Einstein [45] in 1911 who proposed a viscosity model for an infinitely dilute suspension of small solid spheres as follows:

$$\frac{\mu_m}{\mu_c} = 1 + 2.5h_d \quad (30)$$

Where  $\mu_m$  is the mixture viscosity, and  $\mu_c$  is the continuous phase viscosity,  $h_d$  is the dispersed phase holdup. The equation is linear, and the model can't be used for non-spherical particles at high concentrations and for particle size distributions.

Taylor [46] in 1932 modified Einstein's equation to be used in fluid dispersions. He assumed that the tangential stresses on the drop surface cause the internal circulation in the drops. He also assumed spherical drops and infinite dilution.

$$\frac{\mu_m}{\mu_c} = 1 + 2.5 h_d \left( \frac{0.4 + \mu_d/\mu_c}{1 + \mu_d/\mu_c} \right) \quad (31)$$

Where:  $\mu_d$  is the dispersed phase viscosity. Mooney [47] in 1951 extended Einstein's viscosity equation of infinite dilute suspension of spheres and to be used in the suspension of finite concentration.

$$\frac{\mu_m}{\mu_c} = \exp\left(\frac{2.5.h_d}{1-k.h_d}\right) \quad (32)$$

Where:  $k$  is the self-crowding factor ranges from  $1.35 < k < 1.91$  ( $k=1.43$  was used in his paper), Brinkman [48] in 1952 used a simple method for the estimation of the mixture viscosity by using Einstein's [45] model, the result was:

$$\frac{\mu_m}{\mu_c} = (1-h_d)^{-2.5} \quad (33)$$

Same equation was found by Roscoe [49] in 1952, Roscoe showed the effect of size distribution of the suspended spheres on the relative viscosity, Roscoe represented the model using Einstein [45] model of the extreme dilution with the effect of adding particles of small size to a solution.

$$\frac{\mu_m}{\mu_c} = \exp\left(\frac{2.5.h_d}{1-k.h_d}\right) \quad (34)$$

Krieger and Dougherty [50] in 1959 modified Brinkman's equation using Mooney's [47] crowding factor concept:

$$\frac{\mu_m}{\mu_c} = \left(1 - \frac{h_d}{h_{d,max}}\right)^{c.h_{d,max}} \quad (35)$$

Where:  $c = -2.5$ . Furuse [51] in 1972 modified Einstein's model by considering the hydrodynamic effects of neighboring particles:

$$\frac{\mu_m}{\mu_c} = \frac{1 + 0.5h_d}{(1 - h_d)^2} \quad (36)$$

Yaron and Gal-Or [52] in 1972, represented the cell model in which a certain number of drops are confined within a representative cell to achieve a phase fraction that resembles the concentration in the bulk surrounding the cell.

$$\frac{\mu_m}{\mu_c} = 1 + 5.5h_d \left\{ \frac{4h_d^{7/3} + 10 - \left(\frac{84}{11}\right)h_d^{2/3} + (4/K)(1 - h_d^{7/3})}{10(1 - h_d^{10/3}) - 25h_d(1 - h_d^{4/3}) + (10/K)(1 - h_d)(1 - h_d^{7/3})} \right\} \quad (37)$$

Choi and Schowalter [53] in 1975 represented another cell model for finite concentration of the dispersed phase. They studied the effect of shear on drops shape with the influence of neighboring drops.

$$\frac{\mu_m}{\mu_c} = 1 + h_d \left\{ \frac{2(5K+2) - 5(5K-1)h_d^{7/3}}{4(K+1) - 5(5K+2)h_d + 42Kh_d^{5/3} - 5(5K-2)h_d^{7/3} + 4(K-1)h_d^{10/3}} \right\} \quad (38)$$

Where:  $K$  is a constant. Pal and Rhodes [54] developed the following relationship in 1989:

$$\frac{\mu_m}{\mu_c} = \left[ 1 + \frac{0.9415h_d/h_{d,\mu=100}}{1 - 0.9415h_d/h_{d,\mu=100}} \right]^{2.5} \quad (39)$$

Where:  $\mu = \mu_m/\mu_c$ . Phan & Pham [55] in 1997 modeled the suspensions of rigid particles and droplets and of particulate solids consisting of several elastic phases, yielding to expressions of the effective properties, by using the idea of constructing the composite material from an initial material with a series of additions of the compounds

materials until the final volume fractions was reached. At each addition, the effective properties of the composite was found, and then considered as the base properties of the next incremental step. The two phase formula of Suspensions of droplets was:

$$h_d = 1 - \left[ \frac{\mu_c}{\mu_m} \right]^{\frac{2}{5}} \left[ \frac{2\mu_c + 5\mu_d}{2\mu_m + 5\mu_d} \right]^{\frac{3}{5}} \quad (40)$$

$$\left[ \frac{\mu_m}{\mu_c} \right]^{\frac{2}{5}} \left[ \frac{2\eta + 5k}{2 + 5k} \right]^{\frac{3}{5}} = (1 - h_d)^{-1} \quad (41)$$

$$\eta = \frac{\mu_m}{\mu_c}, k = \frac{\mu_d}{\mu_c}$$

Pal [56] derived models for concentrated emulsions of spherical droplets using Taylor [46] model and using the concept of effective medium:

$$\left( \frac{\mu_m}{\mu_c} \right) \left[ \frac{2\left(\frac{\mu_m}{\mu_c}\right) + 5\left(\frac{\mu_d}{\mu_c}\right)}{2 + 5\left(\frac{\mu_d}{\mu_c}\right)} \right]^{1.5} = \exp\left(\frac{2.5h_d}{1 - h_d/h_{d,max}}\right) \quad (42)$$

$$\left( \frac{\mu_m}{\mu_c} \right) \left[ \frac{2\left(\frac{\mu_m}{\mu_c}\right) + 5\left(\frac{\mu_d}{\mu_c}\right)}{2 + 5\left(\frac{\mu_d}{\mu_c}\right)} \right]^{1.5} = \left[ 1 - \frac{h_d}{h_{d,max}} \right]^{-2.5h_{d,max}} \quad (43)$$

Pal [57] in 2001 studied liquid-liquid emulsions, a new equation in this field was proposed. One model was proposed based on single parameter Viscosity-Concentration, where the droplet size was not considered. The model uses Taylor [46] equation, by considering the addition of new particles  $dh_d$  will increase  $\eta$  by  $d\eta$  will make a new homogenous model of viscosity  $\eta$ . applying this assumption in Taylor equation will give:

$$\left( \frac{\mu_m}{\mu_c} \right) \left[ \frac{2\left(\frac{\mu_m}{\mu_c}\right) + 5\left(\frac{\mu_d}{\mu_c}\right)}{2 + 5\left(\frac{\mu_d}{\mu_c}\right)} \right]^{1.5} = \exp(2.5h_d) \quad (44)$$

Other models were proposed by Pal [57] that considers the droplet size and droplet size distribution and the divergence of viscosity:

$$\left(\frac{\mu_m}{\mu_c}\right) \left[ \frac{2\left(\frac{\mu_m}{\mu_c}\right) + 5\left(\frac{\mu_d}{\mu_c}\right)}{2 + 5\left(\frac{\mu_d}{\mu_c}\right)} \right]^{1.5} = \frac{9}{8} \left[ \frac{(h_d/h_{d,max})^{\frac{1}{3}}}{1 - (h_d/h_{d,max})^{\frac{1}{3}}} \right] \quad (45)$$

The dispersed phase and the continuous phase are determined by the location of inversion point. A literature on finding inversion point location is given in the next section.

### 2.2.1.2 Inversion Point

Inversion happens when the continuous phase becomes the dispersed one. This phenomenon can only be seen in liquid-liquid flow. The pressure drop at inversion is noticed to change rapidly and might generate a peak, where in many cases, the maximum or the minimum pressure value is found at the inversion point.

Several experimental works were performed to investigate the phase inversion phenomena and the parameter which influences its location. The main factors which affect the inversion point and can be seen in almost every model are the fluid properties where viscosity has a great effect, other models include the pipe diameter and flow type, turbulent or laminar.

Arirachakaran et al. [9] suggested a method to predict inversion point by means of oil and water viscosity of as below:

$$\epsilon_o = 0.5 + 0.1108 \log \left( \frac{\mu_o}{\mu_w} \right) \quad (46)$$

Where  $\epsilon_o$  is the critical oil holdup at which inversion happens,  $\mu_o$  is the oil viscosity and  $\mu_w$  is the water viscosity. The model was derived based on large numbers of experimental data. Yeh et al [58] suggested the following model:

$$\epsilon_o = \frac{\left( \frac{\mu_o}{\mu_w} \right)^{0.5}}{1 + \left( \frac{\mu_o}{\mu_w} \right)^{0.5}} \quad (47)$$

Nädler and Mewes [11] proposed the following correlation:

$$\epsilon_o = 1 - \frac{1}{1 + k1 \left( \frac{c_o \rho_o^{(1-n_o)} \mu_o^{n_o}}{c_w \rho_w^{(1-n_w)} \mu_w^{n_w}} (d U_M)^{(n_w - n_o)} \right)^{\frac{1}{k2}}} \quad (48)$$

Where  $c_o$ ,  $c_w$ ,  $n_o$ ,  $n_w$  are the Blasius friction factor constants that depend on flow type (laminar or turbulent) for water and oil respectively,  $d$  is the pipe diameter,  $K1$  and  $K2$  are constants ( $=1$ , and  $2$  respectively),  $\rho_o$  and  $\rho_w$  are the density of oil and water respectively, and  $U_m$  is the mixture velocity. The model takes into account the mixture velocity, liquids viscosity, liquids density, flow type (laminar or turbulent), and pipe geometry. The correlation was suggested based on zero shear stress.

Brauner and Ullman [59] proposed the following correlation:

$$\epsilon_o = \frac{\left( \frac{\rho_o}{\rho_w} \right) \left( \frac{\mu_o}{\mu_w} \right)^{0.4}}{1 + \left( \frac{\rho_o}{\rho_w} \right) \left( \frac{\mu_o}{\mu_w} \right)^{0.4}} \quad (49)$$

Poesio and Beretta [60] suggested the following:

$$\epsilon_o = \frac{1 - \left(\frac{\mu_o}{\mu_w}\right)^{-2/5k} + k \left(\frac{\mu_o}{\mu_w}\right)^{-2/5k}}{1 + \left(\frac{\mu_o}{\mu_w}\right)^{-2/5k}} \quad (50)$$

Where  $(1/k)$  is the maximum packing factor and was suggested by Yeh et al. [58] to be 0.74.

Several mixture viscosity models are plotted together in Figure 2-5 to illustrate the differences in these models and to show the expected pressure drop profile for a given oil-water flow.

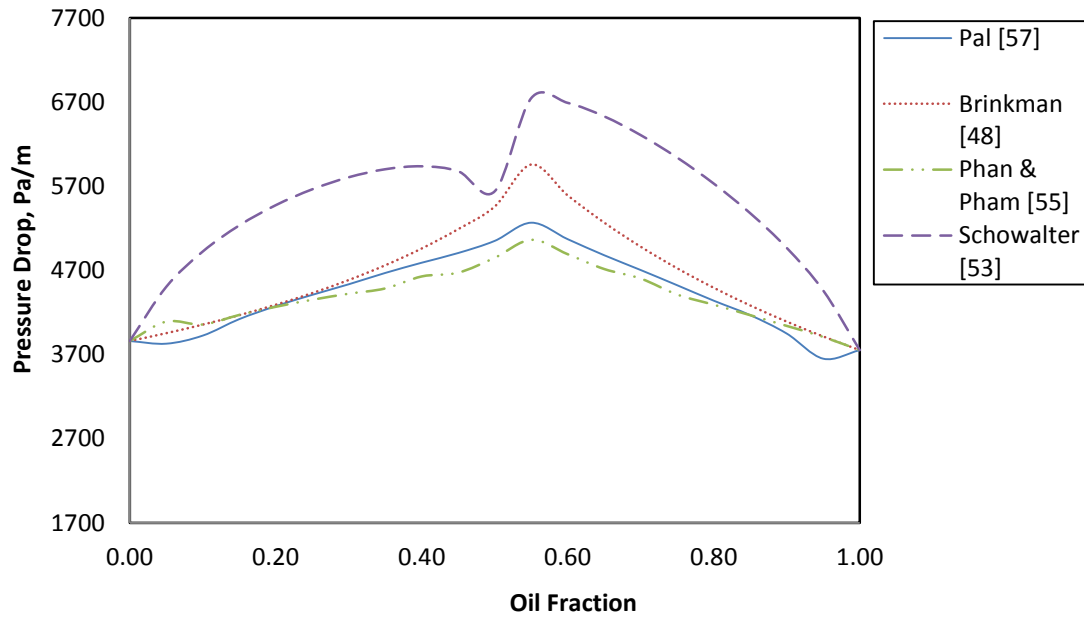


Figure 2-5: The calculated pressure drop using Pal [57], Phan & Pham [55], Brinkman [48], and Schowalter [53] models of mixture viscosity, where inversion point was found by Arirachakaran et al. [9]  $\nu_o = 1.85$  cP,  $\rho_o = 780$  kg/m<sup>3</sup>,  $U_m = 2$  m/s, and  $d = 22.5$  cm.



## 2.2.2 Pressure Drop in Stratified Flow

The Two Fluid Model (TFM) is used to find the pressure drop in stratified flow. A schematic diagram of the stratified flow is shown in Figure 2-6.

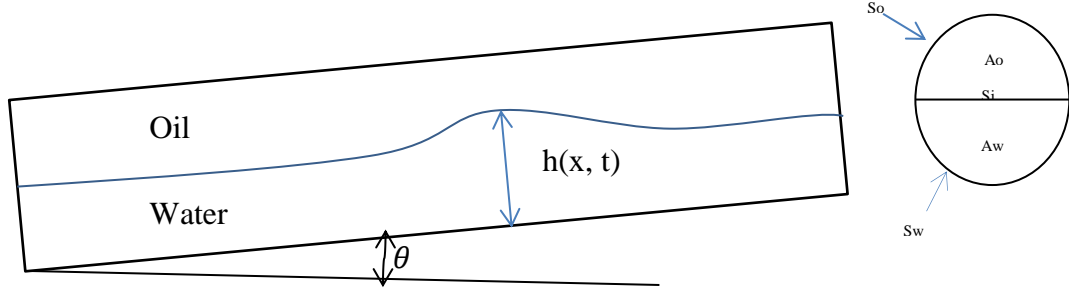


Figure 2-6: Schematic diagram of the stratified flow

The model uses the oil and water momentum equation

$$A_o \left( \frac{dP}{dx} \right) - \tau_o S_o - \tau_i S_i - \rho_o A_o g \sin \theta = 0 \quad (51)$$

$$A_w \left( \frac{dP}{dx} \right) - \tau_w S_w + \tau_i S_i - \rho_w A_w g \sin \theta = 0 \quad (52)$$

Eliminating the pressure drop from these equation gives

$$-\frac{\tau_w S_w}{A_w} + \frac{\tau_o S_o}{A_o} + \tau_i S_i \left( \frac{1}{A_w} + \frac{1}{A_o} \right) - (\rho_w - \rho_o) g \sin(\beta) = 0 \quad (53)$$

The actual holdup can be found from equation (53), and then the pressure drop can be calculated from either equation (51) or equation (52).

Where:

$$\tau_w = f_w \rho_w \frac{U_w^2}{2}$$

$$\tau_o = f_o \rho_o \frac{U_o^2}{2}$$

$$\tau_i = f_o \rho_o \frac{(U_o - U_w)^2}{2} \quad \text{If} \quad U_o > U_w$$

$$\tau_i = -f_w \rho_w \frac{(U_o - U_w)^2}{2} \quad \text{If} \quad U_w > U_o$$

$$f_w = c \left( \frac{D_w U_w \rho_w}{\mu_w} \right)^{-n}$$

$$f_o = c \left( \frac{D_o U_o \rho_o}{\mu_o} \right)^{-n}$$

$$D_w = \frac{4A_w}{(S_i + S_w)}, D_o = \frac{4A_o}{S_o} \quad \text{if} \quad U_w > U_o$$

$$D_o = \frac{4A_o}{(S_i + S_o)}, D_w = \frac{4A_w}{S_w} \quad \text{if} \quad U_o > U_w$$

The pipe perimeters and areas are shown in Figure 2-6 above.

## **CHAPTER 3**

### **EXPERIMENTAL SETUP & PROCEDURE**

The multiphase experimental setup and procedure along with the properties of the used oil are presented in this chapter. Experimental setup includes the test section, and instrumentations.

#### **3.1 Multiphase Flow Facility**

The conducted oil-water experiments were performed in the “Research Institute” building at the King Fahd University of Petroleum and Minerals. The multiphase flow setup was constructed for two and three phase flow experiments. The setup is shown in Figure 3-1. It consists of two tanks for oil and water, two pumps for each fluid, test section, two separation tanks that are attached at the end of the test tube, a return pump close to the separation tanks, and an air compressor. The used tanks have a 1.25 m inner diameter, and a 1.6 m height, and the used pumps have a 3.5 hp capacity. The pumps can deliver oil or water with a maximum velocity of 3 m/s. Also, they can deliver oil and water together with a 3 m/s mixture velocity. A Y-shaped mixing section shown in Figure 3-2 joins the oil and water pipes to the test section which has a 2.25 cm diameter. The pipes are made of PVC. The last section of the pipe was made of a transparent Plexiglas for visual

observation. The velocity range of the conducted experiments was from 0.05 m/s to 3 m/s.

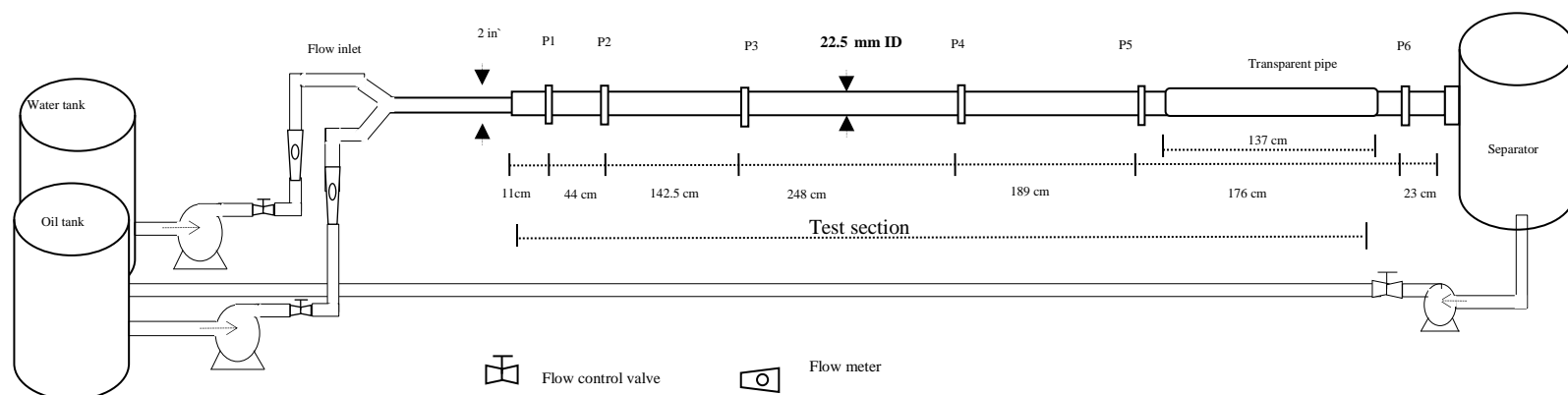


**Figure 3-1: Schematic Representation of the Experimental Setup**

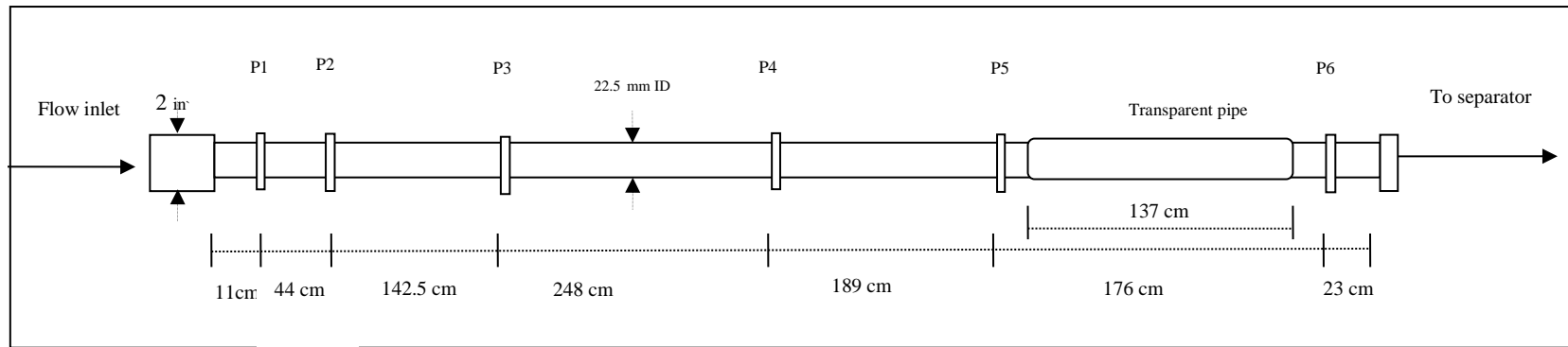


Figure 3-2: Oil-water mixing section

### 3.2 Test section

The test section is shown in Figure3-3. The pipe is made of PVC with ASTM D-1785 standard number and a 2.25 cm inner diameter. The pipe was installed horizontally. It contains two sections, one section is a PVC pipe, used for pressure readings, and the other is transparent made of Plexiglas for visual observation, which is used for flow pattern observation. The total length of the test section is 8 meters as can be seen in Figure3-3. Pressure outlets are distributed along the pipe where the manometer is attached. A picture of the transparent section of the pipe is given in Figure 3-4.

Pressure drop was taken between P4 and P5 using water manometer. The pipe length to diameter ratio until P4 is 200. This ratio is taken from the start of the test section until point P4.



**Figure3-3: The Test Part of the Setup**





**Figure 3-4: The transparent part of the test section.**

### **3.3 Instrumentation**

The instrumentations which were used to control the flow rate, measure the pressure drop, and to determine the flow pattern is presented in this section. The Flow pattern was captured by a camera which was fixed in front of the transparent part of the pipe. The pressure drop was read by a water manometer that is connected to pressure outlets P4, and P5 which can be seen in Figure3-3. The error in the manometer reading was 0.5 mm.

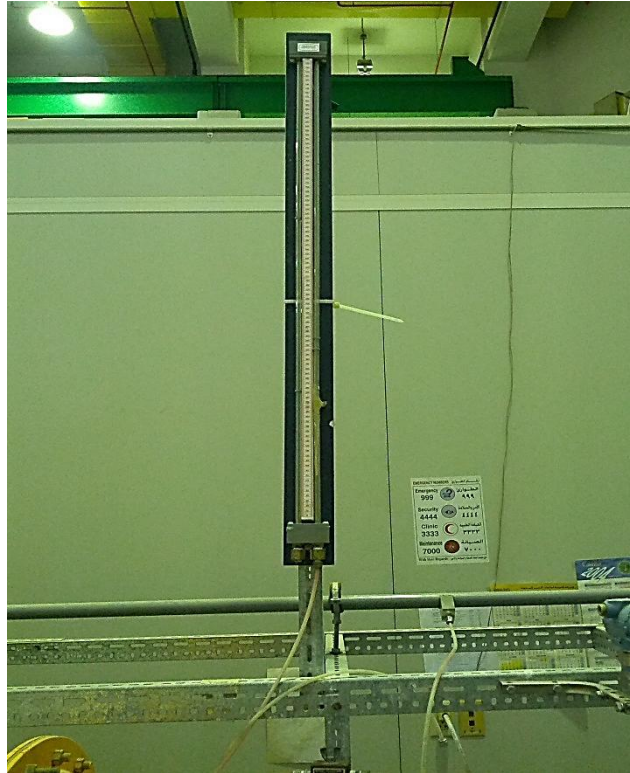


**Figure 3-5: The water manometer**

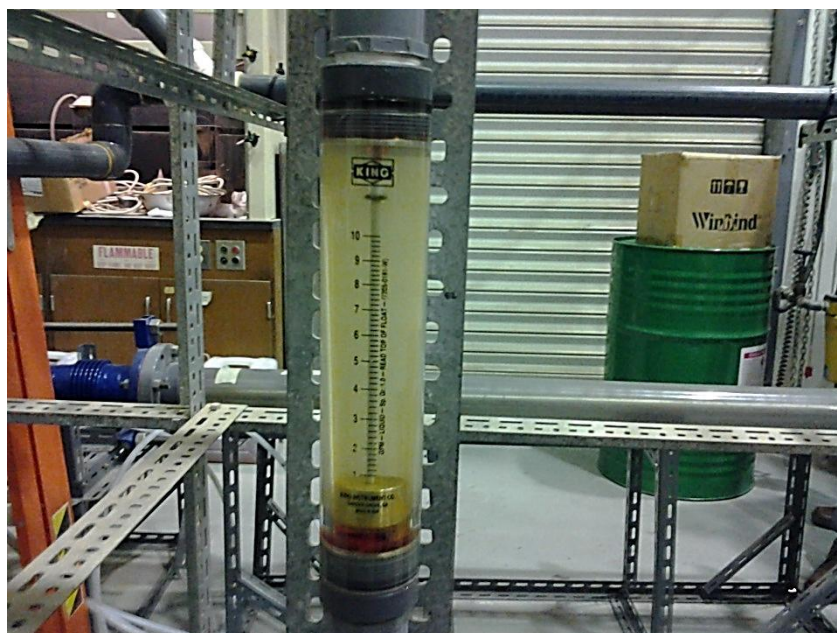


**Figure 3-6: The variable area flow meter**

The flow meters are Variable Area flow meters type from “king instrument co.” as shown in Figure 3-6. Two small flow meters are used for each fluid and two big ones. The small ones have an error of  $\pm 1\%$  of Full Scale, and they ranged from 1 to 10 gpm. The bigger ones have an error of  $\pm 4\%$  of Full Scale, and they ranged from 5 to 40 gpm. A calibration was achieved using a formula provided with the flow meters to allow the usage of the flow meter with oil and saline water.

Figure 3-7 shows four flow meters. Two small flow meters ranged from 1 to 10 gpm were used for low flow rates since the minimum reading of the big flow meters was 5 gpm. Also, two big flow meters ranged from 5 to 40 gpm were used for flow rates higher than 10 gpm. To insure accurate results, small and big flow meters were not used at the same time. Only flow meters from the same size were used at each run.



Figure 3-7: A picture of the “king instrument” flow meters.

In order to use the flow meter for oil (or for saline water), calibration is needed to adjust the density difference. The reading of the flow meter is divided by a factor found from equation (54) to give the actual flow rate, this factor was found to be 1.15 for oil and 0.964 for saline water ( $1065 \text{ kg/m}^3$  density), so if the needed oil and saline water flow rates are 1 gpm, then the actual reading that the flow meter should read is 0.87 gpm for oil and 1.04 gpm for saline water.

$$\text{calibration factor} = \sqrt{\frac{(8.03 - S_g)}{(8.03 - 1)(S_g)}} \quad (54)$$

Where  $S_g$  is the specific gravity of the used fluid. The uncertainty analyses of the used instruments are shown in appendix 1.

### **3.4 Procedure**

The experiments were conducted by the following procedures

1. First running water inside the loop to clean up the pipe and remove bubbles from the manometer connections and pressure inlets.
2. After that, the flow rates are fixed using the flow control valves that are placed before the flow meters, and using a control panel which controls the pump speed to give the required superficial oil and water velocities. The run continues for 2 minutes to achieve stable flow before taking data.
3. Then readings for pressure drop and pictures of the flow patterns were taken. The liquids then flow to the separation tank to be separated.
4. After the run stops, the mixture stays for 15 minutes in the separation tank. After separation, oil and water are returned to oil and water tanks respectively.

### **3.5 Fluids Properties**

The used oil in the experiment is an Aliphatic Solvent-Heavy oil type named as Safrasol 80 which is one type of Kerosene, it is provided by safraco [61]. The oil properties are provided in Table1.

**Table1: “Safrasol 80” oil properties.**

Property	ASTM Test Method	Units	Typical Values	Guarantee
Distillation Range: IBP FBP	D86	C	210 260	200Min. 280Max
Density @ 15 c	D4052	Kg/L	0.806	0.785-0.81
Flash Point	D56	C	88	75Min.
Aromatic Content	D1319	% vol.	18-22	25Max
Color (Saybolt)	D156		25	21Min.
Sulphur Content	D3120	ppmwt	13	20Max
Copper Corrosion	D130	Rating	1a	1Max

A viscosity test was performed at different temperatures in order to cover the variation of lab temperature in summer and winter. The instrument which was used in the test is the “Contraves Low Shear 30 Viscometer”. The Contraves Low Shear 30 Viscometer is a controlled strain, for steady shear measurements of viscosity. Given in Figure 3-8 the oil dynamic viscosity plotted against temperature:

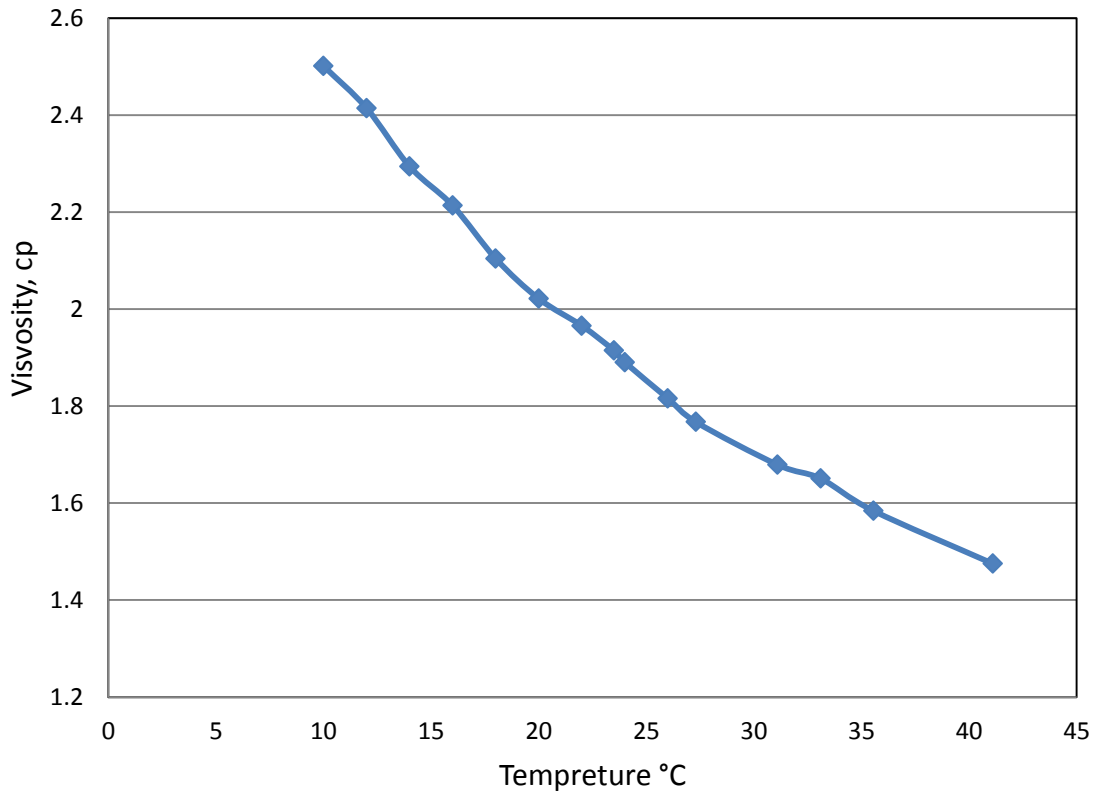


**Figure 3-8: “Safrasol 80” oil viscosity at different temperatures**

The measured density of the oil ranged from  $781 \text{ kg/m}^3$  at  $25^\circ\text{C}$ , to  $806 \text{ kg/m}^3$  at  $15^\circ\text{C}$ . This temperature test was made for density and viscosity to study the temperature effect in the results (section 4.2). Also the oil-air interfacial tension was measured to be  $0.03 \text{ N/m}$  at  $20^\circ\text{C}$ , and the oil-water interfacial tension was measured to be  $0.017 \text{ N/m}$  at  $20^\circ\text{C}$ .

In the conducted experiments, tap water and saline water were used. Saline water produced by adding food salt with an amount of 9% of water weight to the water tank, making its salinity about 75 %. The density of the water was increased from  $998 \text{ kg/m}^3$  to  $1065 \text{ kg/m}^3$  (at  $25^\circ\text{C}$ ). The density and the salinity of the saline and tap water were

found using ATAGO S/Mill-E instrument. Also, viscosity tests were performed on tap and saline water using the Contraves Low Shear 30 Viscometer which was used in oil. It was found that due to the salt addition, the viscosity changed from 0.985 cP to 1.246 cP. Although the density and viscosity differences were slight, but the oil-water density ratio was changed from 0.78 to 0.732, while the oil-water viscosity ratio changed from 1.94 to 1.536. This change had considerable effects on the flow patterns and the pressure drop.



## **CHAPTER 4**

### **EXPERIMENTAL RESULTS**

The results of the conducted experiments for flow pattern and pressure drop of oil-water, and oil-saline water are presented in this chapter. The pressure drop at several flow rates is obtained in order to provide more data to examine the effect of flow pattern and the effect of adding salt to water on pressure drop. Food salt (NaCl) was added as mentioned to water to make its salinity about 75 ‰. This high amount of salt was used to show clearly the effect of the added salt on the oil-water characteristics.

#### **4.1 Flow Pattern Map**

The flow pattern map for the used oil was produced for superficial velocities ranged from 0.05 to 1.6 m/s. The flow pattern was generated using visual observations only. The taken pictures of the oil-water flow were studied to configure and identify the flow pattern type of each run. The flow patterns were classified into seven groups: stratified flow (ST), stratified flow with mixing at the interface (ST-MI), water-in-oil emulsion (W/O), oil-in-water emulsion (O/W), dispersion of oil in water over a water layer (DO/W &W), dispersion of water in oil under an oil layer (DW/O &O), and the dispersion of oil in water and the dispersion of water in oil (DO/W & DW/O). These classifications were proposed earlier by Trallero [10] and Nadler and Mews [11]. Examples of these flow patterns are shown from Figure 4-1 to Figure 4-7.



**Figure 4-1: Stratified flow pattern (ST),  $U_o = 0.1$  m/s,  $U_w = 0.2$  m/s**



**Figure 4-2: Stratified flow with mixing at interface (ST-MI),  $U_o = 0.63$  m/s,  $U_w = 0.2$  m/s**



**Figure 4-3: Oil-in-water emulsion (O/W),  $U_o = 0.5$  m/s,  $U_w = 1.6$  m/s**



**Figure 4-4: Water-in-oil emulsion (W/O),  $U_o = 1.6$  m/s,  $U_w = 0.08$  m/s**



**Figure 4-5: Dispersion of oil in water over a water layer (DO/W & W),  $U_o = 0.08$  m/s,  $U_w = 0.8$  m/s**



**Figure 4-6: Dispersion of oil in water and dispersion of water in oil (DO/W & DW/O),  $U_o = 0.8$  m/s,  $U_w = 1.6$  m/s**

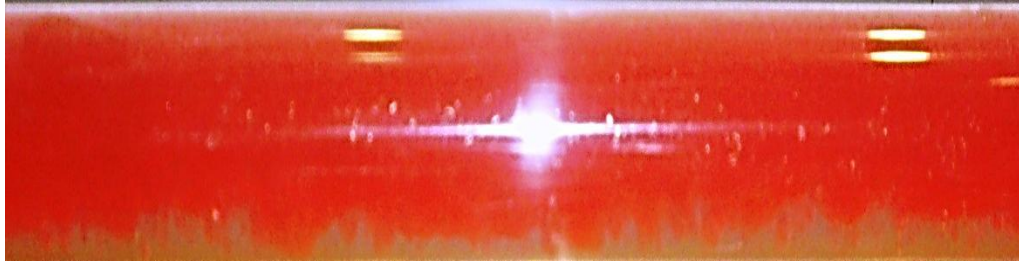


**Figure 4-7: Dispersion of water in oil under an oil layer (DW/O & O),  $U_o=0.6$  m/s,  $U_w=1.26$  m/s**

In Figure 4-1, where the flow pattern is the stratified flow (ST), two layers of oil and water are flowing together with a smooth interface between them. This flow pattern is seen at low oil and water flow rates.

Figure 4-2 shows the stratified flow with mixing at interface (ST-MI) flow pattern. This flow pattern is seen at flow rates higher than that in the stratified flow pattern. In this flow pattern, waves are seen at the interface.

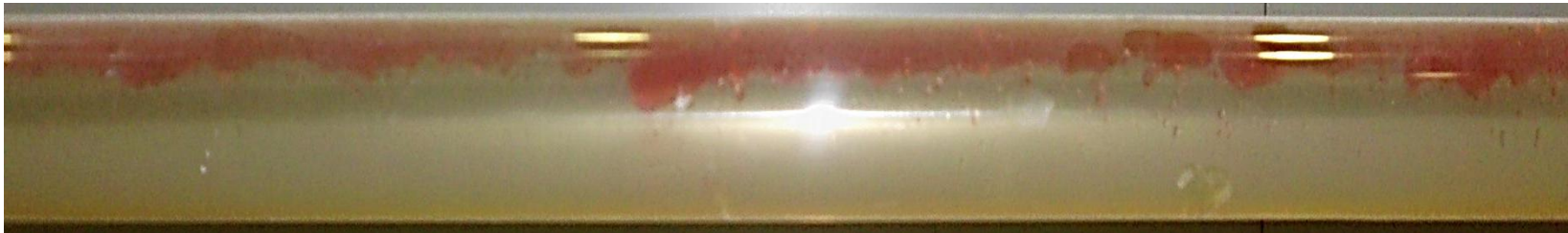
Figure 4-3 shows the oil-in-water emulsion (O/W) flow pattern. This flow pattern is seen at high water flow rates with small oil flow rates. The oil in this flow pattern travels as droplets that are distributed in the water phase. The reason behind that is the high water turbulence which breaks the oil layer into droplets. The opposite case is seen in Figure 4-4, where the flow pattern is water-in-oil emulsion (W/O). In this flow pattern, water flows as droplets that are distributed in the oil phase. It can be seen at high oil flow rates with small water flow rates.

Figure 4-5 shows the dispersion of oil in water over a water layer (DO/W & W) flow pattern. This flow pattern is seen when the oil flow rates are low, and when the water flow rates are high but also lower than that in the oil-in-water emulsion (O/W) flow

pattern. In this flow pattern, oil flows as slugs in some cases, and as droplets that is seen at the top of the pipe in other cases. Also in this flow pattern, a continuous layer of water is seen in the bottom of the pipe without any mixing with the oil phase.

In Figure 4-7, where the flow pattern is dispersion of water in oil under an oil layer (DW/O & O), the opposite of Figure 4-5 is seen. In this flow pattern, a continuous oil layer is seen at the top of the pipe without any water mixing, and a layer of oil-water mixture is seen at the bottom of the pipe. This flow pattern occurs when the water flow rates are small, and when the oil flow rates are high but smaller than that in the Water-in-oil emulsion (W/O) flow pattern. The dispersion of oil in water and dispersion of water in oil (DO/W & DW/O) flow pattern which is seen in Figure 4-6 appears when the oil and water flow rates are both high. Here oil and water phases are mixed together.

To show the salt effect, pictures for salt and tap water were captured at the same oil-water flow rates. The effect of salt can be seen from Figure 4-8 to Figure 4-15.



**Figure 4-8: Dispersion of oil in water over a water layer (DW/O & W),  $U_o = 0.08$  m/s,  $U_w = 0.8$  m/s, Saline water.**



**Figure 4-9: Dispersion of oil in water over a water layer (DW/O & W),  $U_o = 0.08$  m/s,  $U_w = 0.8$  m/s, Tap water**





**Figure 4-10: Dispersion of oil in water over a water layer (DW/O & W),  $U_o=0.5$  m/s,  $U_w=1.26$  m/s, Saline water**



**Figure 4-11: Dispersion of water in oil and oil in water (DW/O & DO/W),  $U_o=0.5$  m/s,  $U_w=1.26$  m/s, Tap water**

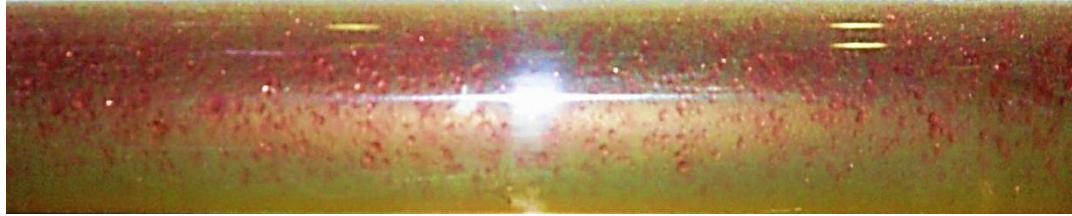


**Figure 4-12: Oil-in-water emulsion (DO/W),  $U_o = 0.1$  m/s,  $U_w = 1.6$  m/s, Saline water**



**Figure 4-13: Oil-in-water emulsion (DO/W),  $U_o = 0.1$  m/s,  $U_w = 1.6$  m/s, Tap water**



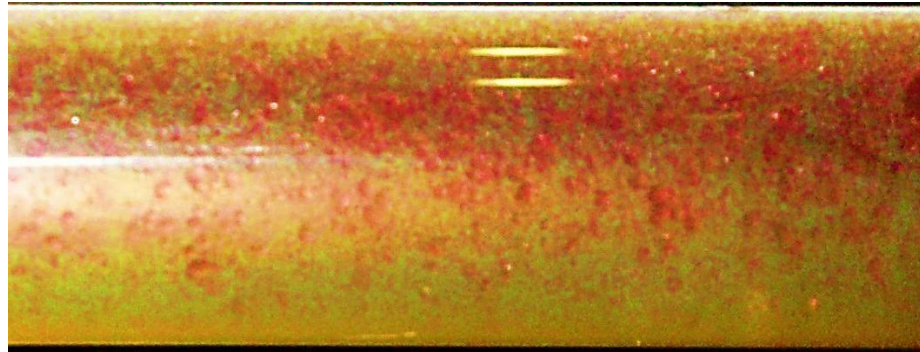


**Figure 4-14: Oil-in-water emulsion (DO/W),  $U_o = 0.1$  m/s,  $U_w = 1.6$  m/s, Saline water**

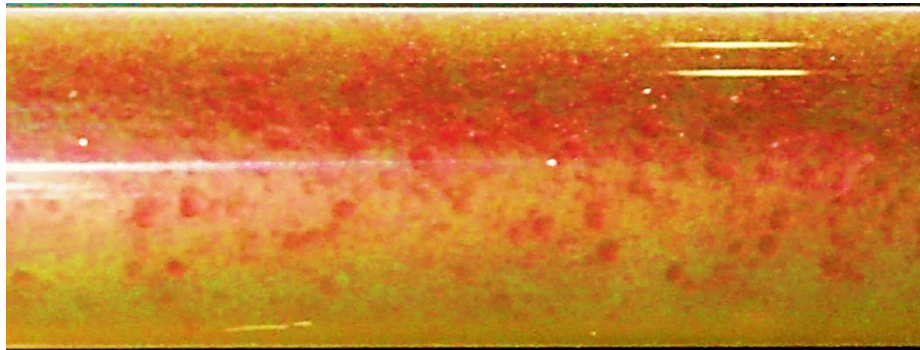


**Figure 4-15: Oil-in-water emulsion (DO/W),  $U_o = 0.1$  m/s,  $U_w = 1.6$  m/s, Tap water**



Figure 4-16: Stratified flow with mixing at the interface (ST-MI),  $U_o = 1$  m/s,  $U_w = 0.5$  m/s, Saline water



Figure 4-17: Stratified flow with mixing at the interface (ST-MI),  $U_o = 1$  m/s,  $U_w = 0.5$  m/s, Tap water

In Figure 4-8 and Figure 4-9, the flow pattern for tap and saline water is dispersion of oil in water over a water layer. But it can be noticed that for tap water, the oil flows in slugs or in separated masses unlike in saline water, where in saline water, a continuous layer of oil-water mixture is seen at the top of the pipe.

In Figure 4-10 and Figure 4-11, the flow pattern in tap water is more as dispersion of water in oil and oil in water. But for saline water, the flow pattern is dispersion of oil in water over a water layer. The dispersion of water in oil and oil in water flow pattern is noticed to happen at higher oil flow rates than the dispersion of oil in water over a water layer flow pattern, see Figure 4-18. This means that salt delayed the transition to the dispersion of water in oil and oil in water flow pattern.

In Figure 4-12 to Figure 4-15, where oil is dispersed in water for both saline and tap water, no difference is noticed between the tap and the saline water.

Figure 4-16 shows wavy interface between oil and salted water as for tap water in Figure 4-17. However, large wave amplitudes can be seen in tap water. Moreover, greater number of oil drops tend to break up from the interface as can be seen.

The flow pattern maps for saline water and tap water flowing with oil having a  $780 \text{ kg/m}^3$  density, and a 1.85 cP viscosity are shown in Figure 4-18, and Figure 4-19.

From Figure 4-20, seven flow patterns are observed. The smooth stratified (ST) flow pattern is found in a region below 0.37 m/s superficial oil velocity. As for dispersion of oil in water over a water layer (DO/W&W) region, it is located in the water dominated region between 0.6 m/s and 1.35 m/s superficial water velocity, and up to 0.55 m/s superficial oil velocity. Above this region for higher water velocities, the dispersion of oil in water (DO/W) region starts.

The dispersion of water in oil under an oil layer (DW/O&O) region can be seen in the oil dominated region, it is located beside the dispersion of oil in water and water in oil (DW/O&DO/W) region. The dispersion of oil in water and water in oil (DW/O&DO/W) region also located in the oil dominated region above 0.1 m/s superficial water velocity, after 1.1 m/s superficial oil velocity for low water superficial velocity, and after 0.6 m/s superficial oil velocity for high water superficial velocity. The dispersion of water in oil (DO/W) region is to be found at superficial oil velocities higher than 1.1 m/s, and after the dispersion of oil in water and water in oil region.

The flow patterns regions, such as for stratified, where plotted in the light of the flow pattern models of Trallero [15] and Brauner [36] which will be investigated in section 5.1 later.

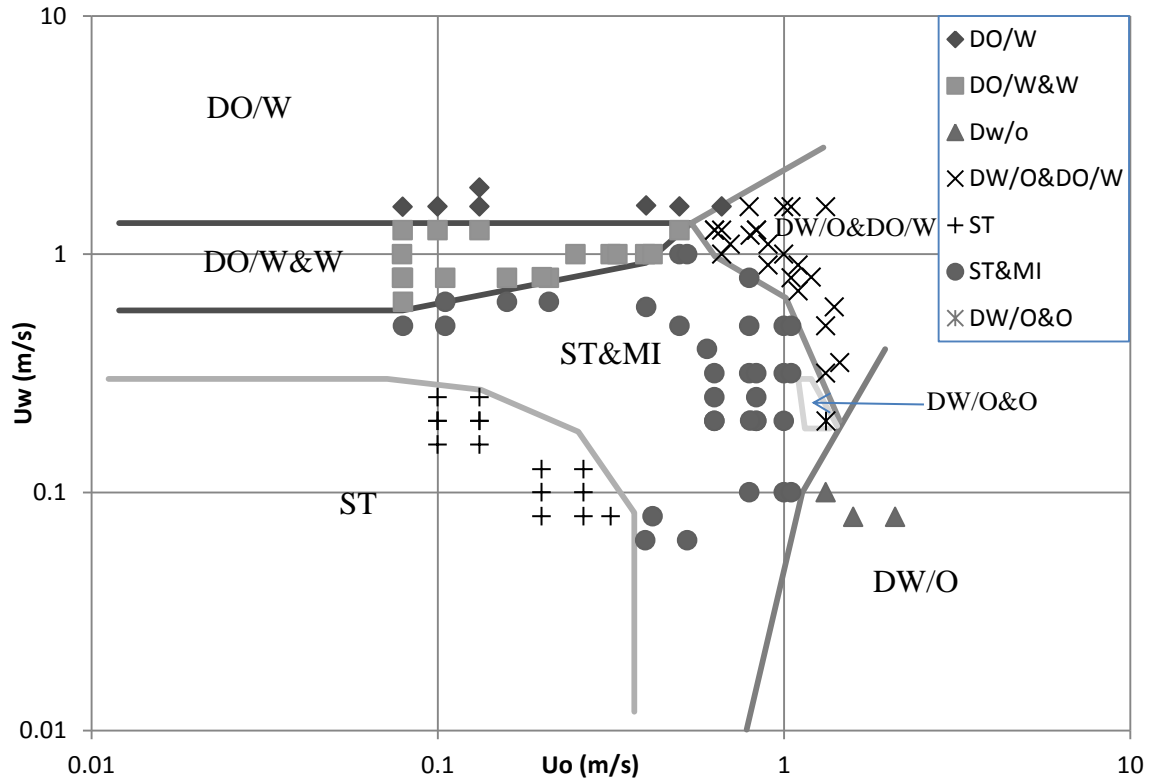


Figure 4-18: Experimental flow pattern map for Tap water,  $\mu_o/\mu_w = 1.94$ ,  $\rho_o/\rho_w = 0.78$ .

In Figure 4-19, six flow patterns are seen in the saline water flow pattern map, since no data are available for the dispersion of water in oil under an oil layer (DW/O&O) flow pattern. The six flow patterns boundaries in Figure 4-19 covers the same regions as in Figure 4-18 except for the dispersion of oil in water over a water layer (DO/W&W) region. This region covers up to 0.43 m/s superficial oil velocity, which is less than that in tap water. This also implies that the dispersion of oil in water and water in oil (DW/O&DO/W) region in saline water cover more region up to 0.43 m/s superficial oil velocity, which is more than that for tap water.

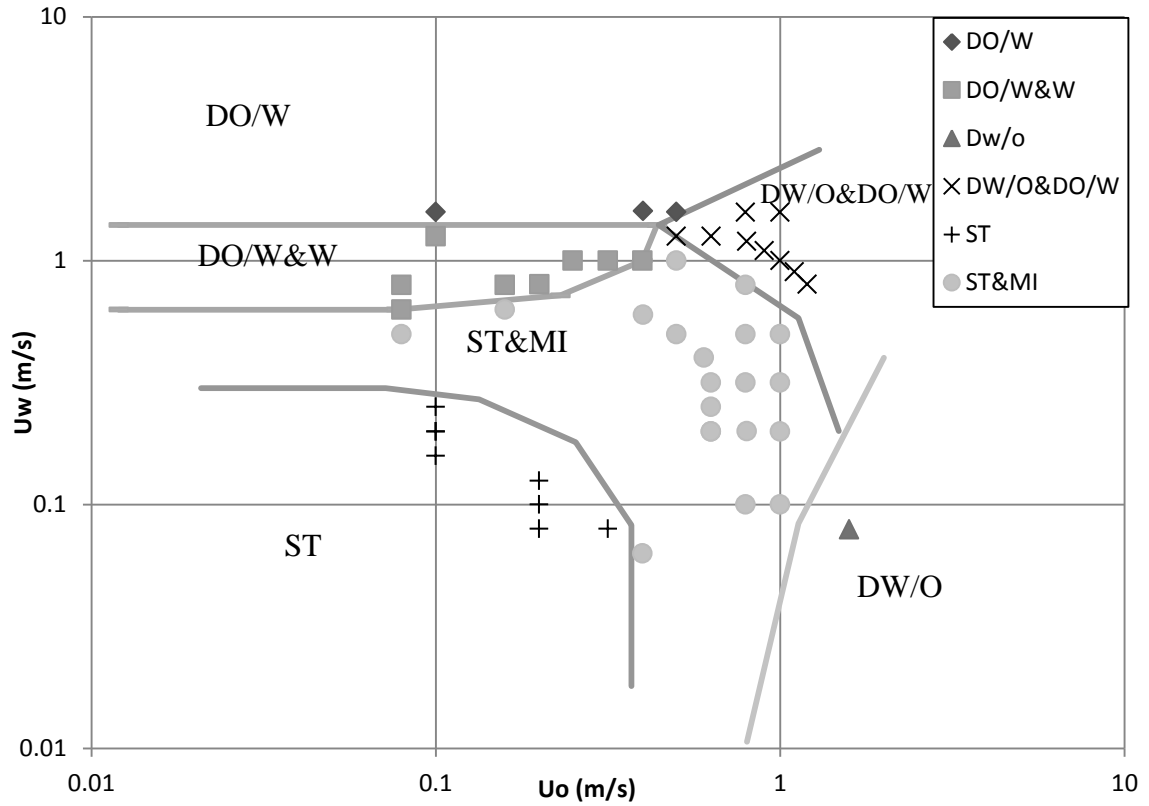


Figure 4-19: Experimental flow pattern map for 75 % saline water,  $\mu_o/\mu_w = 1.536$ ,  $\rho_o/\rho_w = 0.732$

In Figure 4-20, the two flow patterns are plotted together to distinguish the differences in the flow patterns boundaries. A clear difference can be seen in the dispersion of oil in water and water in oil (DW/O&DO/W) region along with the dispersion of oil in water over a water layer (DO/W&W) region. The difference is that the dispersion of oil in water and water in oil (DW/O&DO/W) region in saline water extend to cover greater area at the expense of dispersion of oil in water and water in oil (DW/O&DO/W) region.

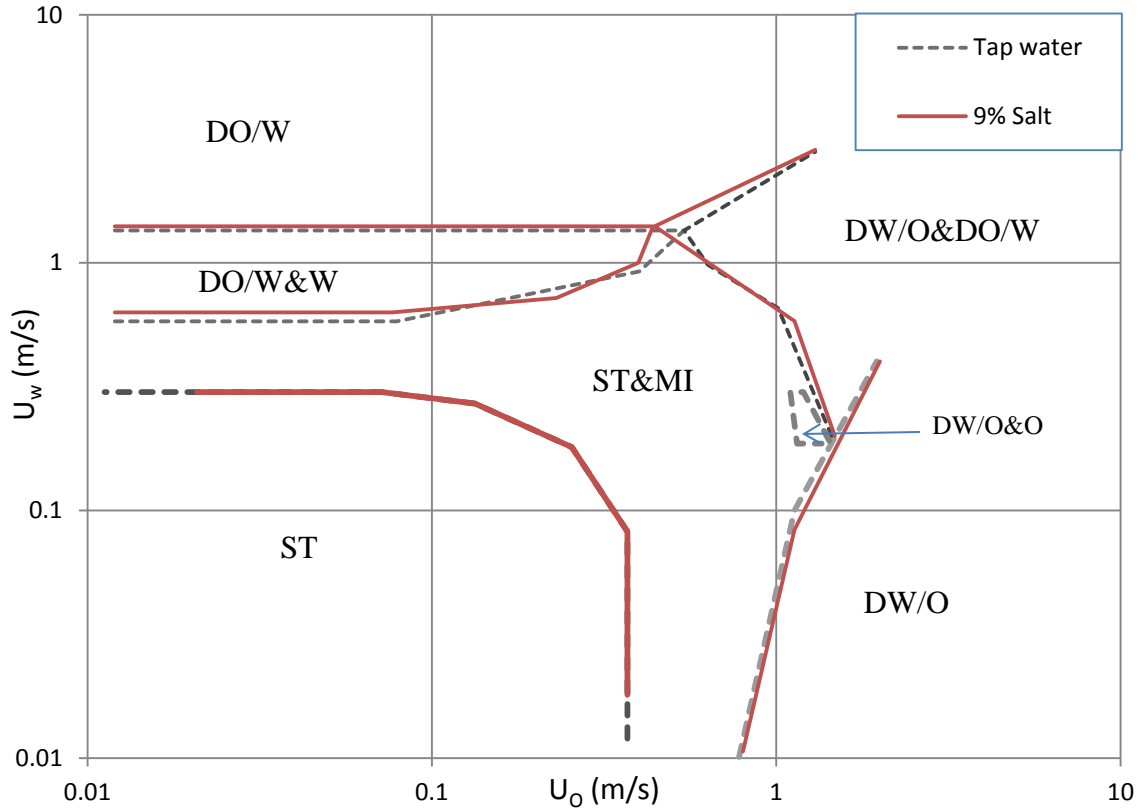


Figure 4-20: Comparison of the flow pattern boundaries between Tap water and saline water.

In Figure 4-18, Figure 4-19, and Figure 4-20, the boundaries which are presented to show the flow patterns regions are not absolute and can be modified as long as they can fit the experimental data. For an example, the dispersion of water in oil region can start from lower or higher superficial oil velocities other than 0.8 m/s.

The obvious reason in the above differences in the flow patterns pictures (from Figure 4-8 to Figure 4-17 ) between tap and saline water which is the density and viscosity difference that salt addition caused. The oil-water density ratio became 0.732 instead of 0.78, whereas the oil-water dynamic viscosity ratio became 1.536 instead of 1.94.

Each point on the flow pattern map of saline water is compared with its equivalent for tap water. The only noticed differences are the one which were presented in Figure 4-8 to Figure 4-17. It should be mentioned that in small oil and water flow rates, no differences were seen in the flow pattern between tap and saline water for the taken set of points. The only differences were seen at high flow rates of oil or water.



## 4.2 Pressure Drop

In this section, a study on the pressure drop is presented for different conditions and different mixture velocities. The used oil density is  $780 \text{ kg/m}^3$  at  $25^\circ\text{C}$ , and its kinematic viscosity is  $1.85 \text{ cP}$  at  $25^\circ\text{C}$ . The influence of salinity on pressure drop is investigated as a comparison is made between water having  $75 \text{ ‰}$  salinity and tap water. Adding food salt will change the water properties only since it only dissolved in water.

The first step is to run a single phase test inside the pipe and record the pressure of that component, this allows to determine the friction factor of the inside wall of the pipe, and allows to determine the accuracy of the used instruments. The single phase pressure drop for oil, water, and saline water are presented in Figure 4-23, Figure 4-22, and Figure 4-23. Calculations for the single phase pressure drop are seen in section 5.2.1.

From Figure 4-23, Figure 4-22, and Figure 4-23, it can be noticed that good agreement is seen between the experimental and the calculated values of the single phase pressure drop.

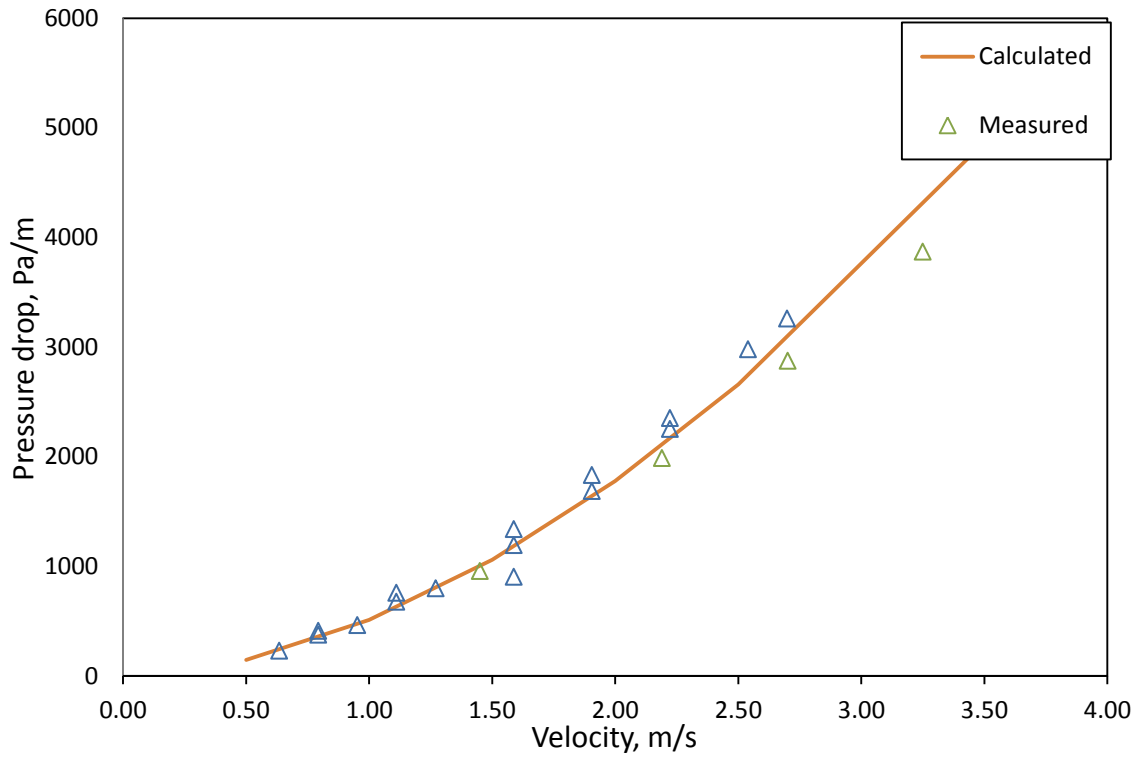


Figure 4-21: Single phase pressure drop for oil, 25 °C

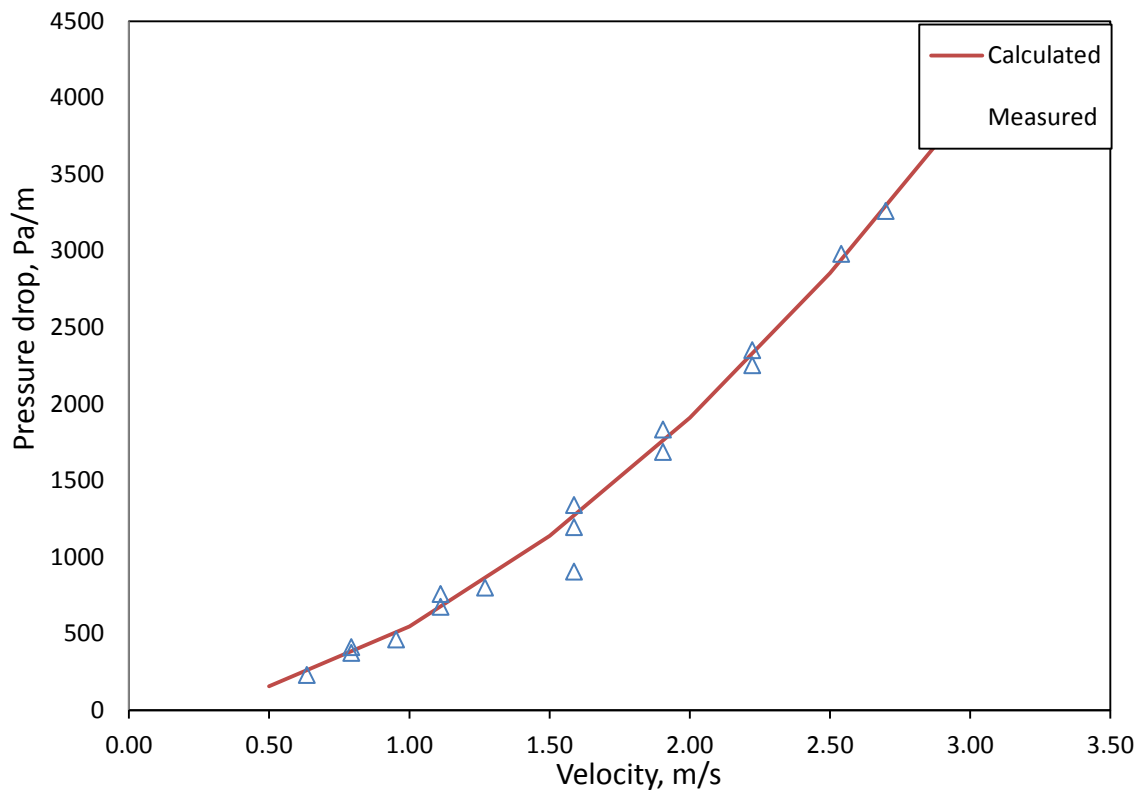
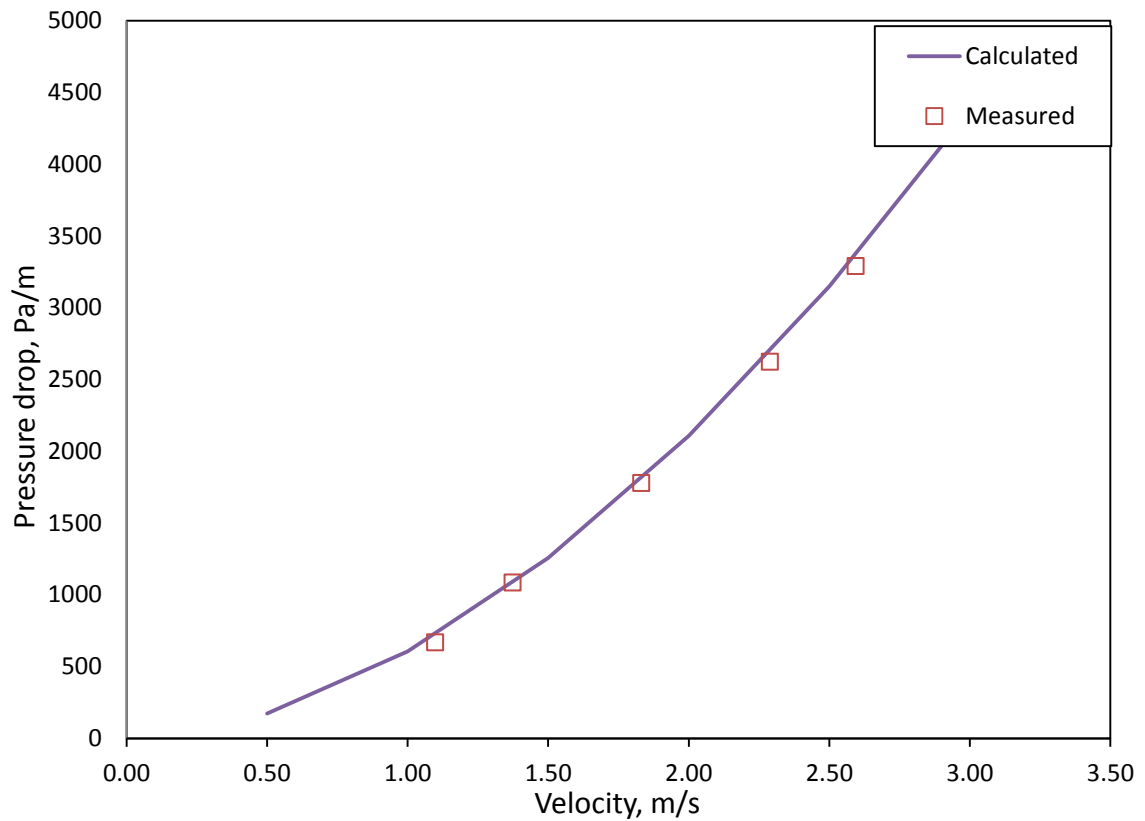
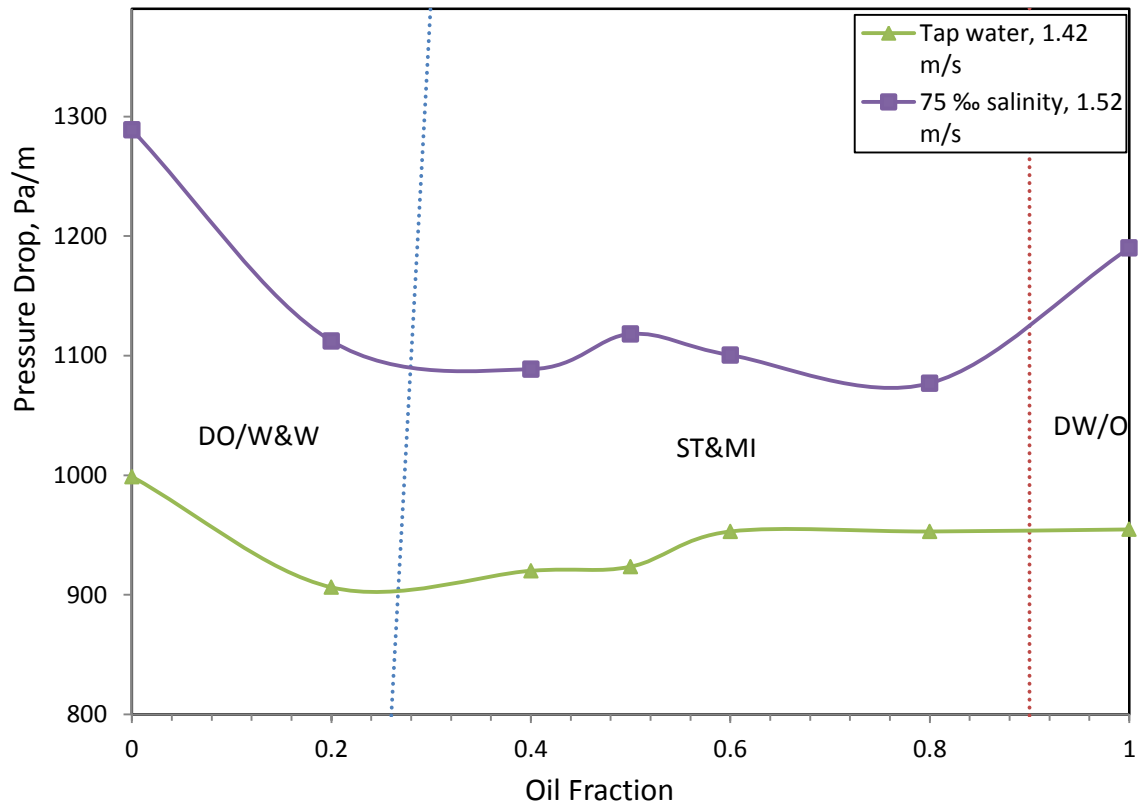


Figure 4-22: Single phase pressure drop for Tap water, 25 °C



**Figure 4-23: Single phase pressure drop for 75 % saline water, 25 °C**

The pressure drop for oil-tap water and for oil-saline water was measured at 1.5 m/s, and 3 m/s mixture velocities. The small mixture velocity uses the small flow meter. The large mixture velocity uses the big one. Both tap water and saline water pressure drops are plotted on the same graph as shown in Figure 4-24 and Figure 4-25. In addition, the flow pattern can be seen in these figures to show the effect of flow pattern change on pressure drop.



**Figure 4-24:** The pressure drop of oil-tap water at 1.42 m/s mixture velocity and of oil-saline water at 1.61 m/s mixture velocity, 25 °C.

In Figure 4-24, the pressure drop profile goes through dispersed flow pattern and stratified with mixing at the interface (ST&MI) flow pattern. The dashed lines represent the transition boundary from one flow pattern to the other. These transition boundaries were found based on Figure 4-18 and Figure 4-19.

The pressure drop profile for tap and saline water which are flowing at 3 m/s mixture velocity is given next in Figure 4-25. The transition boundary of the flow patterns is found based on Figure 4-18 and Figure 4-19.

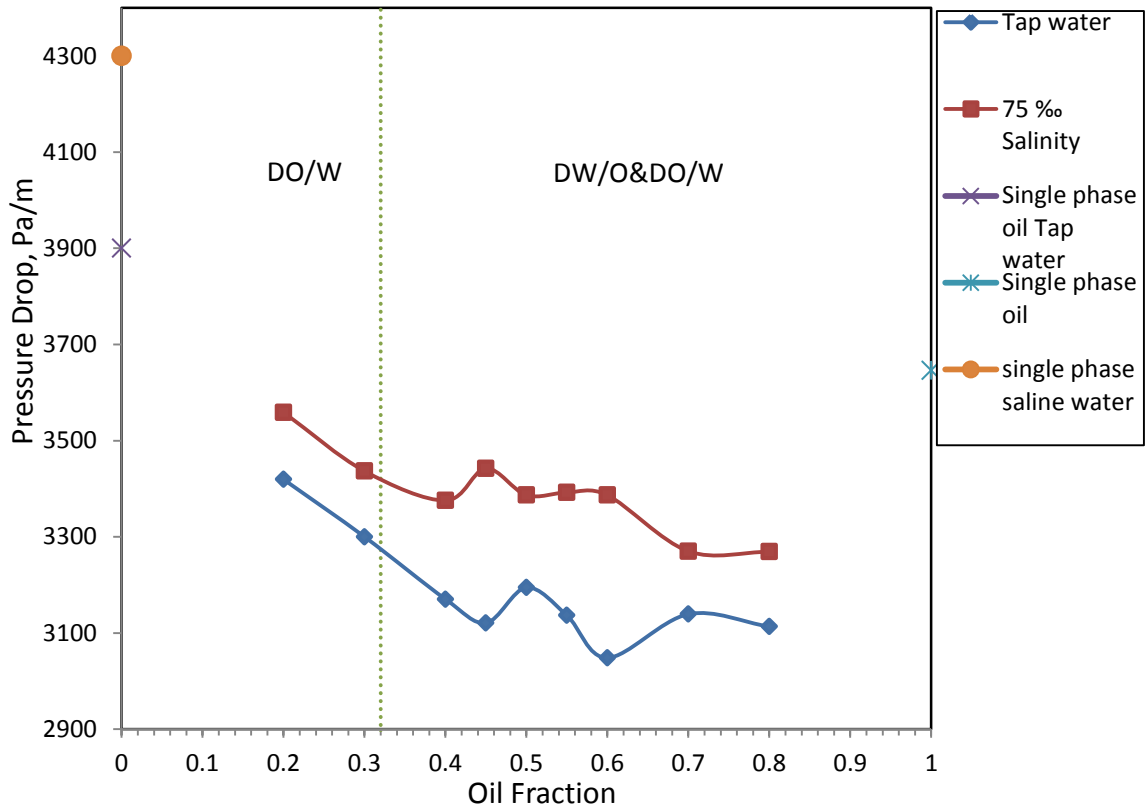


Figure 4-25: The pressure drop of oil with tap and saline water at 2.98 m/s mixture velocity, where the single phases pressure drops are found by calculation, 25 °C.

Figure 4-25 shows the pressure drop profile in each flow pattern, and its behavior between 0.2 to 0.8 oil fractions. The single phase pressure drops at zero and at one oil fraction were found by calculation. As can be seen from the figure, the profile constantly decreases with the increase of the oil fraction until it reaches a region in the middle. This region starts at 0.45 oil fraction for tap water and at 0.4 oil fraction for saline water. At this point, the pressure drop increases and decreases again generating a peak at 0.5 and at 0.45 oil fractions for tap and saline water respectively. After the decrease, pressure drop starts to increase until it reaches the single phase pressure drop of oil.

Inversion point is recognized in this profile when the pressure drop stops decreasing and starts increasing, and when a peak in the pressure drop is generated. This peak was seen at 0.5 oil fraction for tap water and at 0.45 oil fractions for saline water.

After inversion, the pressure drop stops decreasing and starts to increase, this happens at 0.7 oil fraction for both tap and saline water. So the overall behavior for the pressure drop is decreasing, peak, and then increasing as it moves closer to inversion for both saline and tap water.

The peak in the pressure drop can also be seen in Valle and Utvik [62], Soleimani et al. [63] and Karolina et al. [64], where they reported that a peak in the pressure drop appeared at inversion point.

It can be understood that the salt caused the inversion to start earlier than that in tap water, so inversion was affected by the salt addition.

Figure 4-24 shows that the pressure drop profiles is different from that in Figure 4-25, the reason behind that is the small oil-water flow rate, which made the flow pattern to be stratified with mixing at the interface near the 0.5 oil fractions.

Another set of pressure drop profiles for tap water are shown in Figure 4-26 below, where three different mixture velocities were chosen, 2.04 m/s, 2.4 m/s, and 2.8 m/s. The data were taken at 17 °C to show temperature effect on the pressure drop profile.

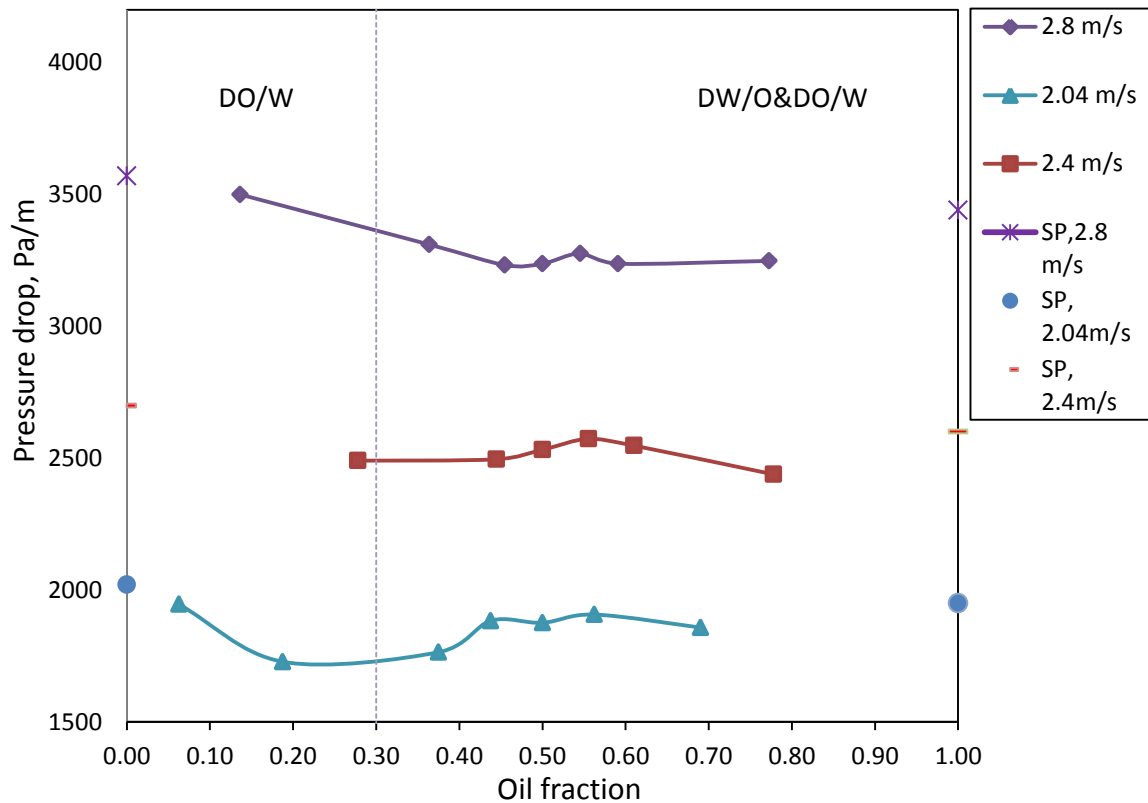


Figure 4-26: The pressure drop of oil-Tap water, where SP is the calculated single phase pressure drop for oil and water, 17 °C

It is noticed from Figure 4-26 that inversion is seen for the 2.8 m/s and the 2.4 m/s pressure drop profiles. The taken data ranged from 0.05 to 0.8 oil fractions, and the single phase pressure drops at zero and at one oil fraction were found by calculation. Inversion in the 2.8 m/s pressure drop profile occurs at 0.55 oil fraction, while for the 2.4 m/s pressure drop profile, inversion is at 0.56 oil fraction.

Comparing the 2.8 m/s and the 2.4 m/s pressure drop profiles in Figure 4-26 with the 2.98 m/s pressure drop profile in Figure 4-25, it is noticed that as the mixture velocity increases, inversion starts at earlier oil fractions. Also, the pressure peak magnitude increases as the mixture velocity increases. Moreover, as the mixture velocity increases, the pressure decrease rate increases.

Similar pressure drop behaviors are seen in Soleimani [65], Elseth's [66], Karolina et al. [64], Lum et al. [67]. In these studies, the oil-water pressure drop is noticed to have a lower value than the single phase water value, or it decreases as the oil fraction approaches a certain value. This behavior according to Soleimani [65], pal [68], Lum et al. [67], and Karolina et al. [64] is due to the drag reduction which present in dispersed liquid-liquid systems. Soleimani [65] mentioned that the presence of drops will repress turbulence and exhibit drag reduction.



The temperature influence on pressure drop is shown in Figure 4-27. Two profiles of pressure drop, one at 17 °C, and the other at 25 °C. The corresponding oil density at 17 °C is 802 kg/m<sup>3</sup>, and its kinematic viscosity is 2.16 cP, while water density is 999 kg/m<sup>3</sup> and its kinematic viscosity is 1.08 cP; see Figure 4-27.

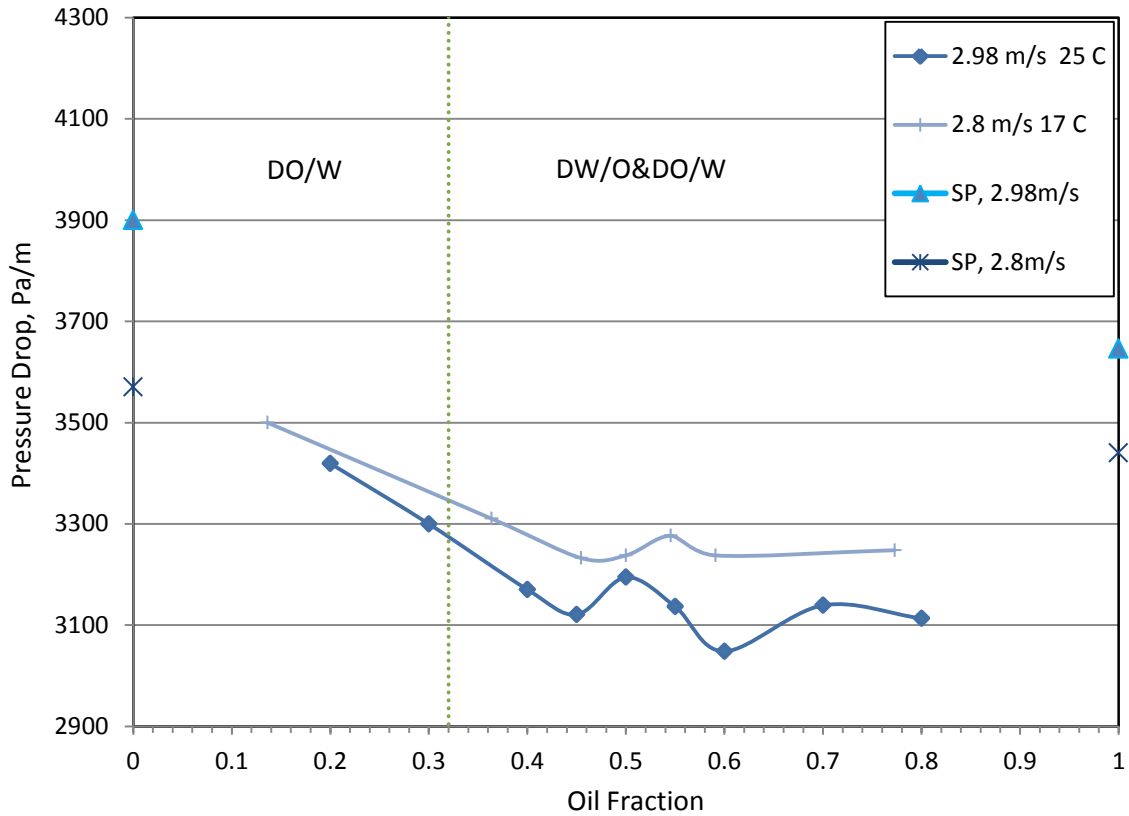


Figure 4-27: The pressure drop of oil -Tap water for 17 °C and 25 °C, where SP is the calculated single phase pressure drops for oil and water.

From Figure 4-27, the pressure for the 2.98m/s mixture velocity is noticed to start at high pressure drop value than that for the 2.8m/s profile, but it has a smaller value at inversion. Two factors should be considered to describe why the profile with the 2.98m/s mixture velocity has smaller pressure drop at inversion than the 2.8m/s profile even it has higher mixture velocity. These factors are the mixture velocity, and the temperature drop. For the mixture velocity, the pressure drop profile is noticed to have greater slope as the mixture velocity increases. For the temperature, the decrease in the temperature cause an increase the oil viscosity and density of the 2.8m/s profile, causing greater pressure drop values at inversion.

Another set of pressure drop points are shown in Figure 4-28 and Figure 4-29 for tap and saline water, were the pressure drop is plotted against the oil fraction with different mixture velocities. No relation exists between the points of the same line. The lines between the points drawn only to show the behavior of the pressure drop as the mixture velocity increases.

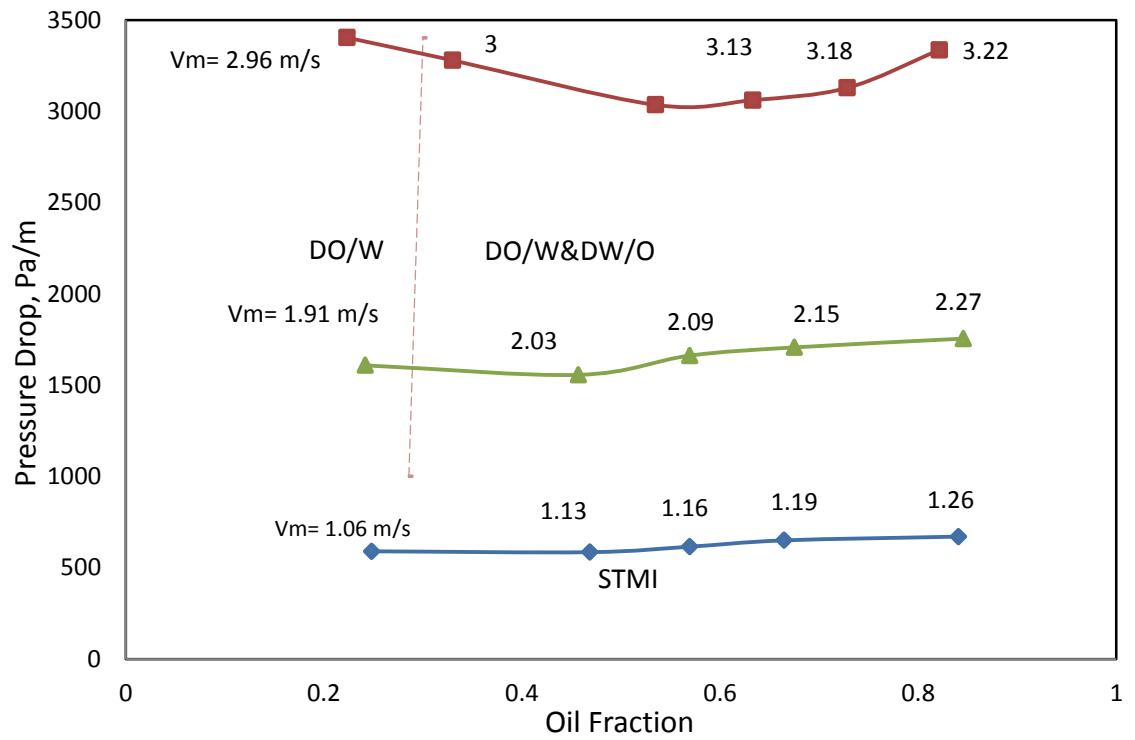


Figure 4-28: Pressure drop of oil -Tap water with mixture velocities (m/s) shown in chart; the flow pattern of first data line was ST&MI, 25 °C.

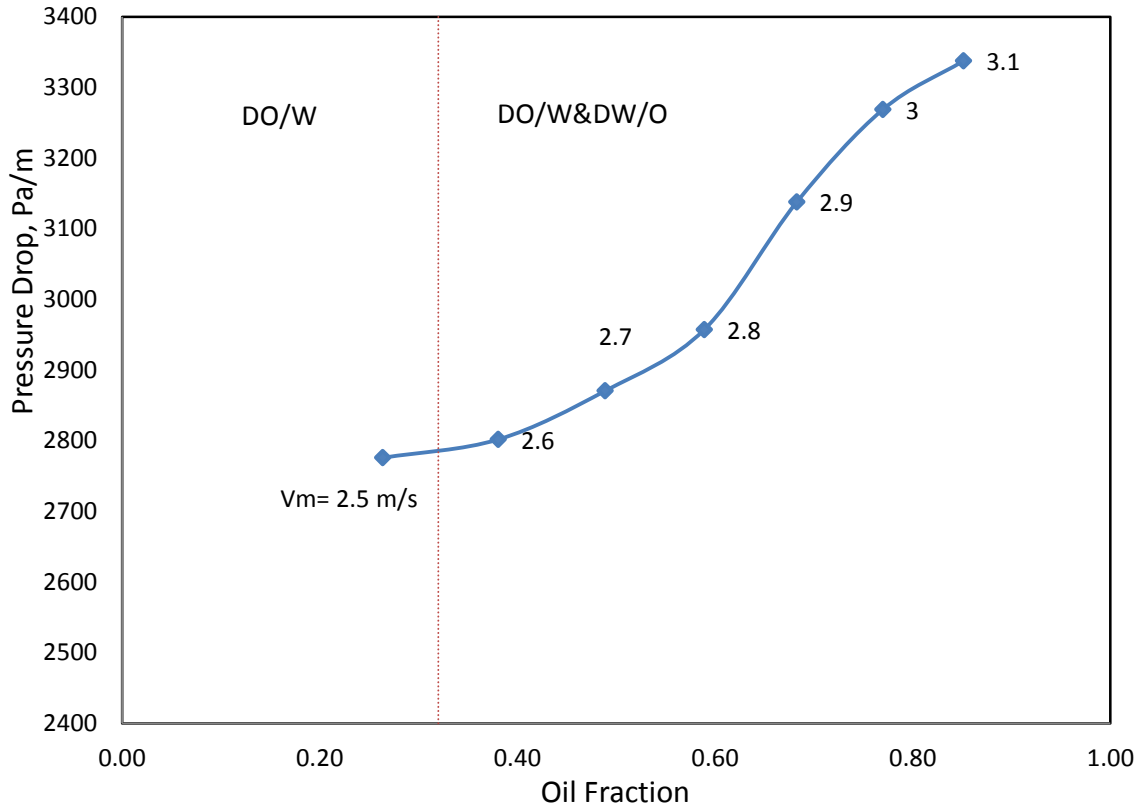
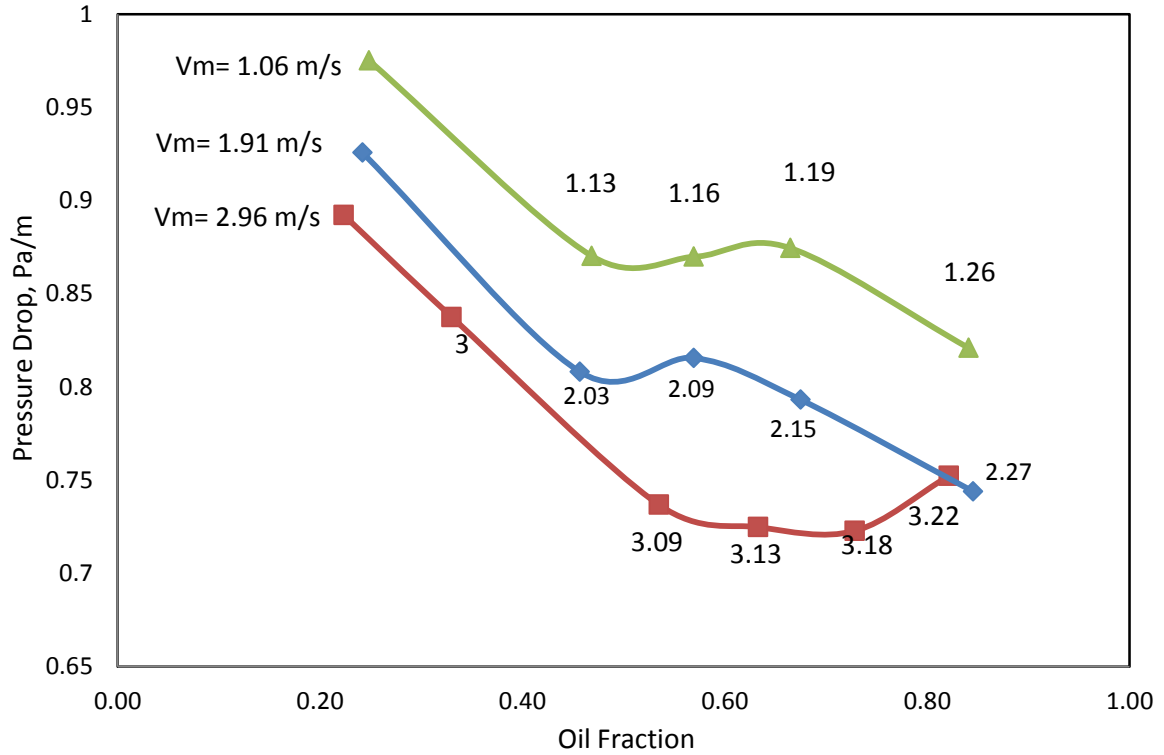


Figure 4-29: Pressure drop of oil -saline water with mixture velocities (m/s) shown in chart, 25 °C.

In Figure 4-28 and Figure 4-29, inversion is identified in the first line (the one which starts with 2.96 m/s mixture velocity) when the pressure drop profile changes its course. This is seen at 0.5 oil fraction. Inversion point is not seen in the other pressure drop lines. In these lines, it is also noticed that the pressure drop is continuously increasing as the mixture velocity increases.

Comparing all the oil-water pressure drop figures, it can be noticed that the exact point of inversion varies, where it ranges from 0.5 to 0.59 oil fractions. So it can be said that its location depends on the mixture velocity. An approximate value for all of the above figures is given to be here 0.52.

The pressure drop profiles in Figure 4-28 are made dimensionless by dividing them over the water single phase pressure drop as in Figure 4-30. It is noticed that the normalized pressure drop value of the two pressure drop profiles which start with 1.06 m/s and 1.91 m/s drop as the oil fraction increases. However for the other pressure drop profile, its normalized pressure drop value is noticed to drop until 0.52 oil fraction and then starts to increase. Looking again at Figure 4-30, it is noticed for the same oil fraction, as the mixture velocity increases, the less normalized pressure drop value is produced. This means that as the mixture velocity increases, the pressure drop profile has greater descent, or the rate of descent increases as the mixture velocity increases. It is also noticed that all of the pressure drop profiles have normalized pressure drop value less than one. This means that as the pressure drop decreases as it approaches inversion point when inversion is seen.



**Figure 4-30: Normalized pressure drop against oil fraction. The mixture velocities (m/s) are shown in chart, 25 °C.**

A new representation of the pressure drop can be plotted as the decrease rate in the pressure drop as the oil fraction changes for saline and tap water. This can be obtained by drawing a straight line from the single phase water pressure drop to the single phase oil pressure drop as in Figure 4-31. Then the experimental pressure drop value is subtracted from its equivalent on the straight line. This step is done for every point of pressure drop for tap and saline water. It was found that the maximum difference in the pressure drop between the experimental curve and the straight line for tap water to be 700 Pa, and the average difference was 620 Pa. While for saline water, the maximum difference was reduced to 630 Pa, with an average difference of 542 Pa. This means that saline water has less change in the pressure with the change of the oil fraction than tap water, or the

pressure decrease rate for saline water is less than that for tap water. Moreover, at inversion point (0.5 for tap water and 0.45 for saline water), the difference between the experimental pressure drop and its corresponding value on the straight line was 585 Pa for tap water and 530 Pa for saline water.

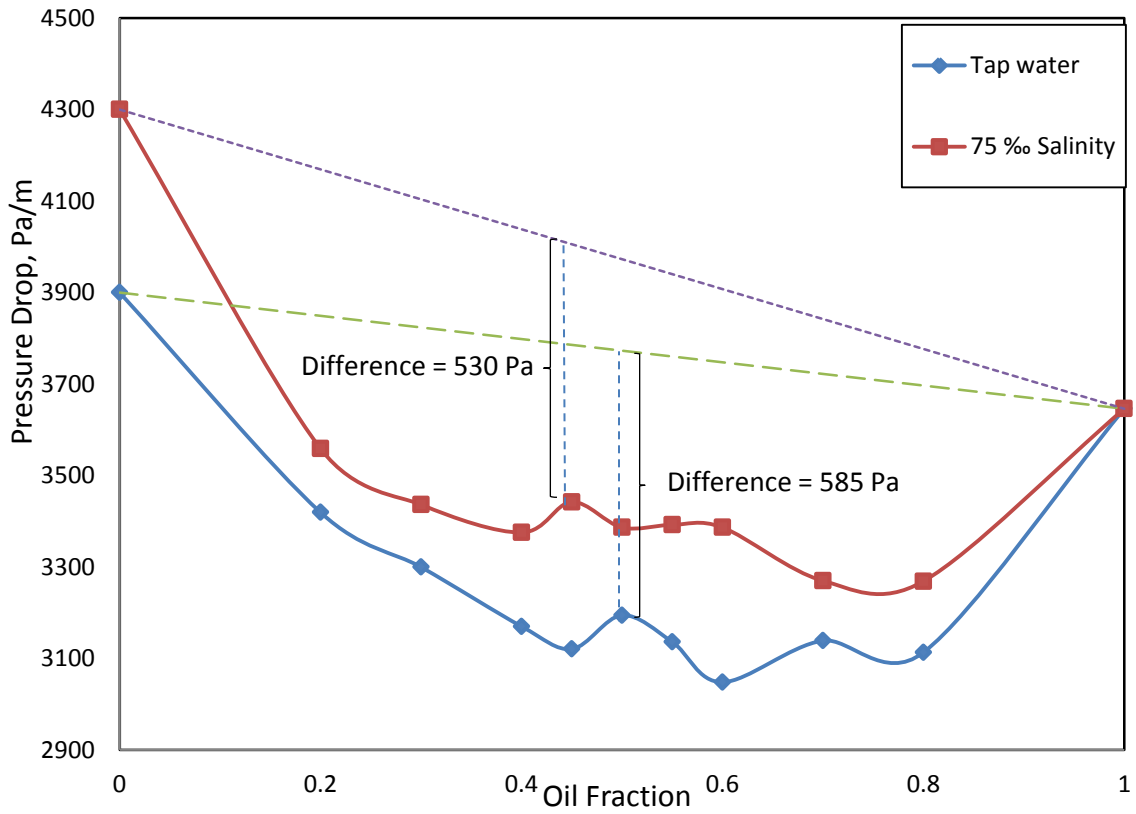


Figure 4-31: Experimental Pressure drop profile along with a straight line profile of  $V_m=2.98\text{m/s}$ ,  $25\text{ }^\circ\text{C}$ .

## **CHAPTER 5**

### **VALIDATION**

In this chapter the results of the present study are compared against several models of flow pattern and pressure drop, along with previous experimental work of oil having approximately similar properties as the one used in this work. The acquired flow pattern map is compared with Trallero [15], Brauner [36], and Torres [43] models of oil-water flow pattern map. The pressure drop data are compared with several models of inversion point and mixture viscosity mentioned in the literature.

#### **5.1 Flow Pattern**

The experimental flow pattern maps of tap and saline water are compared with Trallero [15], Brauner [36], and Torres [43] models of flow pattern map. This comparison is seen in Figure 5-1 to Figure 5-6. Similarly, comparison is made with the flow pattern map of Elseth [66] who used oil with almost similar properties as the one used in this study.



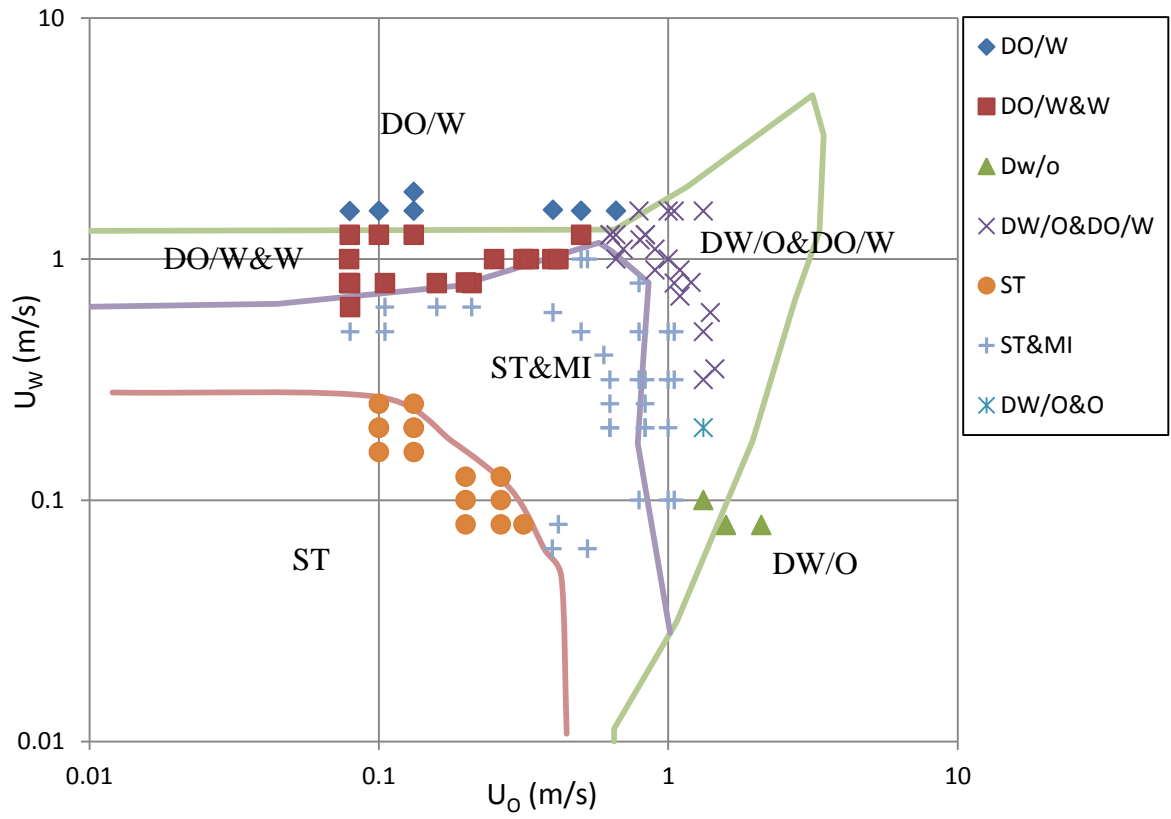


Figure 5-1: Comparison between Trallero [15] flow pattern map (lines) and this study experimental flow pattern map (points), Tap water,  $\mu_o/\mu_w = 1.94$ ,  $\rho_o/\rho_w = 0.78$ .

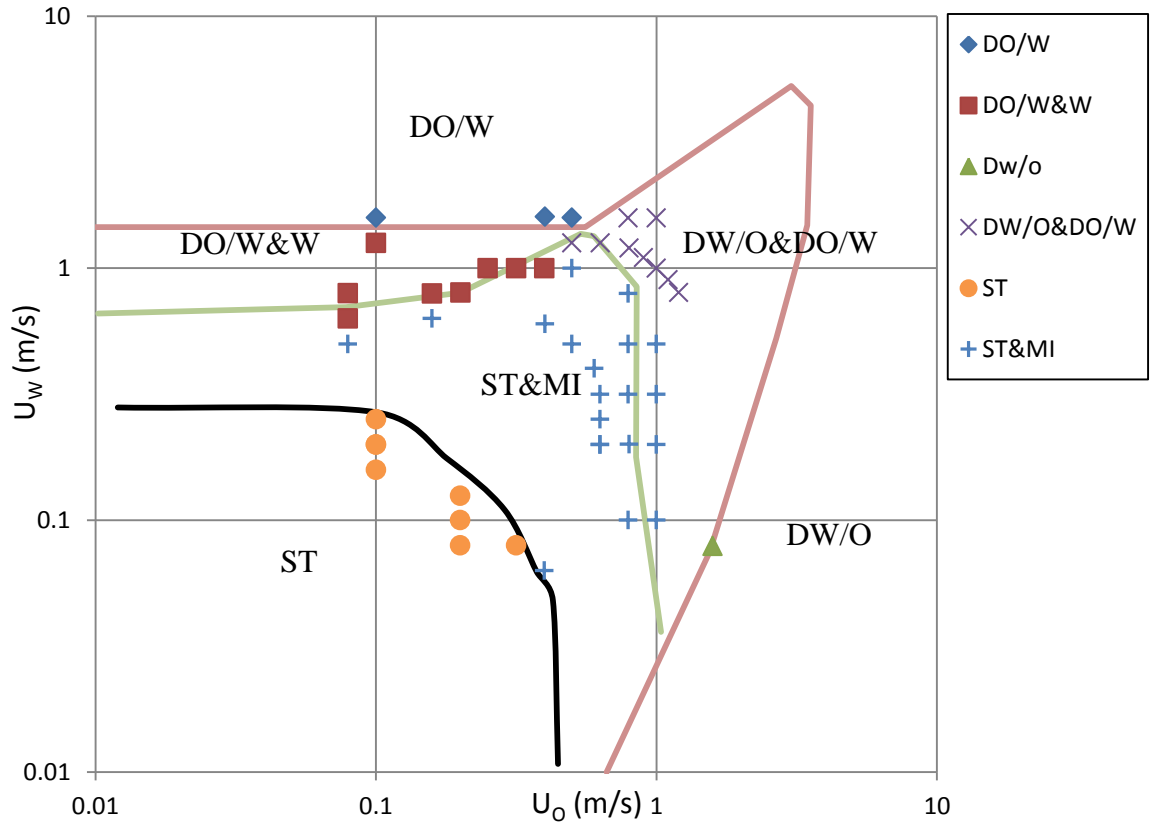
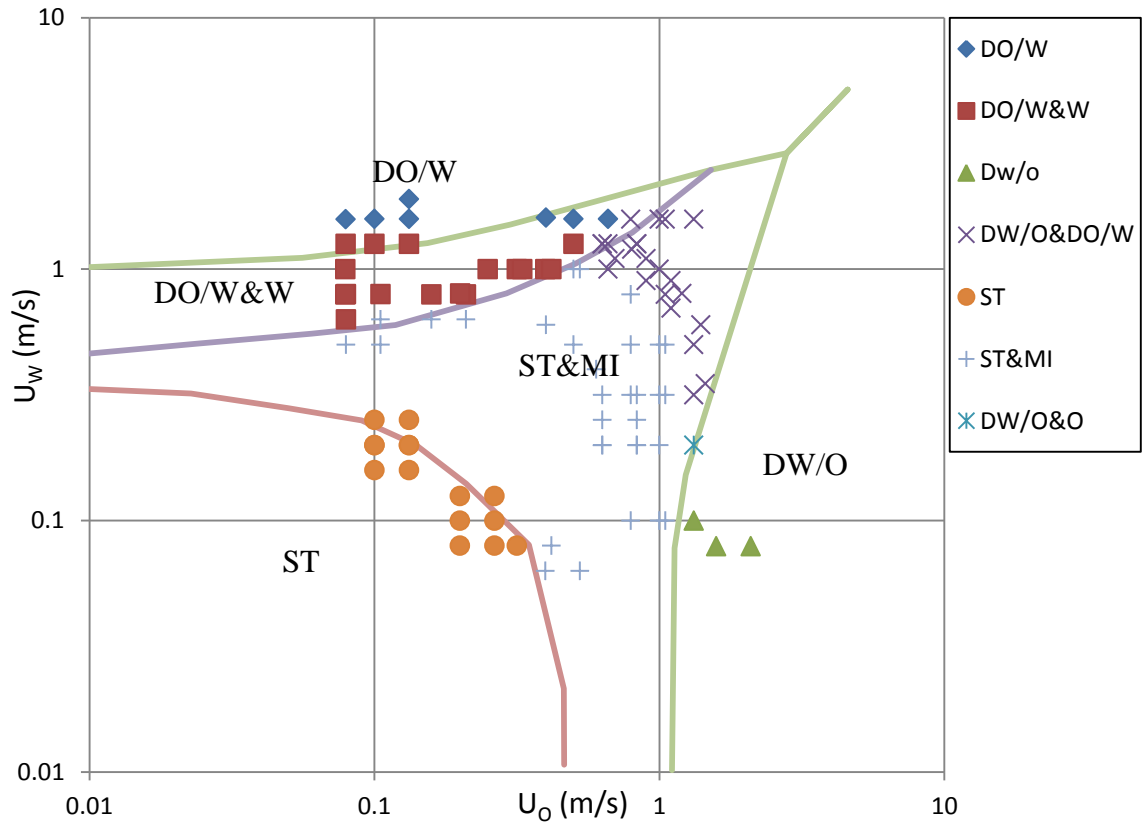


Figure 5-2: Comparison between Trallero [15] flow pattern map (lines) and this study experimental flow pattern map (points), saline water,  $\mu_o/\mu_w = 1.536$ ,  $\rho_o/\rho_w = 0.732$ .



**Figure 5-3: Comparison between Brauner flow pattern map (lines) and this study experimental flow pattern map (points), Tap water,  $\mu_o/\mu_w = 1.94$ ,  $\rho_o/\rho_w = 0.78$ .**

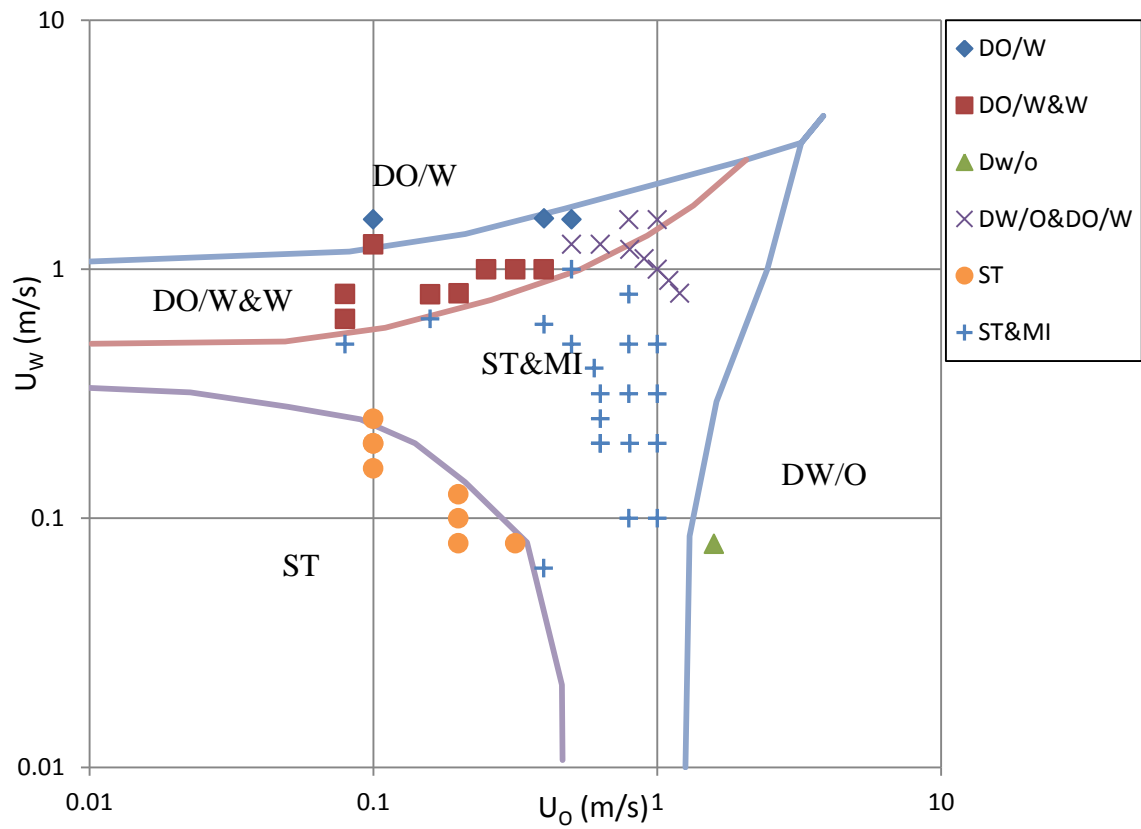
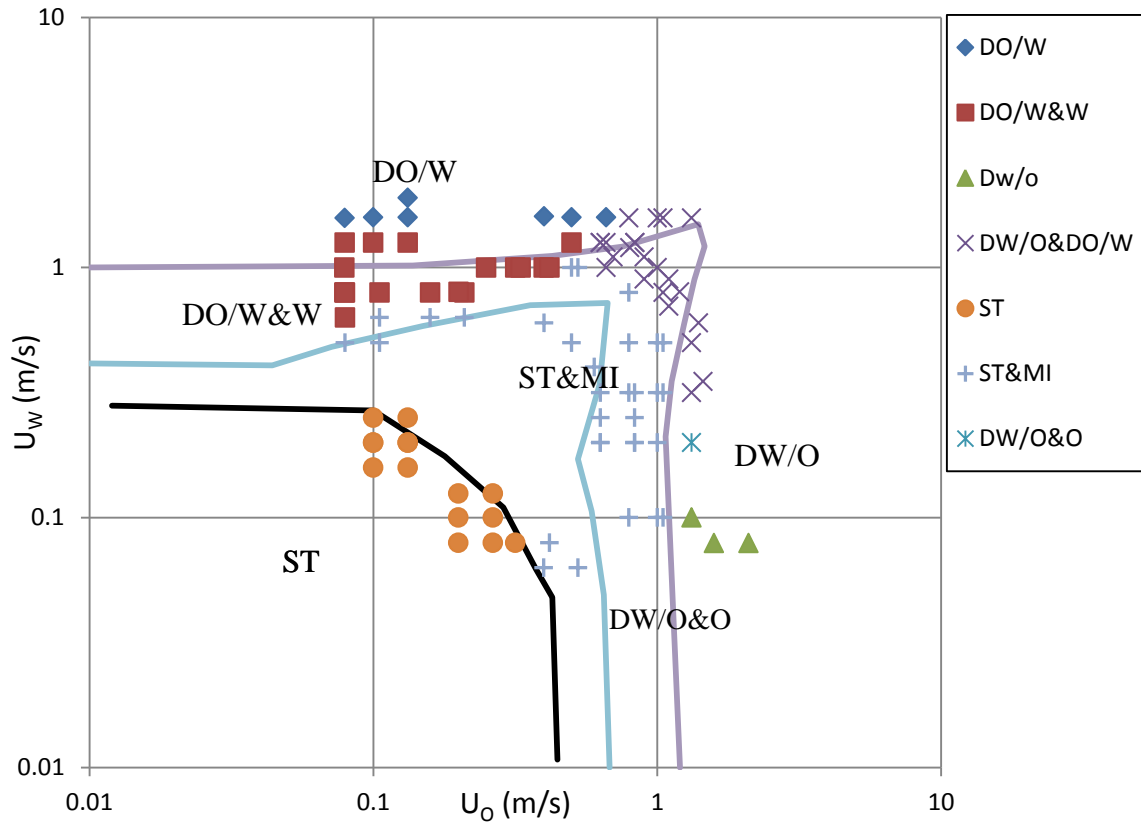
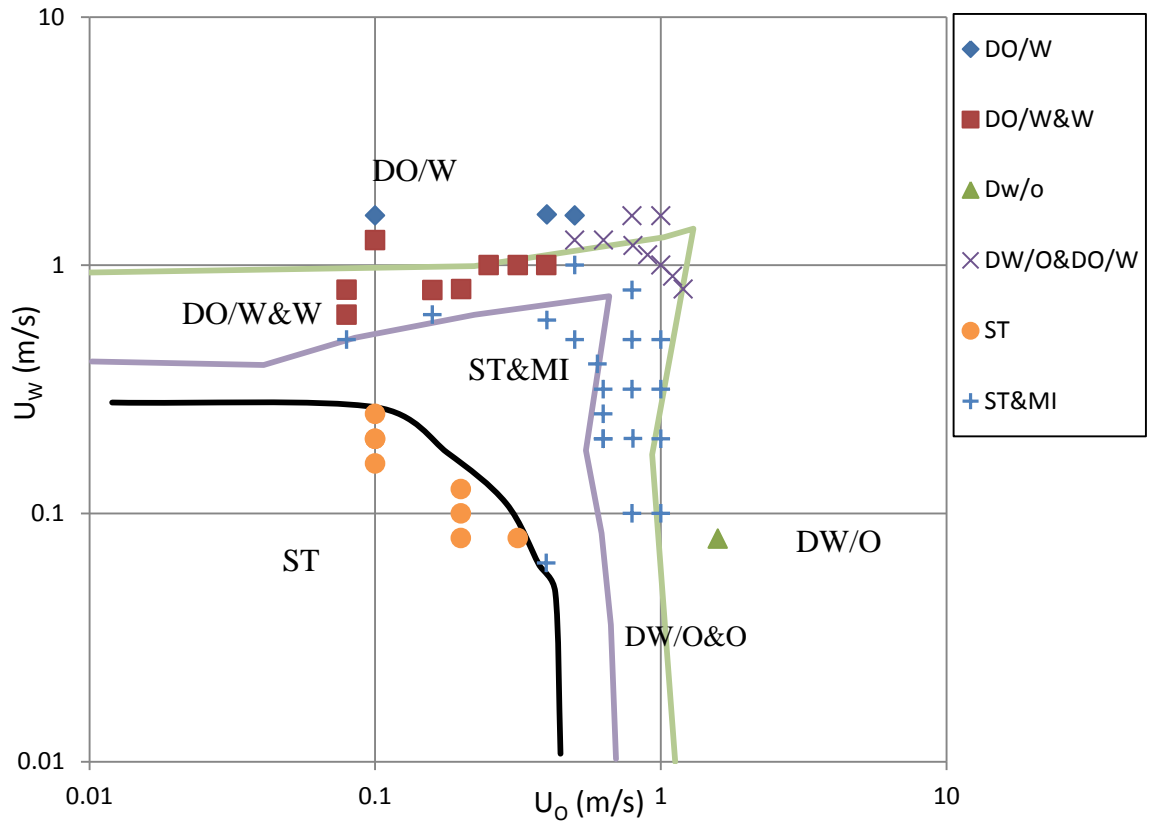


Figure 5-4: Comparison between Brauner flow pattern map (lines) and this study experimental flow pattern map (points), saline water,  $\mu_o/\mu_w = 1.536$ ,  $\rho_o/\rho_w = 0.732$ .



**Figure 5-5: Comparison between Torres [43] flow pattern map (lines) and this study experimental flow pattern map (points), Tap water,  $\mu_o/\mu_w = 1.94$ ,  $\rho_o/\rho_w = 0.78$ .**



**Figure 5-6: Comparison between Torres [43] flow pattern map (lines) and this study experimental flow pattern map (points), saline water,  $\mu_o/\mu_w = 1.536$ ,  $\rho_o/\rho_w = 0.732$ .**

As seen in Figure 5-1 to Figure 5-6, good agreement is observed between the models and the experimental data of this study. This agreement is seen in predicting the transition from smooth interface to mixture at the interface in the stratified flow, also in predicting the transition to semi dispersed flow and to fully dispersed flow.

Trallero [15] model gives excellent agreement with the experimental data in the stratified region, the dispersion of oil in water over a water layer (DO/W&W) region, and the dispersion of oil in water (DO/W) region. The dispersion of water in oil (DW/O) is slightly different than the experimental data.

In Brauner's model, the transition from stratified to stratified with mixing at the interface was obtained from Brauner [14] and [13]. While the transition from semi dispersed flow to fully dispersed flow in the water dominated region and in the oil dominated region was obtained by equation (7). The constant  $C_H$  which can be seen in equation (10) was set to 2 to give the best fitting with the experimental data. Also, the transition from stratified to semi dispersed in the water dominated region was obtained by equation (16), where the constant 4.36 was modified to 6.2 to suit the experimental data. The model shows excellent agreement in predicting the stratified region (ST), the dispersion of oil in water over a water layer (DO/W&W) region, the dispersion of oil in water (DO/W) region, and the dispersion of water in oil (DW/O) region.

The transition criteria in Torres [43] model can be found in equation (21) and equation (23) for semi dispersed flow and fully dispersed flow respectively. While for the stratified region, the same transition criteria of Trallero [15] were used. Good agreement can be seen in the dispersion of oil in water over a water layer (DO/W&W) region, the

dispersion of oil in water (DO/W) region, and the dispersion of water in oil (DW/O) region.

Brauner's [36] and Torres [43] models shows that the dispersion of water in oil over an oil layer region exists at low water flow rates. However, no data are available at that region to show the experimental flow pattern.

In comparing the experimental data of this study with other previous experimental work, similar results can be found in the flow pattern regions and regions boundaries is seen. The comparison considers Elseth [66] and Angeli [69] flow pattern maps since their used oil has the same properties of this study oil.



## 5.2 Pressure Drop

This section validates mixture viscosity models with the present pressure drop data and other published work. But first, the single phase analysis is provided.

### 5.2.1 Single phase Pressure Drop

The single phase pressure drop is calculated by equation (55) below.

$$\left(\frac{dp}{dL}\right)_f = \frac{f \cdot \rho \cdot U^2}{2d} \quad (55)$$

Where  $\left(\frac{dp}{dL}\right)_f$  is the frictional pressure loss inside the pipe,  $f$  is the friction factor,  $\rho$  is the density of the fluid,  $U$  is average the velocity of the fluid inside the pipe, and  $d$  is the pipe diameter. The friction factor correlation for smooth pipe is given as  $f = C \cdot Re^{-n}$ , Where  $C=16$ ,  $n=1$  for laminar flow, and  $C=.079$ ,  $n=0.25$  for turbulent.  $Re$  is the Reynolds number  $Re = \frac{\rho \cdot d \cdot U}{\mu}$ , Where  $\mu$  is the viscosity of the fluid.

The single phase data for oil, water, and saline water flow were validated previously in Figure 4-21, Figure 4-22, and Figure 4-23 in section 4.2, where the mixture velocity was plotted with the calculated and the experimental pressure.

## 5.2.2 Two Phase Pressure Drop

The experimental pressure drop data are compared with different previous studies with similar oil properties in Figure 5-7. The high mixture velocity pressure drop profiles are used from this study and from the other studies. The used pressure profiles from this study have 2.98 m/s (for tap and saline water) mixture velocity. The high mixture velocity profiles help better in displaying the differences between these pressure profiles.

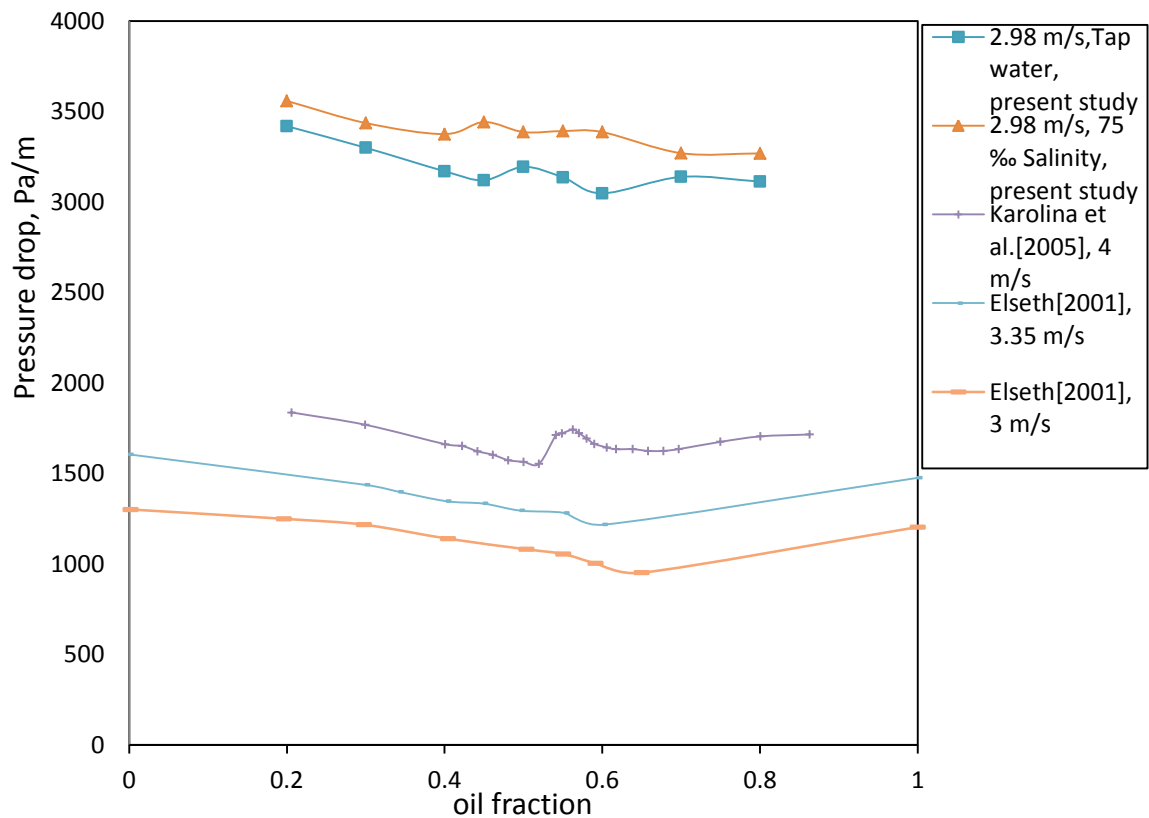


Figure 5-7: Experimental pressure drop of different mixture velocities taken from the present study along with the experimental work of Elseth [66] and Karolina et al. [64]

Figure 5-7 shows the pressure drops of Elseth [52], Karolina et al. [71], and this study. No data for pressure drop in Elseth's [66] work was recorded after 0.35 water cut for the 3.35 m/s and the 3 m/s mixture velocity profiles. No peak in the pressure drop was noticed in Elseth [66] data, this due to that peak might happened in the region where no data are available after 0.35 water cut; or else as he mentioned, the mixture velocity is too low for the peak to appear. Karolina et al. [64] mentioned that phase inversion was noticed at 56% oil fraction when starting from oil continuous phase. They also mentioned that phase inversion was preceded by a large increase in pressure gradient. This large increase is followed by a sharp reduction in pressure gradient after the new continuous phase is established. The properties of the used oil in the other works are shown in Table 2. Higher pressure is observed in this work since in the present work, the used pipe diameter is much smaller than the other works plotted in Figure 5-7. More pressure drop profiles for low viscosity oils are presented in Figure 5-8.

Given a review in Table 2 on previous experimental works with low viscosity oils, these experimental works will help in finding the behavior of pressure drop for this range of viscosity.

**Table 2: Previous experimental studies on oil-water in horizontal pipes with low viscosity range**

Author	Mixture velocity m/s	pipe material	Flow direction	$\rho_o$ kg/m <sup>3</sup>	$\mu_o$ cP	$\sigma$ mN/m	Diameter cm
Present study	2.98, 2.04, 2.8, 2.4	Acrylic	Horizontal	780	1.85	17	2.25
Karolina et al. [64]	3.5, 4	Steel, Acrylic	Horizontal	796	2.19	26.2	6
Elseth [66]	3.35, 3.5	St- steal	Horizontal	790	1.6	43	5.63
Lovick & Angeli [70]	3	St- Steel	Horizontal	828	6	27.6	3.8
Ngan et al. [71]	3	Acrylic	Horizontal	828	5.5	48.14	3.8
Lum et al. [67]	2	St- steal	Vertical	828	5.5	40	3.8
Rodriguez & Oliemans [72]	$U_o=3$ , $U_w=0.02\sim2.5$	Steel	Horizontal	830	7.5	-	8.28
Vielma [73]	$U_o=1.75$ , $U_w=0.02\sim1.77$	Acrylic	Horizontal	850	15	16	5.08
Charles [8]	0.03~1.07	Cellulose acetate-butyrate	Horizontal	998	16.8	45	2.64

The data shown in Table 2 has a kinematic viscosity range from 1.6 to 17 cP, while density ranges from 780 to 998 kg/m<sup>3</sup>. Some of these studies have greater oil (single phase) pressure than water while others have less. The previous works is used in the comparison with several mixture viscosity models will be presented in section 5.2.2.1.

The two phase pressure drops in these studies have lower value than the single phase water pressure drop, where pressure is noticed to decrease as it approaches inversion point or a certain oil fraction, see Figure 5-8.

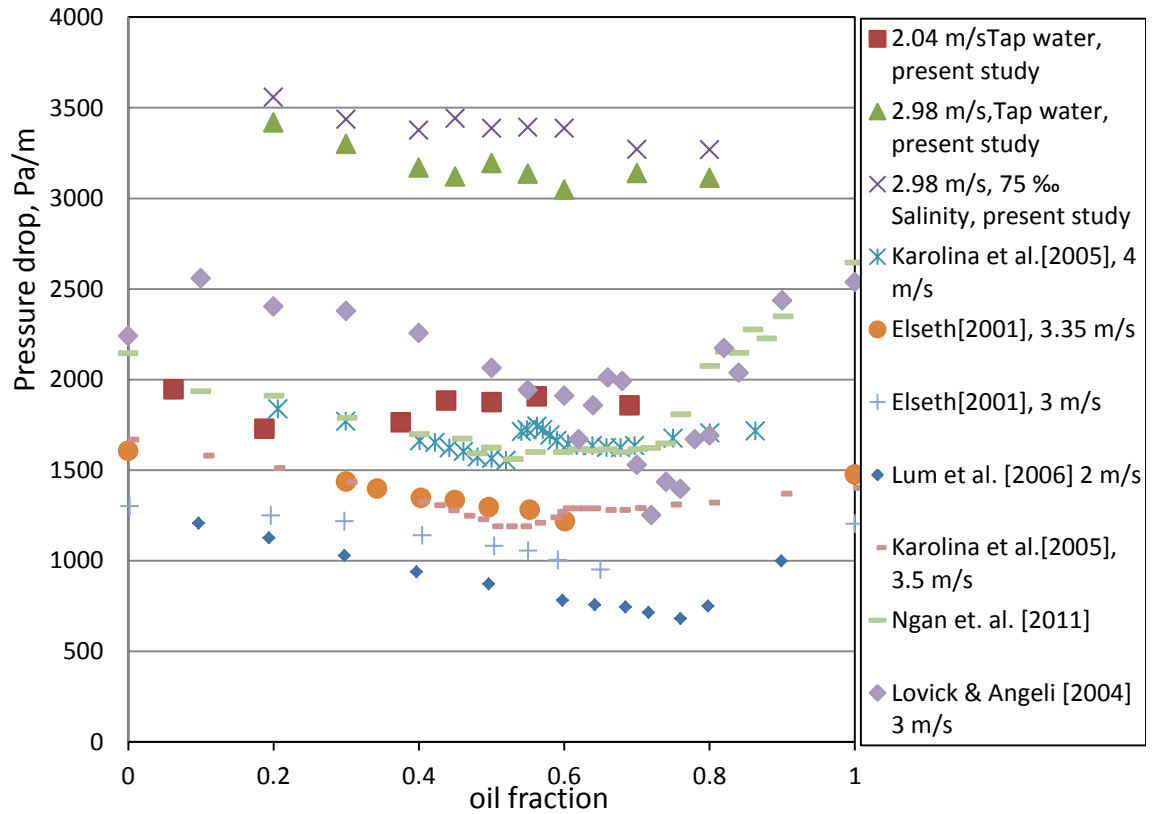


**Figure 5-8: Experimental pressure drop for several previous works taken from Table 2 along with the present study**

### 5.2.2.1 Comparison with models

The experimental data are compared with the Homogenous model of mixture viscosity in dispersed flow, and the Two-Fluid-Model (TFM) in stratified flow. Figure 5-9 below shows both the TFM and the Homogenous model on single plot, where each one predicts a certain region of flow pattern.

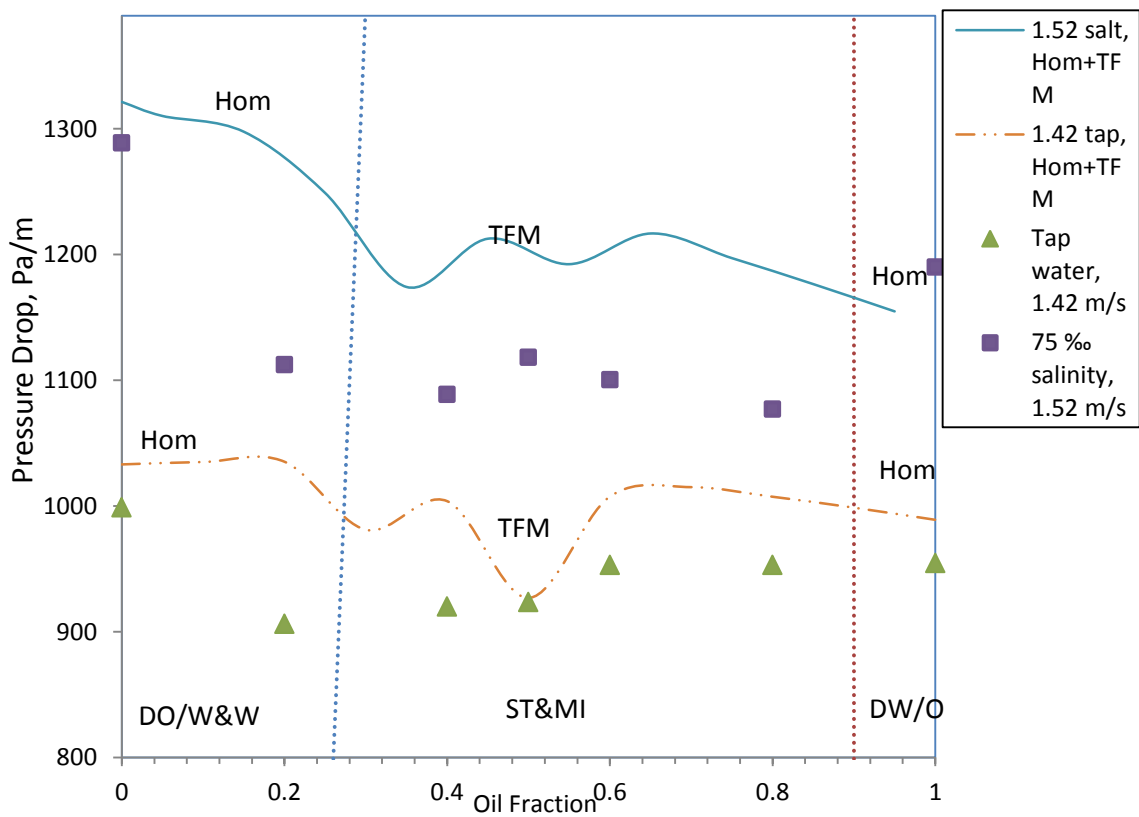


Figure 5-9: Comparison between the Homogenous Model along with the Two-Fluid-Model and the present experimental work

In Figure 5-9, the experiment data are plotted with the Two-Fluid-Model in the stratified region and the homogenous model in the dispersed region. It can be noticed that the TFM predicts well the stratified flow compared with the Homogenous model. Another comparison between the experimental data for tap and saline water with the Homogenous model in dispersed flow are given in Figure 5-10 and Figure 5-11.

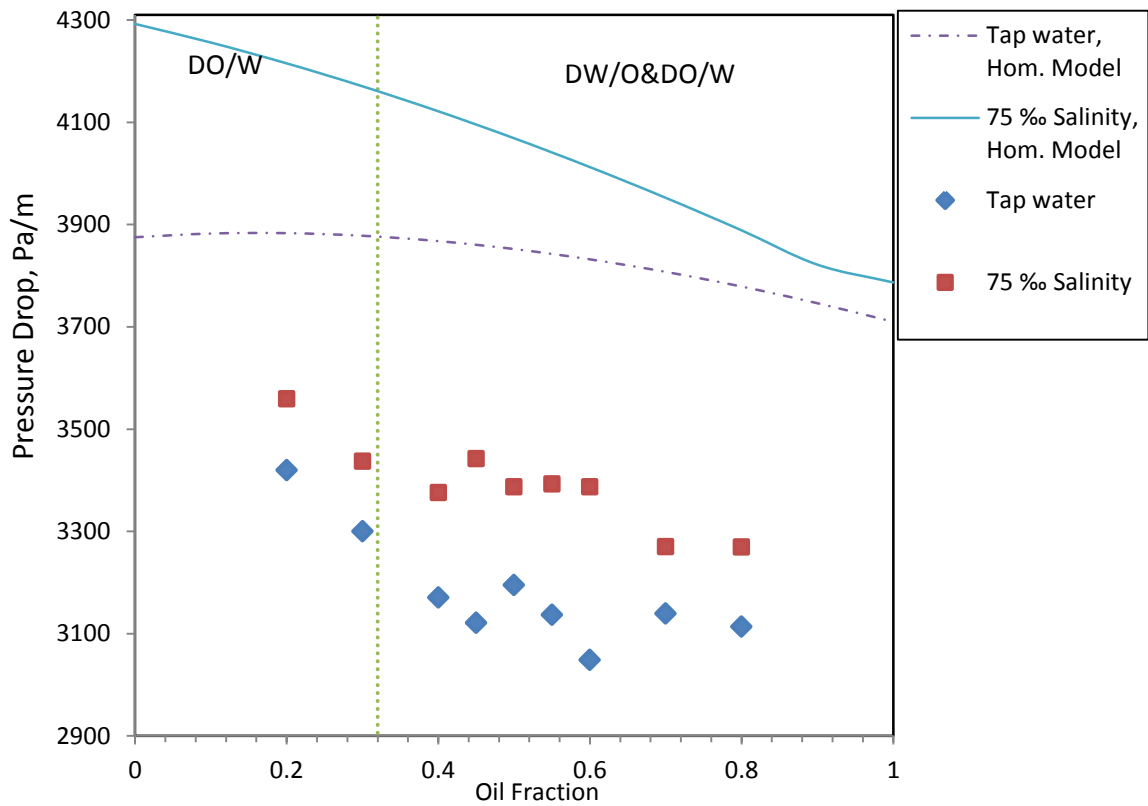


Figure 5-10: Comparison between the Homogenous Model and the present experimental work

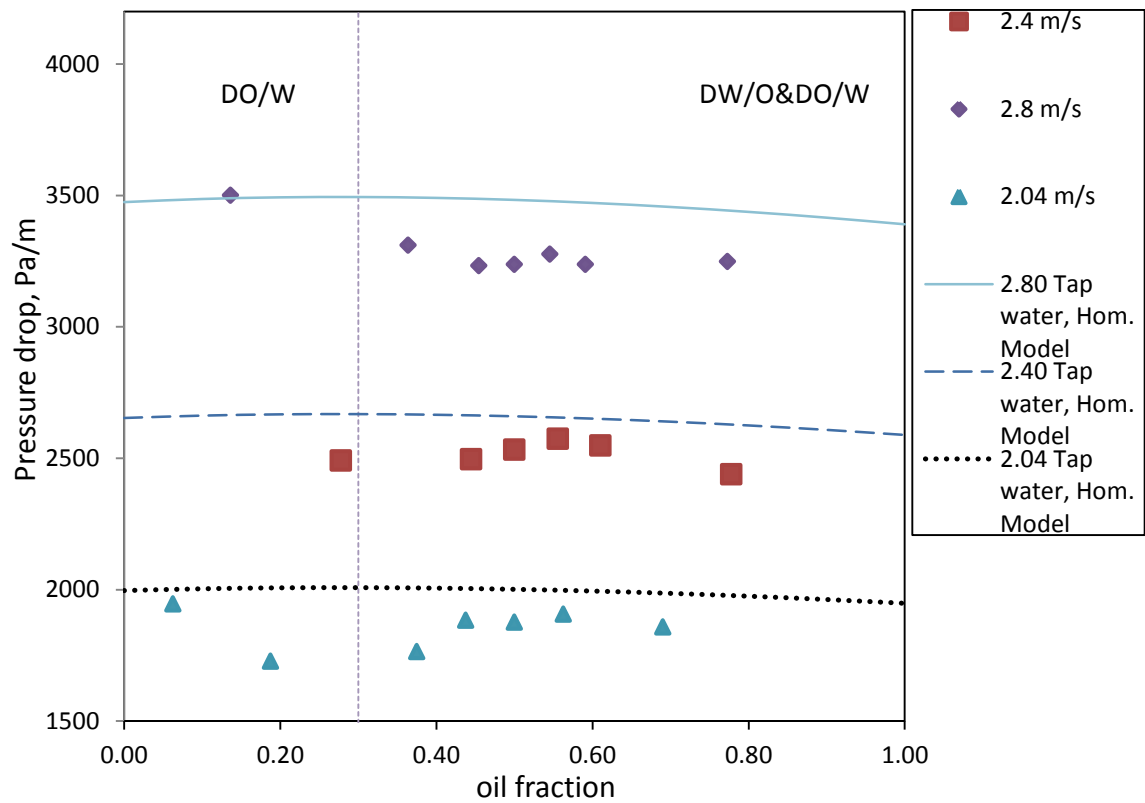
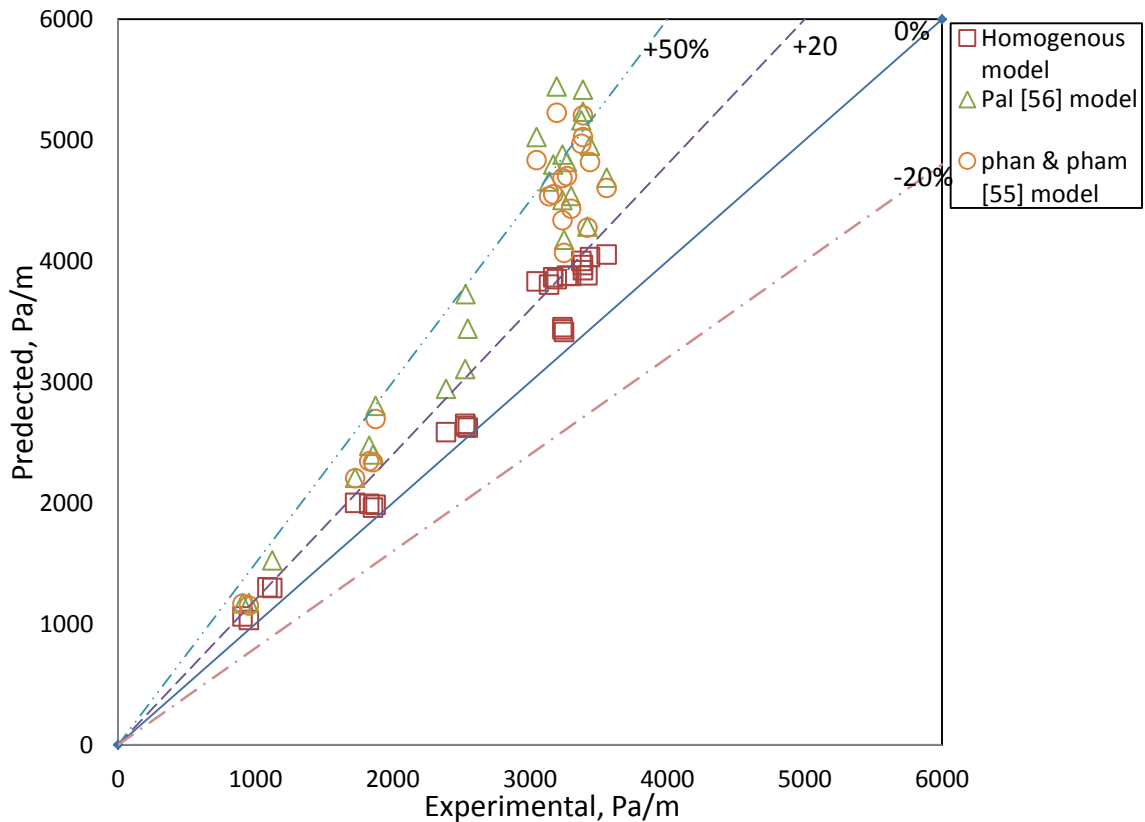


Figure 5-11: Comparison between the Homogenous Model and the present experimental work, 17 °C



In Figure 5-10 and Figure 5-11, the Homogenous model has a straight profile of the pressure drop unlike the experimental data. This means that the corresponding error will be high especially at inversion point (at 0.52 oil fraction).

The other mentioned models in the literature predicts pressure drop for profiles that have maximum pressure drop value at inversion, where pressure drop increases towards inversion point. So, these models will give high error in predicting pressure drop with minimum pressure value at inversion, such as in this study pressure drop profile. To show the error range of these models, the theoretical and experimental values are plotted in Figure 5-12 together with pal [56] and phan and pham [55] models of mixture viscosity.



**Figure 5-12: Comparison between theoretical and experimental values of pressure drop from this study using the Homogenous, pal [56], and phan and pham [55] models**

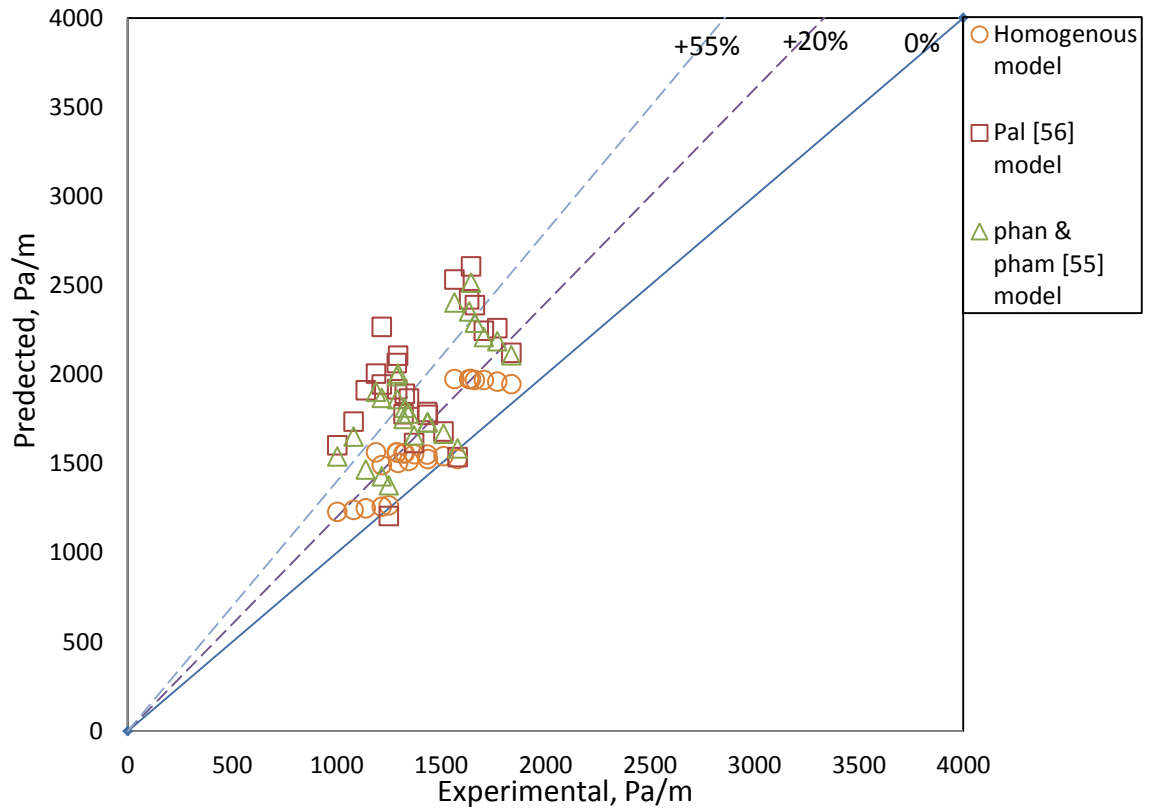


**Figure 5-13: Comparison between theoretical and experimental values of pressure drop of Elseth [66] and Karolina et al. [64] experimental data taken from Figure 5-7.**

As can be seen from Figure 5-12 and Figure 5-13, pal [56] and phan and pham [55] models along with Homogenous model over predict the actual value. It is also noticed that the Homogenous model gives less error and shows better agreement than the other models with low viscosity oils.

### 5.2.2.1.1 Modified Correlation of Mixture Viscosity

A new correlation is suggested to cover the low oil viscosity region. The correlation was developed based on Brinkman's [48] model with a modified dispersion factor as below:

$$\frac{\mu_m}{\mu_c} = (1 - \varepsilon_d)^{0.8 \mu_c / \mu_d} \quad (56)$$

Instead of using the constant -2.5, the model uses the viscosity ratio of the continuous and the dispersed phase multiplied with a factor found experimentally to give a best fitting with the experimental data. The correlation shows better prediction and gives less error than the Homogenous model. The correlation was compared with the given work in Table 2 to show its accuracy in prediction the frictional pressure drop. The comparison is showed in Figure 5-15 and Figure 5-16 below.

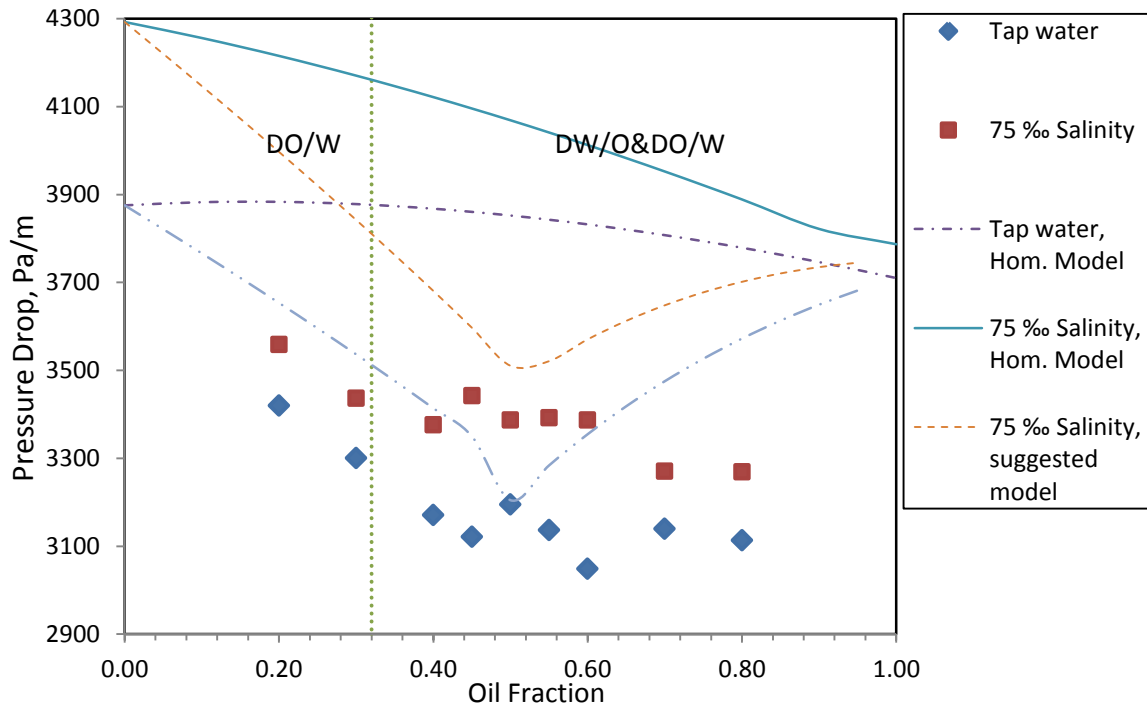


Figure 5-14: Comparison between suggested model and the Homogenous model with the experimental work of this study for  $U_m = 2.98$  m/s.

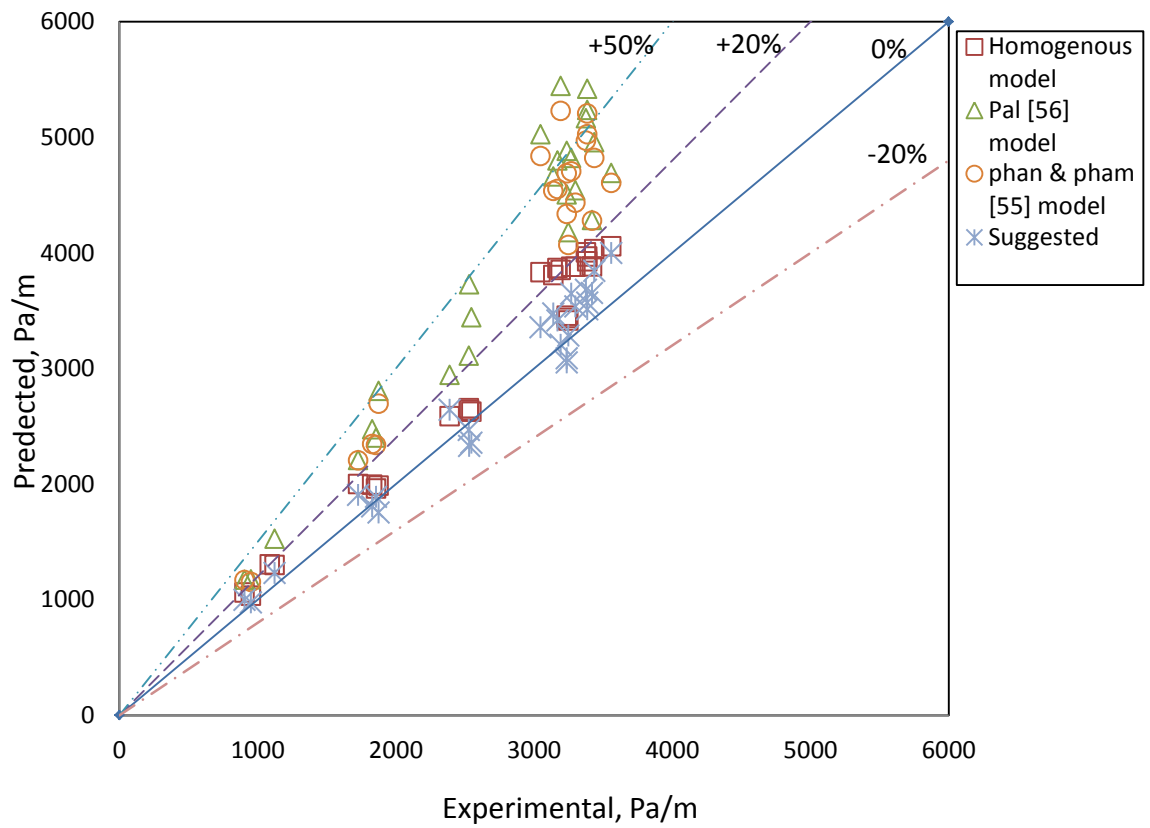
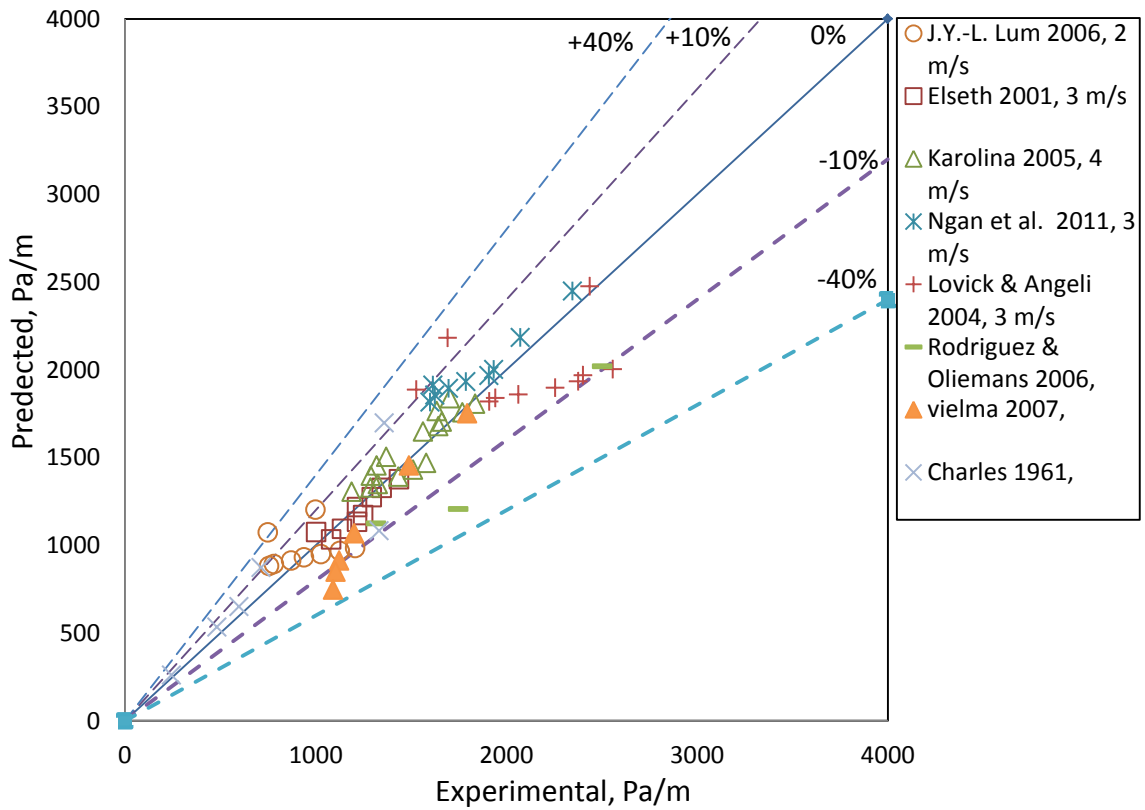


Figure 5-15: Comparison between the suggested model, pal [56] model, and phan and pham [55] model with the experimental work of this study.



**Figure 5-16: Comparison between the suggested model and the experimental work of several works mentioned in Table 2**

As seen in Figure 5-14, Figure 5-15, and Figure 5-16, a better prediction is obtained using the suggested correlation than the other models. The average error was reduced using this study data from 15% when using the Homogenous model to about 5%. Moreover when using the previous works mentioned in Table 2, the average error was less 10% as can be seen from Figure 5-16 and Table 3.

Table 3 shows the average error and the root mean square error for the Homogenous model, suggested correlation, pal [56] model, and phan and pham [55] model. The average and the root mean square errors were found by the following relations:

$$\text{Error} = \frac{|\text{Pre}-\text{Exp}|}{\text{Exp}} * 100\% \quad (57)$$

$$\text{Average Error (AVG)} = \frac{\sum \text{Error}}{n} \quad (58)$$

$$\text{Root Mean Square Error (RMS)} = \sqrt{\frac{\sum \text{Error}^2}{n-1}} \quad (59)$$

Where Pre, Exp, and n are the predicted value, the experimental value, and the number of data respectively.

**Table 3: Percent error in the new correlation**

works in Table 2	Homogenous model	Pal model	Phan & pham	Suggested correlation
Average error %	14.5	42.4	34.4	10.3
Rms %	52.4	66.4	59.8	33.2
The experimental data of this study				
Average error %	13.1	41.4	39.1	6.7
Rms %	37.1	65.3	63.7	26.7

It can be noticed from Table 3 that the minimum average error and the minimum root mean square error value is seen in the suggested correlation. The root mean square error for the suggested correlation is 33 for the experimental data in Table 2 and 27 while using this study experimental data. However the root mean square error value for the homogenous model is 52 for data in Table 2 and 37 for this study experimental data. Higher average error and root mean square error values are seen in pal [56] model, and phan and pham [55] model.

Xu, J. et al. [74] mentioned that the pressure drop at inversion was minimum in the performed experiments, they used high viscosity oil (44 cP viscosity and  $860 \text{ kg/m}^3$  density), where the pressure drop was taken in upward and downward flow. However, the data were compared with the suggested model and showed high error in predicting the pressure drop especially near inversion.

#### **5.2.2.2 Inversion Point**

From the pressure drop figures in section 4.2, the inversion was considered to occur at 0.52 oil fraction for all the mixture velocities as an average value. A comparison is made with the inversion models and presented in

Table 4. The experimental works mentioned in Table 2 will be also included.

**Table 4: Comparison between inversion point models and experimental data**

Method	This study		Karolina et al. [64]	Elseth [66]	Lovick & Angeli [70]	Ngan et al. [71]	Lum et al. [67]
	Tap water	75 % salinity					
Experimental value	0.5~0.56	0.45	0.56	$\geq 0.75$	0.64	0.65	0.8
Arirachakaran et al. [9]	0.53	0.52	0.54	0.52	0.59	0.58	0.58
Yeh et al. [58]	0.58	0.55	0.6	0.56	0.71	0.7	0.7
Brauner and Ullman [59]	0.5	0.46	0.52	0.5	0.63	0.62	0.62

Elseth [66] mentioned that the continuous phase of oil will become the dispersed phase close to 0.35 water cut, the change is considered to happen at this water cut value. No peak in the pressure drop was noticed in Elseth [66] data, this due to that peak might occur after 0.35 water cut, or the mixture velocity is too low for the peak to appear as he mentioned,.

Lum et al. [67] mentioned that the pressure drop decreases as the oil fraction increases until 80% oil fraction, then pressure starts to increase. They mentioned that the change in the pressure happened due the change in the flow pattern from dispersed water-in-oil to dual continuous flow. No peak was noticed at this oil fraction.

In Karolina et al. [64] work, phase inversion happened at 56% oil fraction, and a peak in the pressure is seen at inversion. The pressure drop in Lovick & Angeli [70] work



decreases with the increase of oil fraction until inversion happens at 36% water cut. After that pressure starts to increase towards the single phase oil value. No peak in the pressure is seen at inversion.

It can be noticed from the table that all of the above models can be used to predict the inversion point location. However, more accurate prediction of inversion point is seen in Brauner and Ullman [59] for the experimental data of this study.

The peak in the pressure drop was seen only in this study along with Valle and Utvik [62], Soleimani et al. [63] and Karolina et al. [64]. This phenomenon could be dedicated to the type of oils which was used or their physical properties.

## **CHAPTER 6**

### **CONCLUSIONS AND RECOMMENDATION**

#### **6.1 Conclusions**

1. New experimental data are presented for oil-water flow in an acrylic horizontal pipe, where the oil has a  $781 \text{ kg/m}^3$  density and a 1.85 cP viscosity at  $25^\circ\text{C}$ .
2. The effect of salt on flow pattern map and pressure drop was investigated. It was found that for saline water, the transition from Dispersion of oil in water over a water layer flow pattern to the Dispersion of water in oil and oil in water to the flow pattern was delayed. Moreover, it was noticed in the stratified with mixture at the interface flow pattern, the waves in saline water has less amplitudes than that in tap water.
3. The pressure drop behavior was affected with the salt as follows:
  - a. Inversion point started earlier in saline water (0.45 for saline water, and 0.5 for tap water).
  - b. Saline water has less change in the pressure with the change of the oil fraction than tap water, or the pressure decreasing rate for saline water is less than that for tap water.
4. The flow pattern map of tap water and saline water were compared with Trallero, Brauner, and Torres models of oil-water flow pattern map and a good agreement was noticed.

5. The pressure drop data were compared with several previous model of mixture viscosity, a new correlation was suggested to estimate the pressure drop for low viscosity oils and showed better results in the prediction of the pressure profile.

The disadvantage of adding salt is that the pressure is increased. Thus more pumping power is needed compared with tap water. While the advantage is that salt reduced the rate of change in the pressure due to inversion and the fluctuations in pressure has less peak value.

## 6.2 Recommendation

The following are recommended for future studies:

- Effect of salt on the pressure drop and the flow pattern for high viscosity oils.
- Effect of salt on holdup and droplet size.
- Using saline water with other salt percentages to provide more data on salinity effect

The following are suggested for the experimental facility:

- Installing new techniques to measure the actual holdup, the droplet size, and the flow pattern detection.
- Using larger diameter pipe to reduce the pressure generated at high flow rates which allow reaching higher mixture velocities.

## References

- [1] J. R. Fair, "What You Need to Know to Design Thermosyphon Reboilers," *Petroleum Refiner*, vol. 39, 1960.
- [2] R. Lockhart and R. Martinelli, "Proposed correlation of data for isothermal two-phase, two-component flow in pipes," *Chem. Eng. Prog.*, vol. 45, pp. 39-48, 1949.
- [3] Y. Taitel and A. Dukler, "A model for predicting flow regime transitions in horizontal and near horizontal gas-liquid flow," *AIChE Journal*, vol. 22, pp. 47-55, 1976.
- [4] O. P. Bergelin and C. Gazley, "Cocurrent Gas-Liquid Flow, I. Flow in Horizontal Tubes," *ASME Proc. Heat Transfer and Fluid Mech. Inst.*, pp. 5-18, 1949.
- [5] H. Johnson and A. Abou-Sabe, "Heat transfer and pressure drop for turbulent flow of air-water mixtures in a horizontal pipe," *Trans. ASME*, vol. 74, pp. 977-987, 1952.
- [6] O. Baker, "Simultaneous flow of oil and gas," *Oil and Gas J.*, vol. 53, pp. 185-195, 1954.
- [7] T. Russell, G. Hodgson, and G. Govier, "Horizontal pipeline flow of mixtures of oil and water," *the Canadian Journal of Chemical engineering*, vol. 37, pp. 9-17, 1959.
- [8] M. E. Charles, G. Govier, and G. Hodgson, "The horizontal pipeline flow of equal density oil-water mixtures," *the Canadian Journal of Chemical engineering*, vol. 39, pp. 27-36, 1961.
- [9] S. Arirachakaran, K. Oglesby, M. Malinowsky, O. Shoham, and J. Brill, "An analysis of oil/water flow phenomena in horizontal pipes," 1989.
- [10] J. Trallero, C. Sarica, and J. Brill, "A study of oil-water flow patterns in horizontal pipes," *Oil Production & Facilities*, vol. 12, pp. 165-172, 1997.
- [11] M. Nädler and D. Mewes, "Flow induced emulsification in the flow of two immiscible liquids in horizontal pipes," *International journal of multiphase flow*, vol. 23, pp. 55-68, 1997.
- [12] P. Abduvayt, R. Manabe, T. Watanabe, and N. Arihara, "Analysis of Oil-Water Flow Tests in Horizontal, Hilly-Terrain, and Vertical Pipes," 2004.
- [13] N. Brauner and D. Moalem Maron, "Flow pattern transitions in two-phase liquid-liquid flow in horizontal tubes," *International journal of multiphase flow*, vol. 18, pp. 123-140, 1992.
- [14] N. Brauner and D. Moalem Maron, "Stability analysis of stratified liquid-liquid flow," *International journal of multiphase flow*, vol. 18, pp. 103-121, 1992.
- [15] J. L. Trallero, "Oil-water flow patterns in horizontal pipes," University of Tulsa, 1995.

- [16] E. S. Kordyban and T. Ranov, "Mechanism of slug formation in horizontal two-phase flow," *Journal of Basic Engineering*, vol. 92, p. 857, 1970.
- [17] E. Kordyban, "Some characteristics of high waves in closed channels approaching Kelvin-Helmholtz instability," *Journal of Fluids Engineering*, vol. 99, p. 339, 1977.
- [18] K. Mishima and M. Ishii, "Theoretical prediction of onset of horizontal slug flow," *Journal of Fluids Engineering*, vol. 102, p. 441, 1980.
- [19] G. B. Wallis and J. E. Dodson, "The onset of slugging in horizontal stratified air-water flow," *International journal of multiphase flow*, vol. 1, pp. 173-193, 1973.
- [20] G. Wallis, "One-dimensional Two Phase Flow," ed. New York: McGraw-Hill, 1969.
- [21] P. Lin and T. Hanratty, "Prediction of the initiation of slugs with linear stability theory," *International journal of multiphase flow*, vol. 12, pp. 79-98, 1986.
- [22] H. Wu, B. Pots, J. Hollenberg, and R. Meerhoff, "Flow pattern transitions in two-phase gas/condensate flow at high pressure in an 8-inch horizontal pipe," 1987, pp. 13-21.
- [23] N. Andritsos, L. Williams, and T. Hanratty, "Effect of liquid viscosity on the stratified-slug transition in horizontal pipe flow," *International journal of multiphase flow*, vol. 15, pp. 877-892, 1989.
- [24] D. Barnea, "On the effect of viscosity on stability of stratified gas--liquid flow--application to flow pattern transition at various pipe inclinations," *Chemical engineering science*, vol. 46, pp. 2123-2131, 1991.
- [25] C. Crowley, G. Wallis, and J. Barry, "Validation of a one-dimensional wave model for the stratified-to-slug flow regime transition, with consequences for wave growth and slug frequency," *International journal of multiphase flow*, vol. 18, pp. 249-271, 1992.
- [26] D. Barnea and Y. Taitel, "Kelvin-Helmholtz stability criteria for stratified flow: viscous versus non-viscous (inviscid) approaches," *International journal of multiphase flow*, vol. 19, pp. 639-649, 1993.
- [27] T. J. Hanratty and A. Hershman, "Initiation of roll waves," *AIChE Journal*, vol. 7, pp. 488-497, 1961.
- [28] P. Andreussi, J. Asali, and T. Hanratty, "Initiation of roll waves in gas-liquid flows," *AIChE Journal*, vol. 31, pp. 119-126, 1985.
- [29] D. Barnea and Y. Taitel, "Transient-formulation modes and stability of steady-state annular flow," *Chemical engineering science*, vol. 44, pp. 325-332, 1989.
- [30] D. Barnea and Y. Taitel, "Nonlinear stability and dynamic simulation of annular flow," *Chemical engineering science*, vol. 45, pp. 3367-3371, 1990.
- [31] D. Barnea and Y. Taitel, "Structural and interfacial stability of multiple solutions for stratified flow," *International journal of multiphase flow*, vol. 18, pp. 821-830, 1992.

- [32] D. Barnea and Y. Taitel, "Interfacial and structural stability of separated flow," *International journal of multiphase flow*, vol. 20, pp. 387-414, 1994.
- [33] L. Jurman and M. McCready, "Study of waves on thin liquid films sheared by turbulent gas flows," *Physics of Fluids A: Fluid Dynamics*, vol. 1, p. 522, 1989.
- [34] J. Hinze, "Fundamentals of the hydrodynamic mechanism of splitting in dispersion processes," *AIChE Journal*, vol. 1, pp. 289-295, 1955.
- [35] V. G. Levich and D. B. Spalding, *Physicochemical hydrodynamics* vol. 689: Prentice-Hall Englewood Cliffs, NJ, 1962.
- [36] N. Brauner, "The prediction of dispersed flows boundaries in liquid-liquid and gas-liquid systems," *International journal of multiphase flow*, vol. 27, pp. 885-910, 2001.
- [37] A. N. Kolmogorov, "On the breaking of drops in turbulent flow," *Doklady Akad. Nauk.*, vol. 66, pp. 825-828, 1949.
- [38] D. Barnea, "A unified model for predicting flow-pattern transitions for the whole range of pipe inclinations," *International journal of multiphase flow*, vol. 13, pp. 1-12, 1987.
- [39] R. S. Brodkey, *The Phenomena of Fluid Motions*: Addison-Wesley Reading, MA, 1969.
- [40] A. D. G. A. Guzhov, V.F. Medredev, O.P. Medredeva, "Emulsion formation during the flow of two immiscible liquids," *Neft. Choz. (in Russian)*, pp. 58-61, 1973.
- [41] N. Brauner, "Modelling and control of two-phase phenomena: liquid-liquid two-phase flow systems," *Course notes Udine, PDF available on Internet.[Links]*, 2002.
- [42] N. Brauner, "The onset of drops atomization and the prediction of annular flow boundaries in two-phase pipe flow," Internal Report-5101, Faculty of Engineering, Tel-Aviv, Israel 2000.
- [43] C. F. Torres-Monzon, "Modeling of oil-water flow in horizontal and near horizontal pipes," The University of Tulsa, 2006.
- [44] X. Chen, X. Cai, and J. Brill, "A general model for transition to dispersed bubble flow," *Chemical engineering science*, vol. 52, pp. 4373-4380, 1997.
- [45] A. Einstein, "Berichtigung zu meiner Arbeit:" Eine neue Bestimmung der Moleküldimensionen," Jän 1911.
- [46] G. I. Taylor, "The viscosity of a fluid containing small drops of another fluid," *Proceedings of the Royal Society of London. Series A*, vol. 138, pp. 41-48, 1932.
- [47] M. Mooney, "The viscosity of a concentrated suspension of spherical particles," *Journal of Colloid Science*, vol. 6, pp. 162-170, 1951.
- [48] H. Brinkman, "The viscosity of concentrated suspensions and solutions," *The Journal of Chemical Physics*, vol. 20, p. 571, 1952.

- [49] R. Roscoe, "The viscosity of suspensions of rigid spheres," *British Journal of Applied Physics*, vol. 3, p. 267, 2002.
- [50] I. M. Krieger and T. J. Dougherty, "A mechanism for non-Newtonian flow in suspensions of rigid spheres," *Transactions of the Society of Rheology*, vol. 3, pp. 137-152, 1959.
- [51] H. Furuse, "Viscosity of concentrated solution," *Japanese Journal of Applied Physics*, vol. 11, p. 1537, 1972.
- [52] I. Yaron and B. Gal-Or, "On viscous flow and effective viscosity of concentrated suspensions and emulsions," *Rheologica Acta*, vol. 11, pp. 241-252, 1972.
- [53] S. J. Choi and W. Schowalter, "Rheological properties of nondilute suspensions of deformable particles," *Physics of Fluids*, vol. 18, p. 420, 1975.
- [54] R. Pal and E. Rhodes, "Viscosity/Concentration Relationships for Emulsions," *Journal of Rheology*, vol. 33, pp. 1021-1045, 1989.
- [55] N. Phan-Thien and D. Pham, "Differential multiphase models for polydispersed suspensions and particulate solids," *Journal of Non-Newtonian Fluid Mechanics*, vol. 72, pp. 305-318, 1997.
- [56] R. Pal, "Novel viscosity equations for emulsions of two immiscible liquids," *Journal of Rheology*, vol. 45, pp. 509-520, 2001.
- [57] R. Pal, "Single-parameter and two-parameter rheological equations of state for nondilute emulsions," *Industrial & engineering chemistry research*, vol. 40, pp. 5666-5674, 2001.
- [58] G. C. Yeh, F. H. Haynie Jr, and R. A. Moses, "Phase-volume relationship at the point of phase inversion in liquid dispersions," *AIChE Journal*, vol. 10, pp. 260-265, 1964.
- [59] N. Brauner and A. Ullmann, "Modeling of phase inversion phenomenon in two-phase pipe flows," *International journal of multiphase flow*, vol. 28, pp. 1177-1204, 2002.
- [60] P. Poesio and G. Beretta, "Minimal dissipation rate approach to correlate phase inversion data," *International journal of multiphase flow*, vol. 34, pp. 684-689, 2008.
- [61] Available: [www.safraco.com](http://www.safraco.com)
- [62] A. Valle and O. H. Utvik, "Pressure drop, flow pattern and slip for two phase crude oil/water flow: experiments and model predictions," *ICHMT DIGITAL LIBRARY ONLINE*, vol. 5, 1997.
- [63] A. Soleimani, C. Lawrence, and G. F. Hewitt, "Effect of mixers on flow pattern and pressure drop in horizontal oil-water pipe flow," *ICHMT DIGITAL LIBRARY ONLINE*, vol. 5, 1997.
- [64] K. Ioannou, O. J. Nydal, and P. Angeli, "Phase inversion in dispersed liquid-liquid flows," *Experimental thermal and fluid science*, vol. 29, pp. 331-339, 2005.



- [65] A. Soleimani, "Phase distribution and associated phenomena in oil-water flows in horizontal tubes," Imperial College London (University of London), 1999.
- [66] G. Elseth, "An experimental study of oil/water flow in horizontal pipes," Norwegian University of Science and Technology, 2001.
- [67] J. Y. L. Lum, T. Al-Wahaibi, and P. Angeli, "Upward and downward inclination oil–water flows," *International journal of multiphase flow*, vol. 32, pp. 413-435, 2006.
- [68] R. Pal, "Pipeline flow of unstable and surfactant-stabilized emulsions," *AIChE Journal*, vol. 39, pp. 1754-1764, 1993.
- [69] P. Angeli, "Liquid-liquid dispersed flows in horizontal pipes," Imperial College London (University of London), 1996.
- [70] J. Lovick and P. Angeli, "Experimental studies on the dual continuous flow pattern in oil–water flows," *International journal of multiphase flow*, vol. 30, pp. 139-157, 2004.
- [71] K. H. Ngan, K. Ioannou, L. D. Rhyne, and P. Angeli, "Effect of glycerol addition on phase inversion in horizontal dispersed oil–water pipe flows," *Experimental thermal and fluid science*, vol. 35, pp. 628-635, 2011.
- [72] O. Rodriguez and R. Oliemans, "Experimental study on oil–water flow in horizontal and slightly inclined pipes," *International journal of multiphase flow*, vol. 32, pp. 323-343, 2006.
- [73] M. Vielma, S. Atmaca, C. Sarica, and H. Q. Zhang, "Characterization of oil/water flows in horizontal pipes," in *SPE Annual Technical Conference and Exhibition*, 2007.
- [74] J. Xu, D. Li, J. Guo, and Y. Wu, "Investigations of phase inversion and frictional pressure gradients in upward and downward oil–water flow in vertical pipes," *International journal of multiphase flow*, vol. 36, pp. 930-939, 2010.

## Appendix1: Uncertainty Analysis

Given the percentage error for the big flow meters to be  $\pm 4\%$  at full scale, where they range from 5 to 40 gpm. While for the small flow meters which ranged from 1 to 10 gpm, the error percentage was about  $\pm 1\%$  at full scale. The repeatability of the big and the small flow meters was  $\pm 1\%$ . For the manometer, the error was given to be 1 mm of water. The uncertainties of the instruments are shown in Table 5. Also the error in the S/Mill-E instrument which is used to measure water salinity and water density is provide in the table.

The error in flow meters is found by multiplying the full scale (FS) error by the maximum value on the flow meter range. For an example, the uncertainty in the flow rate  $U_{\dot{m}}$  for the big flow meter which has a 4% error at FS is found by:

$$U_{\dot{m}} = 4\% * 40 = 1.6 \text{ gpm}$$

When the function  $R$  is a function of  $a, b, c, \dots$ , then the uncertainty  $U_R$  is a function of the independent uncertainties of  $a, b, c, \dots$ :

$$U_R = \sqrt{\left(\frac{dR}{da}\right)^2 U_a^2 + \left(\frac{dR}{db}\right)^2 U_b^2 + \left(\frac{dR}{dc}\right)^2 U_c^2 + \dots} \quad (60)$$

Where  $U_a, U_b, U_c$  are the uncertainties of the functions  $a, b$ , and  $c$ . This correlation can be used when counting human error. However no combined uncertainty is used in this study.

**Table 5: Evaluation of the uncertainty analysis**

measured variable	Instrument	Error at FS	Unit	Instrument range	Error value	Used range	Uncertainty (U)
Mass flow rate ( $\dot{m}$ )	Big flow meter	$\pm 4\%$	gpm	5 - 40	$\pm 1.6$ gpm	5 - 18	$U_{\dot{m}} = 1.6$ gpm
Mass flow rate ( $\dot{m}$ )	Small flow meter	$\pm 1\%$	gpm	1 - 10	$\pm 0.1$ gpm	1 - 10	$U_{\dot{m}} = 0.1$ gpm
Pressure (P)	Water manometer	-	mm	1 - 1000	$\pm 1$ mm	10 - 800	$U_P = 1$ mm
Salinity (S)	S/Mill-E	-	parts per thousand (‰)	0 - 100	$\pm 1$	0 - 100	$U_S = 1$ ‰
Specific gravity (Sg)	S/Mill-E	-	-	1 - 1.070	$\pm 0.001$	1 - 1.070	$U_{Sg} = 0.001$

## Appendix2: Pressure Drop Data

Temp. °C	U <sub>o</sub> m/s	U <sub>w</sub> m/s	U <sub>m</sub> m/s	ρ <sub>o</sub> kg/m <sup>3</sup>	ρ <sub>w</sub> kg/m <sup>3</sup>	μ <sub>o</sub> cP	μ <sub>w</sub> cP	Re	dP Pa/m	Additional info
17	-	0.76		808	1000	2.25	1.386	12413	363	Tap water
17	-	1.02		808	1000	2.25	1.386	16551	597	Tap water
17	-	1.27		808	1000	2.25	1.386	20688	892	Tap water
17	-	1.66		808	1000	2.25	1.386	26895	1531	Tap water
17	-	1.91		808	1000	2.25	1.386	31032	1941	Tap water
17	-	2.29		808	1000	2.25	1.386	37239	2709	Tap water
17	-	2.47		808	1000	2.25	1.386	40097	3071	Tap water
17	-	2.55		808	1000	2.25	1.386	41376	3269	Tap water
17	-	2.72		808	1000	2.25	1.386	44156	3605	Tap water
17	-	2.80		808	1000	2.25	1.386	45514	3871	Tap water
17	1.27	-		808	1000	2.25	1.386	9086	841	Tap water
17	2.17	-		808	1000	2.25	1.386	15446	2314	Tap water
17	3.22	-		808	1000	2.25	1.386	22983	4412	Tap water
17	1.22	-		808	1000	2.25	1.386	8700	643	Tap water
17	1.31	-		808	1000	2.25	1.386	9344	732	Tap water
17	1.63	-		808	1000	2.25	1.386	11597	1079	Tap water
17	1.91	-		808	1000	2.25	1.386	13625	1442	Tap water
17	2.48	-		808	1000	2.25	1.386	17716	2314	Tap water
17	2.69	-		808	1000	2.25	1.386	19170	2667	Tap water
17	3.04	-		808	1000	2.25	1.386	21653	3321	Tap water
17	2.21	-		808	1000	2.25	1.386	15752	1873	Tap water
17	2.12	-		808	1000	2.25	1.386	15137	1743	Tap water
17	1.77	-		808	1000	2.25	1.386	12643	1261	Tap water
17	1.44	-		808	1000	2.25	1.386	10299	872	Tap water
17	1.25	-		808	1000	2.25	1.386	8932	675	Tap water
17	1.21	-		808	1000	2.25	1.386	8660	638	Tap water
17	-	1.17		808	1000	2.25	1.386	19027	633	Tap water
17	-	1.46		808	1000	2.25	1.386	23757	944	Tap water
17	-	1.91		808	1000	2.25	1.386	31076	1531	Tap water
17	-	2.18		808	1000	2.25	1.386	35454	1941	Tap water
17	-	2.63		808	1000	2.25	1.386	42668	2709	Tap water
17	-	2.92		808	1000	2.25	1.386	47367	3269	Tap water
17	-	3.21		808	1000	2.25	1.386	52030	3871	Tap water
17	-	1.85		808	1000	2.25	1.386	30007	1437	Tap water
17	-	1.54		808	1000	2.25	1.386	24971	1033	Tap water
17	-	1.40		808	1000	2.25	1.386	22653	867	Tap water
17	-	1.12		808	1000	2.25	1.386	18142	581	Tap water

17	-	0.85		808	1000	2.25	1.386	13751	353	Tap water
17	0.89	-		808	1000	2.25	1.386	6360	643	Tap water
17	1.02	-		808	1000	2.25	1.386	7269	732	Tap water
17	1.27	-		808	1000	2.25	1.386	9086	841	Tap water
17	1.53	-		808	1000	2.25	1.386	10903	1079	Tap water
17	1.78	-		808	1000	2.25	1.386	12720	1442	Tap water
17	2.17	-		808	1000	2.25	1.386	15446	2314	Tap water
17	-	0.64		808	1000	2.25	1.386	10344	280	Tap water
17	-	0.76		808	1000	2.25	1.386	12413	353	Tap water
17	-	1.02		808	1000	2.25	1.386	16551	581	Tap water
17	-	1.02		808	1000	2.25	1.386	16551	638	Tap water
17	-	1.27		808	1000	2.25	1.386	20688	867	Tap water
17	-	1.27		808	1000	2.25	1.386	20688	960	Tap water
17	-	1.40		808	1000	2.25	1.386	22757	1033	Tap water
17	-	1.53		808	1000	2.25	1.386	24826	1240	Tap water
17	-	1.66		808	1000	2.25	1.386	26895	1437	Tap water
17	-	1.91		808	1000	2.25	1.386	31032	1935	Tap water
17	-	2.29		808	1000	2.25	1.386	37239	2745	Tap water
17	-	0.51		808	1000	2.25	1.386	8275	136	Tap water
17	-	0.76		808	1000	2.25	1.386	12413	363	Tap water
17	-	1.02		808	1000	2.25	1.386	16551	597	Tap water
17	-	1.02		808	1000	2.25	1.386	16551	633	Tap water
17	-	1.27		808	1000	2.25	1.386	20688	892	Tap water
17	-	1.27		808	1000	2.25	1.386	20688	944	Tap water
17	-	1.53		808	1000	2.25	1.386	24826	1214	Tap water
17	-	1.66		808	1000	2.25	1.386	26895	1385	Tap water
17	-	1.66		808	1000	2.25	1.386	26895	1531	Tap water
17	-	1.91		808	1000	2.25	1.386	31032	1941	Tap water
17	-	2.29		808	1000	2.25	1.386	37239	2709	Tap water
17	-	2.55		808	1000	2.25	1.386	41376	3269	Tap water
17	-	2.80		808	1000	2.25	1.386	45514	3871	Tap water
17	0.64	-		808	1000	2.25	1.386	4543	638	Tap water
17	0.76	-		808	1000	2.25	1.386	5451	675	Tap water
17	0.76	-		808	1000	2.25	1.386	5451	236	Tap water
17	1.02	-		808	1000	2.25	1.386	7269	872	Tap water
17	1.02	-		808	1000	2.25	1.386	7269	394	Tap water
17	1.27	-		808	1000	2.25	1.386	9086	1261	Tap water
17	1.27	-		808	1000	2.25	1.386	9086	571	Tap water
17	1.53	-		808	1000	2.25	1.386	10903	1743	Tap water
17	1.53	-		808	1000	2.25	1.386	10903	690	Tap water
17	1.78	-		808	1000	2.25	1.386	12720	1873	Tap water

17	1.91	-		808	1000	2.25	1.386	13628	1126	Tap water
17	2.80	-		808	1000	2.25	1.386	19988	3871	Tap water
17	0.80	-		808	1000	2.25	1.386	5704	441	Tap water
17	1.00	-		808	1000	2.25	1.386	7129	841	Tap water
17	1.20	-		808	1000	2.25	1.386	8555	1333	Tap water
17	1.40	-		808	1000	2.25	1.386	9981	2029	Tap water
17	1.70	-		808	1000	2.25	1.386	12120	3347	Tap water
17	0.60	-		808	1000	2.25	1.386	4278	236	Tap water
17	0.80	-		808	1000	2.25	1.386	5704	394	Tap water
17	1.00	-		808	1000	2.25	1.386	7129	571	Tap water
17	1.20	-		808	1000	2.25	1.386	8555	690	Tap water
17	1.50	-		808	1000	2.25	1.386	10694	1126	Tap water
17	-	0.40		808	1000	2.25	1.386	6494	136	Tap water
17	-	0.60		808	1000	2.25	1.386	9740	363	Tap water
17	-	0.80		808	1000	2.25	1.386	12987	597	Tap water
17	-	1.00		808	1000	2.25	1.386	16234	892	Tap water
17	-	1.20		808	1000	2.25	1.386	19481	1214	Tap water
17	-	1.30		808	1000	2.25	1.386	21104	1385	Tap water
17	-	0.50		808	1000	2.25	1.386	8117	280	Tap water
17	-	0.80		808	1000	2.25	1.386	12987	638	Tap water
17	-	1.00		808	1000	2.25	1.386	16234	960	Tap water
17	-	1.20		808	1000	2.25	1.386	19481	1240	Tap water
17	-	1.50		808	1000	2.25	1.386	24351	1935	Tap water
17	-	1.80		808	1000	2.25	1.386	29221	2745	Tap water
17	-	2.47	2.47	808	1000	2.25	1.386		3591	Tap water
17	0.62	1.85	2.47	808	1000	2.25	1.386		3035	Tap water
17	1.11	1.36	2.47	808	1000	2.25	1.386		3009	Tap water
17	1.23	1.23	2.47	808	1000	2.25	1.386		2968	Tap water
17	1.36	1.11	2.47	808	1000	2.25	1.386		2760	Tap water
17	1.85	0.62	2.47	808	1000	2.25	1.386		2807	Tap water
17	2.47	-	2.47	808	1000	2.25	1.386		3367	Tap water
17	0.12	2.35	2.47	808	1000	2.25	1.386		3072	Tap water
17	0.37	2.10	2.47	808	1000	2.25	1.386		2880	Tap water
17	0.74	1.73	2.47	808	1000	2.25	1.386		2838	Tap water
17	1.23	1.23	2.47	808	1000	2.25	1.386		2724	Tap water
17	1.36	1.11	2.47	808	1000	2.25	1.386		2677	Tap water
17	1.48	0.99	2.47	808	1000	2.25	1.386		2594	Tap water
17	1.73	0.74	2.47	808	1000	2.25	1.386		2651	Tap water
17	2.10	0.37	2.47	808	1000	2.25	1.386		2382	Tap water
17	2.35	0.12	2.47	808	1000	2.25	1.386		2501	Tap water
17	0.62	1.60	2.22	808	1000	2.25	1.386		2677	Tap water

17	0.86	1.36	2.22	808	1000	2.25	1.386		2838	Tap water
17	0.99	1.23	2.22	808	1000	2.25	1.386		2963	Tap water
17	1.11	1.11	2.22	808	1000	2.25	1.386		2823	Tap water
17	1.23	0.99	2.22	808	1000	2.25	1.386		2900	Tap water
17	1.73	0.49	2.22	808	1000	2.25	1.386		3227	Tap water
17	2.22	-	2.22	808	1000	2.25	1.386		2449	Tap water
17	0.12	2.10	2.22	808	1000	2.25	1.386		2672	Tap water
17	0.37	1.85	2.22	808	1000	2.25	1.386		2418	Tap water
17	0.74	1.48	2.22	808	1000	2.25	1.386		2205	Tap water
17	0.99	1.23	2.22	808	1000	2.25	1.386		2242	Tap water
17	1.11	1.11	2.22	808	1000	2.25	1.386		2257	Tap water
17	1.23	0.99	2.22	808	1000	2.25	1.386		2205	Tap water
17	1.48	0.74	2.22	808	1000	2.25	1.386		2683	Tap water
17	1.85	0.37	2.22	808	1000	2.25	1.386		2729	Tap water
17	2.10	0.12	2.22	808	1000	2.25	1.386		2999	Tap water
17	0.12	2.10	2.22	808	1000	2.25	1.386		2698	Tap water
17	0.62	1.60	2.22	808	1000	2.25	1.386		2491	Tap water
17	0.99	1.23	2.22	808	1000	2.25	1.386		2496	Tap water
17	1.11	1.11	2.22	808	1000	2.25	1.386		2532	Tap water
17	1.23	0.99	2.22	808	1000	2.25	1.386		2574	Tap water
17	1.36	0.86	2.22	808	1000	2.25	1.386		2548	Tap water
17	1.73	0.49	2.22	808	1000	2.25	1.386		2439	Tap water
17	2.10	0.12	2.22	808	1000	2.25	1.386		2558	Tap water
17	0.12	2.59	2.72	808	1000	2.25	1.386		3539	Tap water
17	0.37	2.35	2.72	808	1000	2.25	1.386		3409	Tap water
17	0.86	1.85	2.72	808	1000	2.25	1.386		3316	Tap water
17	0.99	1.73	2.72	808	1000	2.25	1.386		3347	Tap water
17	1.11	1.60	2.72	808	1000	2.25	1.386		3326	Tap water
17	1.23	1.48	2.72	808	1000	2.25	1.386		3243	Tap water
17	1.36	1.36	2.72	808	1000	2.25	1.386		3207	Tap water
17	1.48	1.23	2.72	808	1000	2.25	1.386		3357	Tap water
17	2.10	0.62	2.72	808	1000	2.25	1.386		3248	Tap water
17	2.59	0.12	2.72	808	1000	2.25	1.386		3175	Tap water
17	0.12	2.59	2.72	808	1000	2.25	1.386		3668	Tap water
17	0.37	2.35	2.72	808	1000	2.25	1.386		3450	Tap water
17	0.62	2.10	2.72	808	1000	2.25	1.386		3233	Tap water
17	0.99	1.73	2.72	808	1000	2.25	1.386		3274	Tap water
17	1.23	1.48	2.72	808	1000	2.25	1.386		3222	Tap water
17	1.36	1.36	2.72	808	1000	2.25	1.386		3269	Tap water
17	1.48	1.23	2.72	808	1000	2.25	1.386		3196	Tap water
17	1.60	1.11	2.72	808	1000	2.25	1.386		3238	Tap water

17	1.73	0.99	2.72	808	1000	2.25	1.386		3155	Tap water
17	1.85	0.86	2.72	808	1000	2.25	1.386		3020	Tap water
25	-	0.48		781	998	1.85	0.985	11778	114	Tap water
25	-	1.11		781	998	1.85	0.985	27481	597	Tap water
25	-	1.59		781	998	1.85	0.985	39259	1162	Tap water
25	-	1.42		781	998	1.85	0.985	35110	2630	Tap water
25	-	0.95		781	998	1.85	0.985	23555	540	Tap water
25	-	1.43		781	998	1.85	0.985	35333	1000	Tap water
25	-	1.91		781	998	1.85	0.985	47110	1759	Tap water
25	-	2.38		781	998	1.85	0.985	58888	2610	Tap water
25	-	2.94		781	998	1.85	0.985	72692	3565	Tap water
25	-	3.00		781	998	1.85	0.985	74176	3620	Tap water
25	-	1.10		781	1065	1.85	1.246	29093	667	saline water
25	-	1.37		781	1065	1.85	1.246	36366	1084	saline water
25	-	1.83		781	1065	1.85	1.246	48488	1778	saline water
25	-	2.29		781	1065	1.85	1.246	60609	2623	saline water
25	-	2.59		781	1065	1.85	1.246	68691	3290	saline water
25	-	3.00		781	1065	1.85	1.246	79442	1302	saline water
25	1.81	-		781	998	1.85	0.985	17888	1199	Tap water
25	1.28	-		781	998	1.85	0.985	12648	825	Tap water
25	3.25	-		781	998	1.85	0.985	32163	3871	Tap water
25	2.19	-		781	998	1.85	0.985	21683	1987	Tap water
25	2.70	-		781	998	1.85	0.985	26742	2875	Tap water
25	3.00	-		781	998	1.85	0.985	29692	3371	Tap water
25	-	1.59		781	998	1.85	0.985	39259	903	Tap water
25	-	1.27		781	998	1.85	0.985	31407	799	Tap water
25	-	0.95		781	998	1.85	0.985	23555	462	Tap water
25	-	0.64		781	998	1.85	0.985	15703	228	Tap water
25	-	0.79		781	998	1.85	0.985	19629	402	Tap water
25	-	0.79		781	998	1.85	0.985	19629	416	Tap water
25	-	1.11		781	998	1.85	0.985	27481	675	Tap water
25	-	1.11		781	998	1.85	0.985	27481	689	Tap water
25	-	1.59		781	998	1.85	0.985	39259	1149	Tap water
25	-	1.59		781	998	1.85	0.985	39259	1163	Tap water
25	-	1.91		781	998	1.85	0.985	47110	1551	Tap water
25	-	1.91		781	998	1.85	0.985	47110	1551	Tap water
25	-	2.22		781	998	1.85	0.985	54962	1996	Tap water
25	-	2.22		781	998	1.85	0.985	54962	1981	Tap water
25	-	2.54		781	998	1.85	0.985	62814	2556	Tap water
25	-	2.70		781	998	1.85	0.985	66740	2872	Tap water
25	3.25	-		781	998	1.85	0.985	32163	3871	Tap water



25	2.70	-		781	998	1.85	0.985	26742	2875	Tap water
25	2.19	-		781	998	1.85	0.985	21683	1987	Tap water
25	1.45	-		781	998	1.85	0.985	14351	955	Tap water
25	1.81	-		781	998	1.85	0.985	17888	1199	Tap water
25	1.28	-		781	998	1.85	0.985	12648	825	Tap water
25	-	1.42	1.42	781	998	1.85	0.985		986	Tap water
25	0.28	1.14	1.42	781	998	1.85	0.985		908	Tap water
25	0.57	0.85	1.42	781	998	1.85	0.985		939	Tap water
25	0.71	0.71	1.42	781	998	1.85	0.985		908	Tap water
25	0.85	0.57	1.42	781	998	1.85	0.985		986	Tap water
25	1.14	0.28	1.42	781	998	1.85	0.985		970	Tap water
25	1.42	-	1.42	781	998	1.85	0.985		950	Tap water
25	0.28	1.14	1.42	781	998	1.85	0.985		903	Tap water
25	0.57	0.85	1.42	781	998	1.85	0.985		913	Tap water
25	0.71	0.71	1.42	781	998	1.85	0.985		918	Tap water
25	0.85	0.57	1.42	781	998	1.85	0.985		924	Tap water
25	1.14	0.28	1.42	781	998	1.85	0.985		944	Tap water
25	-	1.42	1.42	781	998	1.85	0.985		1012	Tap water
25	0.28	1.14	1.42	781	998	1.85	0.985		908	Tap water
25	0.57	0.85	1.42	781	998	1.85	0.985		908	Tap water
25	0.71	0.71	1.42	781	998	1.85	0.985		944	Tap water
25	0.85	0.57	1.42	781	998	1.85	0.985		950	Tap water
25	1.14	0.28	1.42	781	998	1.85	0.985		944	Tap water
25	1.42	-	1.42	781	998	1.85	0.985		960	Tap water
25	0.00	1.61	1.61	781	998	1.85	0.985		1302	Tap water
25	0.32	1.29	1.61	781	998	1.85	0.985		1124	Tap water
25	0.64	0.97	1.61	781	998	1.85	0.985		1100	Tap water
25	0.81	0.81	1.61	781	998	1.85	0.985		1130	Tap water
25	0.97	0.64	1.61	781	998	1.85	0.985		1112	Tap water
25	1.29	0.32	1.61	781	998	1.85	0.985		1088	Tap water
25	1.61	0.00	1.61	781	998	1.85	0.985		1190	Tap water
25	0.60	2.38	2.98	781	998	1.85	0.985		3450	Tap water
25	1.19	1.79	2.98	781	998	1.85	0.985		3144	Tap water
25	1.49	1.49	2.98	781	998	1.85	0.985		3243	Tap water
25	2.38	0.60	2.98	781	998	1.85	0.985		3129	Tap water
25	0.89	2.09	2.98	781	998	1.85	0.985		3321	Tap water
25	1.19	1.79	2.98	781	998	1.85	0.985		3165	Tap water
25	1.34	1.64	2.98	781	998	1.85	0.985		3113	Tap water
25	1.49	1.49	2.98	781	998	1.85	0.985		3150	Tap water
25	1.64	1.34	2.98	781	998	1.85	0.985		3113	Tap water
25	1.79	1.19	2.98	781	998	1.85	0.985		3041	Tap water

25	2.38	0.60	2.98	781	998	1.85	0.985		3030	Tap water
25	0.60	2.38	2.98	781	998	1.85	0.985		3425	Tap water
25	0.89	2.09	2.98	781	998	1.85	0.985		3279	Tap water
25	1.19	1.79	2.98	781	998	1.85	0.985		3175	Tap water
25	1.34	1.64	2.98	781	998	1.85	0.985		3129	Tap water
25	1.49	1.49	2.98	781	998	1.85	0.985		3165	Tap water
25	1.64	1.34	2.98	781	998	1.85	0.985		3160	Tap water
25	1.79	1.19	2.98	781	998	1.85	0.985		3056	Tap water
25	2.09	0.89	2.98	781	998	1.85	0.985		3150	Tap water
25	0.60	2.38	2.98	781	998	1.85	0.985		3383	Tap water
25	1.49	1.49	2.98	781	998	1.85	0.985		3269	Tap water
25	2.09	0.89	2.98	781	998	1.85	0.985		3129	Tap water
25	0.60	2.38	2.98	781	1065	1.85	1.246		3553	saline water
25	1.19	1.79	2.98	781	1065	1.85	1.246		3359	saline water
25	1.34	1.64	2.98	781	1065	1.85	1.246		3392	saline water
25	1.49	1.49	2.98	781	1065	1.85	1.246		3381	saline water
25	1.64	1.34	2.98	781	1065	1.85	1.246		3387	saline water
25	1.79	1.19	2.98	781	1065	1.85	1.246		3392	saline water
25	0.60	2.38	2.98	781	1065	1.85	1.246		3553	saline water
25	1.19	1.79	2.98	781	1065	1.85	1.246		3376	saline water
25	1.34	1.64	2.98	781	1065	1.85	1.246		3475	saline water
25	1.49	1.49	2.98	781	1065	1.85	1.246		3392	saline water
25	1.64	1.34	2.98	781	1065	1.85	1.246		3487	saline water
25	1.79	1.19	2.98	781	1065	1.85	1.246		3459	saline water
25	2.09	0.89	2.98	781	1065	1.85	1.246		3270	saline water
25	2.38	0.60	2.98	781	1065	1.85	1.246		3159	saline water
25	0.60	2.38	2.98	781	1065	1.85	1.246		3570	saline water
25	1.19	1.79	2.98	781	1065	1.85	1.246		3376	saline water
25	1.34	1.64	2.98	781	1065	1.85	1.246		3442	saline water
25	1.49	1.49	2.98	781	1065	1.85	1.246		3437	saline water
25	1.64	1.34	2.98	781	1065	1.85	1.246		3437	saline water
25	0.89	2.09	2.98	781	1065	1.85	1.246		3437	saline water
25	1.34	1.64	2.98	781	1065	1.85	1.246		3442	saline water
25	1.49	1.49	2.98	780	1065	1.85	1.246		3414	saline water
25	1.64	1.34	2.98	780	1065	1.85	1.246		3392	saline water
26	0.26	0.80	1.06	780	998	1.85	0.985		590	Tap water
26	0.53	0.60	1.13	780	998	1.85	0.985		585	Tap water
26	0.66	0.50	1.16	780	998	1.85	0.985		612	Tap water
26	0.79	0.40	1.19	780	998	1.85	0.985		659	Tap water
26	1.06	0.20	1.26	780	998	1.85	0.985		659	Tap water
26	0.66	0.50	1.16	780	998	1.85	0.985		628	Tap water

26	0.79	0.40	1.19	780	998	1.85	0.985		721	Tap water
26	1.06	0.20	1.26	780	998	1.85	0.985		763	Tap water
26	0.66	0.50	1.16	780	998	1.85	0.985		607	Tap water
26	0.79	0.40	1.19	780	998	1.85	0.985		695	Tap water
26	1.06	0.20	1.26	780	998	1.85	0.985		675	Tap water
26	0.66	0.50	1.16	780	998	1.85	0.985		592	Tap water
26	0.79	0.40	1.19	780	998	1.85	0.985		612	Tap water
26	1.06	0.20	1.26	780	998	1.85	0.985		664	Tap water
26	0.66	0.50	1.16	780	998	1.85	0.985		638	Tap water
26	0.79	0.40	1.19	780	998	1.85	0.985		633	Tap water
26	1.06	0.20	1.26	780	998	1.85	0.985		685	Tap water
26	0.46	1.45	1.91	780	998	1.85	0.985		1608	Tap water
26	0.93	1.10	2.03	780	998	1.85	0.985		1518	Tap water
26	1.19	0.90	2.09	780	998	1.85	0.985		1676	Tap water
26	1.45	0.70	2.15	780	998	1.85	0.985		1712	Tap water
26	1.92	0.35	2.27	780	998	1.85	0.985		1795	Tap water
26	1.19	0.90	2.09	780	998	1.85	0.985		1702	Tap water
26	1.45	0.70	2.15	780	998	1.85	0.985		1686	Tap water
26	1.92	0.35	2.27	780	998	1.85	0.985		1832	Tap water
26	1.19	0.90	2.09	780	998	1.85	0.985		1686	Tap water
26	1.45	0.70	2.15	780	998	1.85	0.985		1790	Tap water
26	1.92	0.35	2.27	780	998	1.85	0.985		1899	Tap water
26	1.19	0.90	2.09	780	998	1.85	0.985		1645	Tap water
26	1.45	0.70	2.15	780	998	1.85	0.985		1723	Tap water
26	1.92	0.35	2.27	780	998	1.85	0.985		1795	Tap water
26	1.19	0.90	2.09	780	998	1.85	0.985		1645	Tap water
26	1.45	0.70	2.15	780	998	1.85	0.985		1697	Tap water
26	1.92	0.35	2.27	780	998	1.85	0.985		1697	Tap water
26	1.19	0.90	2.09	780	998	1.85	0.985		1619	Tap water
26	1.45	0.70	2.15	780	998	1.85	0.985		1697	Tap water
26	1.92	0.35	2.27	780	998	1.85	0.985		1733	Tap water
26	0.66	2.30	2.96	780	998	1.85	0.985		3404	Tap water
26	0.66	2.30	2.96	780	998	1.85	0.985		2646	Tap water
26	0.99	2.01	3.00	780	998	1.85	0.985		2786	Tap water
26	1.65	1.44	3.09	780	998	1.85	0.985		2880	Tap water
26	1.98	1.15	3.13	780	998	1.85	0.985		2973	Tap water
26	2.31	0.86	3.18	780	998	1.85	0.985		3124	Tap water
26	2.64	0.57	3.22	780	998	1.85	0.985		3300	Tap water
26	0.99	2.01	3.00	780	998	1.85	0.985		3279	Tap water
26	1.65	1.44	3.09	780	998	1.85	0.985		2833	Tap water
26	1.98	1.15	3.13	780	998	1.85	0.985		3061	Tap water

26	2.31	0.86	3.18	780	998	1.85	0.985		3124	Tap water
26	1.65	1.44	3.09	780	998	1.85	0.985		2838	Tap water
26	1.98	1.15	3.13	780	998	1.85	0.985		2973	Tap water
26	2.31	0.86	3.18	780	998	1.85	0.985		3082	Tap water
26	2.64	0.57	3.22	780	998	1.85	0.985		3269	Tap water
26	1.65	1.44	3.09	780	998	1.85	0.985		2880	Tap water
26	1.98	1.15	3.13	780	998	1.85	0.985		2999	Tap water
26	2.31	0.86	3.18	780	998	1.85	0.985		3129	Tap water
26	2.64	0.57	3.22	780	998	1.85	0.985		3336	Tap water
26	0.66	1.84	2.50	780	998	1.85	0.985		2776	Saline water
26	0.99	1.61	2.60	780	998	1.85	0.985		2802	Saline water
26	1.32	1.38	2.70	780	998	1.85	0.985		2862	Saline water
26	1.65	1.15	2.80	780	998	1.85	0.985		2979	Saline water
26	1.98	0.92	2.90	780	998	1.85	0.985		3096	Saline water
26	2.31	0.69	3.00	780	998	1.85	0.985		3207	Saline water
26	2.64	0.46	3.10	780	998	1.85	0.985		3346	Saline water
26	1.32	1.38	2.70	780	998	1.85	0.985		2800	Saline water
26	1.65	1.15	2.80	780	998	1.85	0.985		2856	Saline water
26	1.98	0.92	2.90	780	998	1.85	0.985		3084	Saline water
26	2.31	0.69	3.00	780	998	1.85	0.985		3185	Saline water
26	2.64	0.46	3.10	780	998	1.85	0.985		3346	Saline water
26	1.32	1.38	2.70	780	998	1.85	0.985		3140	Saline water
26	1.65	1.15	2.80	780	998	1.85	0.985		3129	Saline water
26	1.98	0.92	2.90	780	998	1.85	0.985		3235	Saline water
26	2.31	0.69	3.00	780	998	1.85	0.985		3296	Saline water
26	1.32	1.38	2.70	780	998	1.85	0.985		2667	Saline water
26	1.65	1.15	2.80	780	998	1.85	0.985		2756	Saline water
26	1.98	0.92	2.90	780	998	1.85	0.985		3068	Saline water
26	2.31	0.69	3.00	780	998	1.85	0.985		3079	Saline water
26	2.64	0.46	3.10	780	998	1.85	0.985		3246	Saline water
26	1.32	1.38	2.70	780	998	1.85	0.985		2884	Saline water
26	1.65	1.15	2.80	780	998	1.85	0.985		3068	Saline water
26	1.98	0.92	2.90	780	998	1.85	0.985		3207	Saline water
26	2.31	0.69	3.00	780	998	1.85	0.985		3251	Saline water
26	2.64	0.46	3.10	780	998	1.85	0.985		3413	Saline water

### Appendix3: Flow Pattern Data

Temp. °C	U <sub>o</sub> m/s	U <sub>w</sub> m/s	ρ <sub>o</sub> kg/m <sup>3</sup>	ρ <sub>w</sub> kg/m <sup>3</sup>	μ <sub>o</sub> cP	μ <sub>w</sub> cP	Flow Pattern	Additional info
25	0.226	1.9	781	998	1.85	0.985	DO/W	Tap water
25	0.079	0.794	781	998	1.85	0.985	DO/W&W	Tap water
25	0.079	1	781	998	1.85	0.985	DO/W&W	Tap water
25	0.079	1.58	781	998	1.85	0.985	DO/W	Tap water
25	0.079	1.259	781	998	1.85	0.985	DO/W&W	Tap water
25	0.0795	0.795	781	998	1.85	0.985	DO/W&W	Tap water
25	0.0795	0.631	781	998	1.85	0.985	DO/W&W	Tap water
25	0.0795	0.5	781	998	1.85	0.985	ST&MI	Tap water
25	0.1	0.1995	781	998	1.85	0.985	ST	Tap water
25	0.1	0.1585	781	998	1.85	0.985	ST	Tap water
25	0.1	0.2511	781	998	1.85	0.985	ST	Tap water
25	0.1	1.259	781	998	1.85	0.985	Do/w&w	Tap water
25	0.1	1.585	781	998	1.85	0.985	DO/W	Tap water
25	0.1	0.1995	781	998	1.85	0.985	st	Tap water
25	0.105	0.795	781	998	1.85	0.985	DO/W&W	Tap water
25	0.105	0.631	781	998	1.85	0.985	ST&MI	Tap water
25	0.105	0.5	781	998	1.85	0.985	ST&MI	Tap water
25	0.132	1.259	781	998	1.85	0.985	DO/W&W	Tap water
25	0.132	1.585	781	998	1.85	0.985	DO/W	Tap water
25	0.132	0.1995	781	998	1.85	0.985	ST	Tap water
25	0.1585	0.631	781	998	1.85	0.985	ST&MI	Tap water
25	0.1585	0.794	781	998	1.85	0.985	DO/W&W	Tap water
25	0.1995	0.1	781	998	1.85	0.985	ST	Tap water
25	0.1995	0.125	781	998	1.85	0.985	ST	Tap water
25	0.1995	0.0794	781	998	1.85	0.985	ST	Tap water
25	0.21	0.631	781	998	1.85	0.985	ST&MI	Tap water
25	0.21	0.794	781	998	1.85	0.985	DO/W&W	Tap water
25	0.25	1	781	998	1.85	0.985	DO/W&W	Tap water
25	0.316	0.0794	781	998	1.85	0.985	ST&MI	Tap water
25	0.316	1	781	998	1.85	0.985	DO/W&W	Tap water
25	0.33	1	781	998	1.85	0.985	DO/W&W	Tap water
25	0.398	0.063	781	998	1.85	0.985	ST&MI	Tap water
25	0.398	1	781	998	1.85	0.985	DO/W&W	Tap water
25	0.4178	1	781	998	1.85	0.985	DO/W&W	Tap water
25	0.5	1	781	998	1.85	0.985	ST&MI	Tap water
25	0.5	1.259	781	998	1.85	0.985	DW/O&DO/W	Tap water

25	0.5	1.585	781	998	1.85	0.985	DO/W	Tap water
25	0.526	1	781	998	1.85	0.985	ST&MI	Tap water
25	0.63	0.1995	781	998	1.85	0.985	ST&MI	Tap water
25	0.63	0.2511	781	998	1.85	0.985	ST&MI	Tap water
25	0.63	0.316	781	998	1.85	0.985	ST&MI	Tap water
25	0.63	0.1995	781	998	1.85	0.985	ST&MI	Tap water
25	0.631	1.259	781	998	1.85	0.985	DW/O&DO/W	Tap water
25	0.631	1.259	781	998	1.85	0.985	DW/O&DO/W	Tap water
25	0.661	1	781	998	1.85	0.985	DW/O&DO/W	Tap water
25	0.661	1.259	781	998	1.85	0.985	DW/O&DO/W	Tap water
25	0.661	1.585	781	998	1.85	0.985	DO/W	Tap water
25	0.794	0.1	781	998	1.85	0.985	ST&MI	Tap water
25	0.794	0.5	781	998	1.85	0.985	ST&MI	Tap water
25	0.794	0.794	781	998	1.85	0.985	ST&MI	Tap water
25	0.794	0.316	781	998	1.85	0.985	ST&MI	Tap water
25	0.794	1.58	781	998	1.85	0.985	DW/O&DO/W	Tap water
25	0.833	0.1995	781	998	1.85	0.985	ST&MI	Tap water
25	0.8343	1.259	781	998	1.85	0.985	DW/O&DO/W	Tap water
25	0.8343	1.259	781	998	1.85	0.985	DW/O&DO/W	Tap water
25	1	0.1	781	998	1.85	0.985	ST&MI	Tap water
25	1	0.5	781	998	1.85	0.985	ST&MI	Tap water
25	1	0.316	781	998	1.85	0.985	ST&MI	Tap water
25	1	0.1995	781	998	1.85	0.985	ST&MI	Tap water
25	1	1.58	781	998	1.85	0.985	DW/O&DO/W	Tap water
25	1.05	0.1	781	998	1.85	0.985	ST&MI	Tap water
25	1.05	0.5	781	998	1.85	0.985	DW/O&O	Tap water
25	1.05	0.794	781	998	1.85	0.985	DW/O&DO/W	Tap water
25	1.05	0.316	781	998	1.85	0.985	ST&MI	Tap water
25	1.05	1.58	781	998	1.85	0.985	DW/O&DO/W	Tap water
25	1.32	0.1	781	998	1.85	0.985	DW/O	Tap water
25	1.32	0.5	781	998	1.85	0.985	DW/O&DO/W	Tap water
25	1.322	0.316	781	998	1.85	0.985	DW/O&DO/W	Tap water
25	1.32	0.1995	781	998	1.85	0.985	DW/O&O	Tap water
25	1.32	1.58	781	998	1.85	0.985	DW/O&DO/W	Tap water
25	1.585	0.079	781	998	1.85	0.985	Dw/o	Tap water
25	2.1	0.079	781	998	1.85	0.985	DW/O	Tap water
25	0.0795	0.795	781	1065	1.85	1.246	DO/W&W	Saline water
25	0.0795	0.631	781	1065	1.85	1.246	DO/W&W	Saline water
25	0.0795	0.5	781	1065	1.85	1.246	ST&MI	Saline water

25	0.1	0.1995	781	1065	1.85	1.246	ST	Saline water
25	0.1	0.1585	781	1065	1.85	1.246	ST	Saline water
25	0.1	0.2511	781	1065	1.85	1.246	ST	Saline water
25	0.1	1.259	781	1065	1.85	1.246	Do/w&w	Saline water
25	0.1	1.585	781	1065	1.85	1.246	DO/W	Saline water
25	0.1	0.1995	781	1065	1.85	1.246	st	Saline water
25	0.1585	0.631	781	1065	1.85	1.246	ST&MI	Saline water
25	0.1585	0.794	781	1065	1.85	1.246	DO/W&W	Saline water
25	0.1995	0.1	781	1065	1.85	1.246	ST	Saline water
25	0.1995	0.125	781	1065	1.85	1.246	ST	Saline water
25	0.1995	0.0794	781	1065	1.85	1.246	ST	Saline water
25	0.25	1	781	1065	1.85	1.246	DO/W&W	Saline water
25	0.316	0.0794	781	1065	1.85	1.246	ST&MI	Saline water
25	0.316	1	781	1065	1.85	1.246	DO/W&W	Saline water
25	0.398	0.063	781	1065	1.85	1.246	ST&MI	Saline water
25	0.398	1	781	1065	1.85	1.246	DO/W&W	Saline water
25	0.5	1	781	1065	1.85	1.246	ST&MI	Saline water
25	0.5	1.259	781	1065	1.85	1.246	DO/W&W	Saline water
25	0.5	1.585	781	1065	1.85	1.246	DO/W	Saline water
25	0.63	0.1995	781	1065	1.85	1.246	ST&MI	Saline water
25	0.63	0.251	781	1065	1.85	1.246	ST&MI	Saline water
25	0.63	0.316	781	1065	1.85	1.246	ST&MI	Saline water
25	0.63	0.1995	781	1065	1.85	1.246	ST&MI	Saline water
25	0.631	1.259	781	1065	1.85	1.246	DW/O&DO/W	Saline water
25	0.631	1.259	781	1065	1.85	1.246	DW/O&DO/W	Saline water
25	0.794	0.1	781	1065	1.85	1.246	ST&MI	Saline water
25	0.794	0.5	781	1065	1.85	1.246	ST&MI	Saline water

25	0.794	0.794	781	1065	1.85	1.246	ST&MI	Saline water
25	0.794	0.316	781	1065	1.85	1.246	ST&MI	Saline water
25	0.794	1.58	781	1065	1.85	1.246	DW/O&DO/W	Saline water
25	1	0.1	781	1065	1.85	1.246	ST&MI	Saline water
25	1	0.5	781	1065	1.85	1.246	ST&MI	Saline water
25	1	0.316	781	1065	1.85	1.246	ST&MI	Saline water
25	1	0.1995	781	1065	1.85	1.246	ST&MI	Saline water
25	1	1.58	781	1065	1.85	1.246	DW/O&DO/W	Saline water
25	1.585	0.079	781	1065	1.85	1.246	Dw/o	Saline water



## Vitae

Name : Ayman Wajeeh Mukhaimer

Nationality : Palestinian

Date of Birth : 5/22/1986

Email : ayman\_mukh@yahoo.com

Address : Palestine

Academic Background :

MSc Mechanical Engineering, King Fahd University of  
Petroleum and Minerals, Saudi Arabia.

BSc Mechanical Engineering, An-Najah National  
University, Palestine.